Facoltà di Ingegneria

Corso di Laurea in Ingegneria Aerospaziale

Implementation of a Real-Time Test-Bed for LISA Pathfinder

Tesi di Laurea

Anno Accademico 2005-2006

16 Aprile 2007

Allievo:

MARIANNA VITELLI

Relatori:

PROF. G. MENGALI

DR.-ING. W. FICHTER

DIPL.-ING. T. ZIEGLER

[…] La tua ragione e la tua passione
sono timone e vele dell'anima che naviga.
Dovessero guastarsi o le vele o il timone
non potresti se non scuoterti a vuoto
e andare alla deriva,
o rimanere immoto in mezzo al mare.
La ragione, regnando incontrastata, è forza vincolante;
e la passione, senza alcun controllo,
è una fiamma che arde
fino alla distruzione di se stessa.

GIBRAN, *Il profeta*

[…] Your reason and your passion
are the rudder and the sails of your seafaring soul.
If either your sails or your rudder be broken,
you can but loss and drift,
or else be held at a standstill in mid-seas.
For reason, ruling alone, is a force confining;
And passion, unattended, is a flame
that burns to its own destruction.

GIBRAN, *The prophet*

Ai miei genitori e
a mio nonno Meco

To my parents and
to my grandpa Meco

Preface

The document on hand is a Diploma Thesis in the field of Aerospace Engineering, at the University of Pisa.

The work on this Diploma Thesis was performed over 10 months at the EADS Astrium GmbH, Earth Observation Navigation and Science, in Friedrichshafen, Germany. It is a contribution to the Drag-Free and Attitude Control System (DFACS) of the LISA Pathfinder Mission.

Abstract

LISA Pathfinder is intended to demonstrate the key technologies for LISA, the Laser Interferometer Space Antenna for gravitational waves detection. At the heart of the LISA Pathfinder (LPF) mission lies the high-precision inertial sensor package, the so-called LTP (LISA Technology Package).

The LTP package basically consists of two Inertial Sensors and a laser interferometer. Each Inertial Sensor contains a free floating Test Mass (TM), which will ideally follow a purely gravitational trajectory. The positions of the proof masses with respect to the spacecraft will be measured electrostatically (capacitive sensing) using electrodes embedded in the Inertial Sensor (IS) housing. A Drag-Free Control System will cause the satellite to follow the trajectories of the test masses by means of Field Emission Electric Propulsion (FEEP) micro-Newton thrusters. The LTP laser interferometer will provide a measurement of the relative displacement of the TMs, allowing a direct assessment of the differential acceleration of the masses. The top science requirement of LPF is to demonstrate that the differential acceleration along the direct connection line between the centers of mass of the two TMs can be kept below a certain limit. Since the performance goal cannot be verified on the ground, a high level of modeling and detailed simulations are required to ensure the LISA Pathfinder mission success. Therefore, an End-to-End Simulator has been developed, it will be backed by Real-Time Test-Beds (RTB) with hardware in-loop to validate the performance of the sensors, actuators and control systems in a closed/open loop environmental simulation.

To this end, a preliminary Real-Time Test-Bed has been built during this work.

All actuator and sensor models, the spacecraft and test masses nonlinear dynamics, the environmental and internal disturbance models as well as the Drag-Free Algorithm Control System (DFACS) software have been

implemented on a dSPACE® Real-Time Computer (RTC). A real interferometer, similar to the LTP one, for the readout of the differential TMs displacement has been built-up. In this interferometer, the test mass tip/tilt angles are represented by piezo actuated tip/tilt mirrors controlled according to the test mass motion as derived from the computed equations of motion. Furthermore, the complete hardware set-up (consisting of the interferometer and its electronics devices) has been calibrated.
This Test-Bed represents the first step toward an LTP RTB that can be used for the DFACS closed loop functional testing as well as for the testing of the initial acquisition of the optical metrology system.

LISA Pathfinder ha lo scopo di dimostrare il funzionamento delle tecnologie necessarie per la realizzazione del progetto LISA (Laser Interferometer Space Antenna) per la rilevazione delle onde gravitazionali. Il carico pagante della missione LISA Pathfinder è costituito dal LTP (LISA Technology Package), in pratica tutto l'insieme dei sensori inerziali di alta precisione.
L'LTP contiene due sensori inerziali ed un interferometro laser. Ciascun sensore inerziale contiene una massa-prova soggetta alla sola forza gravitazionale in un moto di quasi perfetta caduta libera. La posizione delle masse-prova rispetto al satellite sarà misurata elettrostaticamente utilizzando degli elettrodi situati nella scatola a vuoto contenente la massa. Un sistema di controllo Drag-Free permetterà al satellite di spostarsi seguendo le traiettorie delle masse-prova, tramite l'utilizzo di micro propulsori elettrici ad emissione di campo (FEEP). L'interferometro laser del LTP misurerà la posizione relativa tra le masse-prova, permettendo una stima diretta dell'accelerazione differenziale. Il principale obiettivo del LTP è quello di dimostrare che il valore dell'accelerazione differenziale, lungo la linea di connessione dei centri di massa delle masse di prova, può essere mantenuto al di sotto di un certo limite. Dato che le prestazioni reali del satellite non possono essere verificate a terra, per assicurare il successo della missione LISA Pathfinder, si rendono

necessarie modellizzazioni e simulazioni molto precise e accurate. Un simulatore *end-to-end* è attualmente in via di sviluppo e sarà presto affiancato da simulazioni ambientali su banchi-prova *real-time* per verificare le prestazioni di sensori, attuatori e sistemi di controllo in ciclo chiuso/aperto.

A questo scopo, durante il periodo di sviluppo della presente tesi, è stato costruito e testato un banco-prova *real-time* preliminare.
Tutti i modelli degli attuatori e dei sensori, la dinamica non lineare delle masse di prova e del satellite, i modelli relativi all'ambiente circostante il satellite e ai disturbi interni ad esso insieme con il software del sistema di controllo (DFACS), in grado di garantire un moto di quasi perfetta caduta libera delle masse di prova, sono stati implementati su un computer *real-time* fornito dall'azienda tedesca dSPACE®. Inoltre, è stato costruito un interferometro, simile a quello del LTP, in grado di misurare lo spostamento relativo tra le due masse di prova e nel quale ciascuna massa è rappresentata da uno specchio in grado di riprodurre i valori angolari di due dei tre angoli di Eulero, ottenuti dalla soluzione delle equazioni del moto. In seguito, il pacchetto hardware (comprendente l'interferometro e i relativi dispositivi elettronici) è stato opportunamente calibrato.
L'attuale banco prova *real-time* rappresenta il primo passo verso un altro sistema di questo tipo mirante a testare sia il DFACS in ciclo chiuso che la fase iniziale di acquisizione del sistema di metrologia ottica.

Acknowledgements

When a so long-waited and suffered goal is reached, the people, that contribute to realize it, should be thanked.
The first thanks go to my professor G. Mengali and to Stefano Lucarelli that gave me the opportunity to develop my thesis in Astrium. Special thanks go to W. Fichter to have introduced me to his team and to offer to me the opportunity to continue working after my graduation.
I thank my advisor Tobias for his positive attitude in our work and for always answering to my thousands of questions. Thank to the DFACS guys that made the work environment affable and friendly.
I really thank my dear friends, Checca and Dondo, for their help in the difficulties and for our long talks during the cold Immenstaad's nights.

My special and loving thanks go to my parents. My gratefulness can not be explained with words. During these years, they gave me the strength I needed. I dedicate this work and the joy of this moment to them that had known my sufferings and always helped me. I can not forget, however, all my family.

My warm thanks go to Marco, my irreplaceable travel mate. We traveled this track together, step by step. Over these years, we shared joys and sorrows, helping each other.

I thank my best friend Serena for always trusting in our friendship especially in this last difficult period.

Finally, thank to my university mates, Luca, Pierpa, Manu and Vale, for making these years special and to put the bases of a strong friendship.

Ringraziamenti

Al raggiungimento di un traguardo tanto agognato e sofferto, non si può non ringraziare coloro che hanno contribuito a realizzarlo.

Ringrazio il mio professore G. Mengali e Stefano Lucarelli che mi hanno dato la possibilità di poter svolgere la mia tesi in Astrium e W. Fichter per avermi introdotto nel suo team e offerto l'opportunità di continuare a farne parte, anche dopo la laurea.
Ringrazio il mio relatore Tobias per il suo costante interesse verso il lavoro da me svolto e la sua disponibilità. Come non rivolgere un pensiero ai "ragazzi del DFACS" che hanno sempre reso l'ambiente lavorativo, e non solo, cordiale e amichevole.
Un ringraziamento particolare a Checca e Dondo, ai quali mi sento particolarmente legata, per la loro presenza nei momenti difficili, per le nostre chiacchierate fino a tardi nelle fredde notti di Immenstaad; senza di loro l'esperienza tedesca non sarebbe stata la stessa.

Ringrazio mamy e babbo; la mia gratitudine verso di loro va al di là di ogni parola. Loro il mio riferimento, loro sempre al mio fianco, nel corso di questi anni mi hanno dato tutta la sicurezza e la forza di cui avevo bisogno, sopportando i miei colpi di testa. A loro che, piu' di chiunque altro, hanno conosciuto le mie sofferenze condividendole con me, dedico questo lavoro e la gioia di questo momento. Un grazie va, comunque, a tutti i miei familiari per la loro costante presenza.

Ringrazio Marco, mio insostituibile compagno d'avventura. Passo dopo passo, abbiamo percorso questo cammino arricchendoci l'un l'altro, partecipando insieme alle gioie e ai dolori di questi anni, sostenendoci a vicenda. Non so descrivere la grandissima felicità e, allo stesso tempo, la tristezza che provo nell'essere giunti insieme a questo traguardo e nel doverci ora separare.

Grazie per esserci sempre stato e non aver mai messo in dubbio il nostro rapporto anche nei momenti piu' difficili.

Ringrazio la mia "amicicia" Serena perché, nonostante l'università ci abbia portato in città diverse, è sempre stata al mio fianco anche quando, soprattutto nell'ultimo periodo, sono stata poco presente e troppo presa dallo studio.

Un affettuoso pensiero va anche ai miei compagni di università, Luca, Pierpa, Manu e Vale che hanno contribuito tutti, in maniera diversa, a rendere speciali questi anni, gettando le basi per un'amicizia che va al di là del semplice rapporto universitario.

List of Figures

1.1-1 Spectrum of predicted gravitational wave amplitudes as function of frequency for a range of astrophysical sources
1.2-1 Artists's concept
1.2-2 Orbital configuration of the LISA mission concept
1.3-1 LISA and LISA Pathfinder configurations
1.3-2 Test masses and laser interferometer
2.1-1 E2E-Simulator top-level architecture
2.2-2 Real Time Interface (RTI) board library
2.3-1 General Implementation procedure diagram
3.1-1 LPF four interferometers
3.1-2 OMS principle of operation
3.1-3 Test masses degrees of freedom
3.2-1 HP interferometer
3.2-2 LPF x_2-x_1 interferometer
3.3.1-1 Laser Head HP5517B
3.3.1-2 HP IFO electronic principle of operation
3.3.2-1 Polarization at the Laser Head
3.3.2-2a Polarization at the polarizing beam splitter 1
3.3.2-2b Polarization at the polarizing beam splitter 2
3.3.2-3 Polarizer principle of operation
3.3.2-4 Receiver: beams overlap
3.3.2-5 Laser beam at the tip/tilt mirror
3.3.2-6 Constructive and destructive interference at the photodetector
3.4.1-1 Interferometer partial view
3.4.1-2 Examples of mounting on the optical bench (PBS)
3.4.1-3 Adjusting beam height
3.4.1-4a Adjusting mirror position
3.4.1-4b Adjusting mirror position
3.4.2-1 New mirror mount

4.1.1 Laboratory instrumentation and interconnections between individual components
4.2.1-1 Transformation algorithm philosophy
4.2.1-2 Transformation algorithm: Simulink block
4.2.3-1 Voltage divider's circuitry
4.2.4-1 Picture of the DK2/35 mirror
4.2.4-2 Linearity between the voltage and the deflection angle
4.2.4-3 Electronic devices connections
4.2.4-4 Piezoelectric mirror
4.2.4-5 Piezo actuator layouts and wiring
4.2.4-6 Linearity between the output voltage anf the deflection angle
4.2.4-7 Closed loop operational mode
4.2.5-1 In-line electronic devices and their gain factors
4.2.6-1 HP 10780A receiver
4.2.6-2 Receiver circuitry
4.2.7-1 HP laser Axis Board and VXI board
4.2.7-2 Laser Axis Board
4.2.8-1 Closed loop configuration
4.2.8-2 Connection between IFO, Laser Axis Board and visualization PC
5.1-1 HP interferometer final configuration
5.2.1-1 Test signal disturbed by 3 slightly touches of the optical bench
5.2.2-1 Noise PSD of three hours measurements
5.2.2-2 DFACS control error and sensitivity of the HP interferometer
5.2.3-1 X-axis measurement by applying a shift equal to 1 mm
5.2.3-2 Shift along the x-axis
6.1 Beam measurement
6.1-1 Inline electronics: ideal case
6.1-2 Inline electronics: real case
6.1-3 Successive measurements
6.2-1 Detrending of data
6.2.2-1 Principle of parameter identification
6.3.2-1 Measurement raw data

6.3.2-2 Detrended data
6.3.2-3 Cross-correlation function
6.3.2-4a Filtering effects
6.3.2-4b Filtering effects
6.3.2-5 Processed data
7.2-1 Developing procedure for the LTP-RTB
7.2-2 RTB: Combination of A1 and A2 modes
7.2-3 RTB: Combination of B1 and B2 modes
A.1-1 Simplified *SolarForceTorque* model
A.1-2 Simplified *GravityField* model
A.2-1 Solver Pane
A.2-2 Optimizations
A.2-3 Real-Time Workshop® pane
A.4-1 Euler angles of TM1
A.4-2 Euler angles of TM2
A.4-3 Position displacement of TM1
A.4-4 Position displacement of TM2
B.1-1 Principle of operation
B.2-1 First layout of the telecommand interface
B.2-2 Second layout of the telecommand interface
B.2-3 Third layout of the telecommand interface
B.2-4 Fourth layout of the telecommand interface
B.2-5 Fifth layout of the telecommand interface
C.1-1 Zeeman splitting
C.2-1 Off-line calibration
C.3-1 Test signal: PSD
C.3-2 Quadratic effect
D.1-1 Multi-port plug
D.2-1 laser Axis Board
D.3-1 Sine wave ControlDesk layout
D.3-2 Sine wave ControlDesk capture layout
E.2-1 Upload and visualization file: block diagram

List of Tables

3.1 LTP and HP interferometers

3.2 The phase difference and Δx for bright and dark fringes

4.1 Scaling factors

4.2 HP Laser Axis Board resolution

6.1 Parameter identification results

C.1a Off-line calibration of the piezoelectric mirror

C.1b Off-line calibration of the voice-coil mirror

C.2 Off-line calibration: definitive results

E.1 Initialization file: front panel

Acronyms

EADS	European Aeronautic Defence and Space Company
LISA	Laser Interferometer Space Antenna
LPF	LISA Pathfinder
LTP	LISA Technology Package
TM	Test Mass
IS	Inertial Sensor
FEEP	Field Emission Electric Propulsion
RTB	Real-Time Test-Bed
DFACS	Drag-Free Algorithm Control System
LIGO	Laser Interferometer Gravitational-Wave Observatory
ESA	European Space Agency
NASA	National Aeronautics and Space Administration
RTC	Real-Time Computer
S/C	Spacecraft
E2E	End-to-End
HP	Hewlett Packard
RTW	Real-Time Workshop®
I/F	Interface
PPC	Power PC
I/O	Input/Output
A/D	Analog/Digital
D/A	Digital/Analog
OMS	Optical Metrology System
OB	Optical Bench
PFE	Phasemeter Front-End
DMU	Data Management Unit
AOM	Acousto-Optical Modulator
ACU	Amplitude Control Unit
EoM	Equations of Motion
DAC	Digital to Analog Converter

LVPZT	Low Voltage Piezoelectric Translator
LVDT	Linear Variable Differential Transformers
PBS	Polarizing Beam Splitter
API	Application Programming Interface
PSD	Power Spectral Density
OMU	Optical Metrology Unit
RTI	Real-Time Interface

Table of Contents

I Introduction

1 Introduction. 2
1.1 Gravitational Waves.. 2
1.2 The LISA Mission. 5
1.3 The LISA Pathfinder Mission.. 4
1.3.1 The Science Requirements. 7
1.3.2 Optical Metrology System Requirement. 8
1.4 Contributions of the Thesis.. 9
1.5 Outline of the Thesis. 10

II The End-to-End Simulator and the Real-Time Environment

2 End-to-End Performance Simulator Implementation. 13
2.1 End-to-End Performance Simulator. 13
2.2 Real-Time Workshop® Software and dSPACE® System.. . . . 15
2.3 The Implementation Procedure. 17
2.3.1 The General Implementation Procedure. 17
2.3.2 Specifics of the E2E-Simulator Implementation Procedure. 19
2.4 Telecommand Interface. 20
2.4.1 Telecommand Implementation on the dSPACE® System. 20

III Laboratory Instrumentation

3 Laser Interferometry.. 24

3.1 LTP Optical Metrology System. 24

3.2 Differences between the LTP and HP Interferometers. 27

3.3 Detailed Description of HP Interferometer. 30

3.3.1 Electronic Principle of Operation. 30

3.3.2 Optic Principle of Operation. 31

3.4 Practical Design Knowledge of the Interferometer Built-Up

3.4.1 Interferometer Build-Up. 38

3.4.2 Stability Problems. 41

4 Overview of the Laboratory Build-Up. 44

4.1 Principle of Operation. 44

4.2 System Level Overview. 46

4.2.1 Transformation Algorithm. 46

4.2.2 Digital to Analog Converter. 48

4.2.3 Voltage Dividers. 49

4.2.4 Tip/Tilt Mirrors. 50

4.2.5 Functional Overview of the DAC, Voltage Divider and Tip/Tilt Mirrors Electronics. 56

4.2.6 The HP Receiver. 57

4.2.7 Laser Electronics. 59

4.2.8 LabVIEW® Computer. 62

5 Complete Setup and Performance. 65

5.1 Interferometer Final Configuration. 65

5.1.1 Maintenance of the Interferometer. 66

5.2 System Performance. 66

5.2.1 Stability. 66

5.2.2 Reached Noise Level Performance.. 67

5.2.3 X-Axis Test. 70

IV Calibration and Testing of the Real-Time Test-Bed

6 Calibration of the RTB. 73

6.1 Calibration Procedure. 73

6.2 General Aspects of the Used Estimation Procedure 78

6.2.1 Data Processing. 78

6.2.2 Principle of Parameter Identification 81

6.3 Calibration Results - 83

6.3.1 Set-Up of Identification Experiment 83

6.3.2 Raw Data Processing. 84

6.3.3 Final Results Obtained from Statistical Estimation Methods.. 88

7 Summary and Outlook. 90

7.1 Conclusions. 90

7.2 Prospects for Future Work. 91

Appendix A. 95

A.1 E2E-Simulator S-functions Modifications. 95

A.2 Implementation Procedure. 96

A.3 User Makefile. 98

A.4 Simulink/Real-Time Simulations: Matching of Results. . . . 101

Appendix B. 104

B.1 Telecommands Modification. 104

B.2 Telecommands Interface. 105

Appendix C. 108

C.1 The Zeeman Splitting 108

C.2 The Off-line Calibration 111

C.3 Quadratic Effect. 113

Appendix D. 116

D.1 Starting a Measurement: Step by Step Procedure. 118

D.2 Importance of the LEDs on the Laser Axis Board. 118

D.3 Managing dSPACE Control Desk. 119

Appendix E. 121

E.1 Laser Axis Board Initialization File. 122

E.2 Laser Axis Board Upload and Visualization File. 123

Part I

Introduction

Chapter 1

Introduction

1.1 Gravitational Waves

Gravitational waves are disturbances in the theoretical, four-dimensional fabric, called space-time, which enmeshes anything of mass in the universe, according to Einstein's Theory of General Relativity. The theory asserts that no physical effect can travel faster than light; therefore, when stars move and thus change the gravitational field they create, these changes cannot be felt everywhere in space instantly. They move through space as a ripple of changing gravity. In Einstein's theory, gravity is represented by the curvature of space and time. Gravitational waves stretch and compress space as they move through it, they can be seen as ripples in space-time.

The effects of gravity waves on matter are very weak. A free mass will oscillate in response to a passing gravity wave, but the amplitude of the oscillation is very small, even if the energy carried by them is quite large. This weakness of the interaction of gravitational waves makes them hard to detect. Since they produce tiny jiggles between masses that are floating freely in space, isolated from all forces other than gravity, one powerful technique to detect gravitational waves is to measure the distances between the masses using laser interferometry. An early generation of such systems has been deployed on the ground and one of the most impressive examples is LIGO (Laser Interferometer Gravitational-Wave Observatory), which is sited in Livingstone Louisiana and its twin in Harford, Washington.

The LIGO detector senses the changes in space by comparing the lengths of two perpendicular arms using a Michelson interferometer in order to detect a gravitationally induced sensitive strain of $\sim 10^{-20} / \sqrt{\text{Hz}}$ over a detection band of

40 Hz to 50 Hz and of ~$10^{-21}/\sqrt{\text{Hz}}$ in a 200 Hz to 100 Hz band (fig. 1.1-1). This strain corresponds to a displacement, over a 4 km baseline, of only 10^{-18} $\text{m}/\sqrt{\text{Hz}}$.

On the ground it is possible to detect only high-frequency gravitational waves, which means waves with oscillation periods shorter than about one second. These are produced in astronomical events that last only one second or less, and such events are rare. They include supernova explosions, collisions of Black Holes that were formed from stars in earlier supernova explosions. At lower frequencies, or longer periods, there should be many other interesting gravitational waves. But the Earth environment is too noisy to allow gravitational waves detectors to operate at lower frequencies. Therefore, after extensive studies, ESA and NASA decided to develop a space-based detector, LISA, able to detect gravitational waves from massive Black Holes and galactic binaries in a low-frequency band.

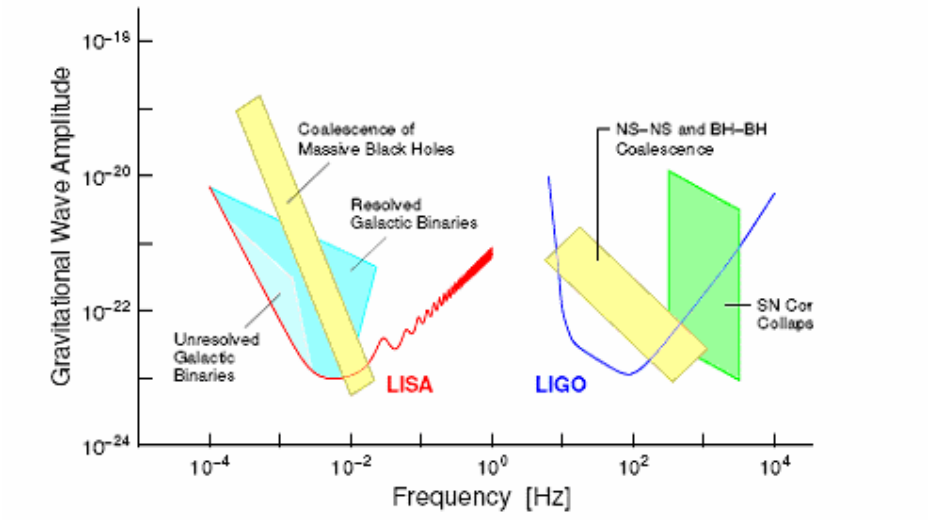

Fig. 1.1-1 *Spectrum of predicted gravitational wave amplitudes as function of frequency for a range of astrophysical sources*

1.1 The LISA Mission

The LISA mission goal is the detection of low frequency (measurement bandwidth: 0.1 mHz - 100 mHz) gravitational radiation with a strain sensitivity of $4 \cdot 10^{-21}/\sqrt{\text{Hz}}$ at 1 mHz.

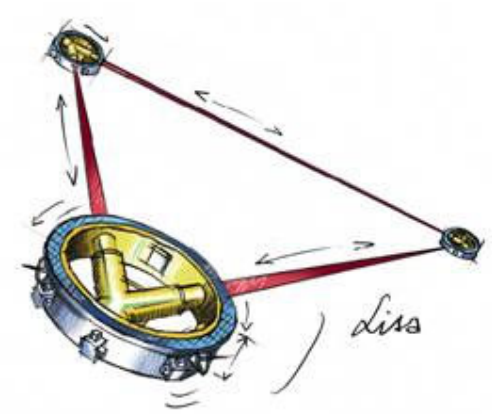

Fig. 1.2-1 *Artist's concept*

It comprises three identical spacecraft located $5 \cdot 10^6$ km apart forming an equilateral triangle, in an Earth-trailing orbit at some 20 degrees behind the Earth (fig. 1.2-2).

Each of the three identical spacecraft carries a V-shaped payload which is the measurement system of two test masses, associated laser interferometer measurement systems and electronics. Provided that the proof masses are maintained in a disturbance-free environment, low-frequency gravity waves will cause small motions in the test masses relative to one another.

The precision interferometry system will be able to measure the gravity waves as path length changes up to 50 pm.

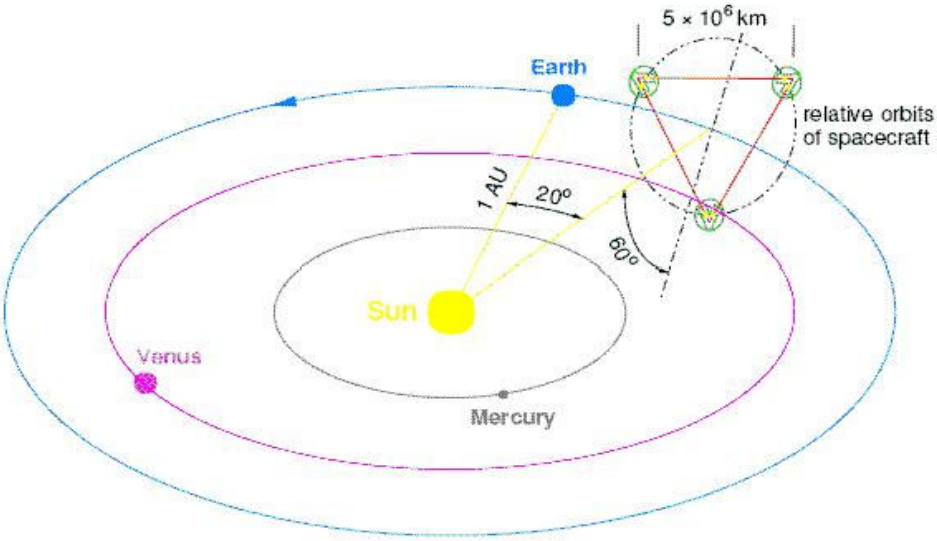

Fig. 1.2-2 *Orbital configuration of the LISA mission concept*

In order to meet the sensitivity goal, two key technologies are required for LISA:

- LISA must detect path length changes of a few pm within the measurement bandwidth
- A disturbance reduction mechanism must shield the proof mass from the outside environment in such a way that only gravity waves will cause measurable displacements.

Critical elements of these technologies can only be proven in orbit:

- inertial sensor to measure disturbances on free-flying test masses
- precise low noise actuators (micro thrusters and electrostatic positioning system)
- Drag-Free Attitude Control System (disturbance control system)

1.3 The LISA Pathfinder Mission

LISA's launch will be preceded several years by LISA Pathfinder, a technology-demonstration mission. It will prove the LISA measurement principle and key technologies that cannot be tested on the ground, thus eliminating any risk from the future science program.
The core of the LISA Pathfinder spacecraft is the LISA Technology Package (LTP): The basic idea behind the LTP is that of squeezing one LISA arm from $5 \cdot 10^6$ km to few centimeters and in placing it on board a single spacecraft (S/C) (fig. 1.3-1).
Thus the key elements are two nominally free flying proof masses and a laser interferometer whose purpose is to read the distance between them (fig. 1.3-2).
The LTP package basically consists of two Inertial Sensors and a laser interferometer. Each Inertial Sensor contains one test mass (TM), which will ideally follow a purely gravitational trajectory.

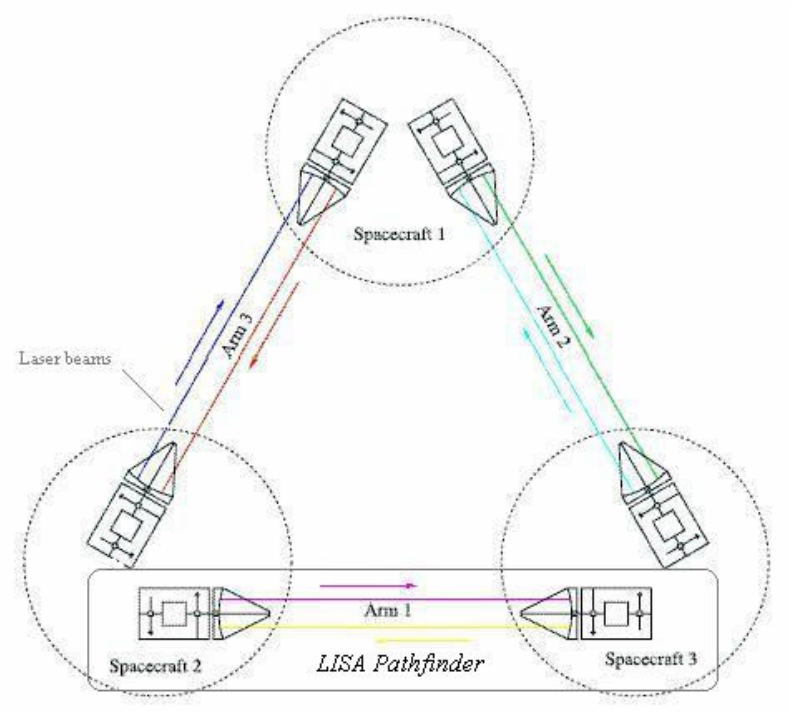

Fig. 1.3-1 *LISA and LISA Pathfinder configurations*

The positions of the proof masses with respect to the spacecraft will be measured optically (laser interferometry) and electrostatically (capacitive sensing) using electrodes embedded in the Inertial Sensor housing.

A Drag-Free Control System will cause the satellite to follow the trajectories of the test masses by means of Field Emission Electric Propulsion μN-thrusters. The LTP laser interferometer will provide a measurement of the relative displacement of the TMs, allowing a direct assessment of the differential acceleration of the masses (fig. 1.3-2).

The major mission objectives consist of:

- testing a Drag-Free and Attitude Control System in a single spacecraft with two test masses
- testing the feasibility of the Optical Metrology System (laser interferometry) at the level accuracy envisaged for LISA
- testing endurance of the different instruments and hardware in the space environment

1.3.1 The Science Requirement

The primary goal of the LISA Pathfinder mission is to verify that a test mass can be put in pure gravitational free-fall by limiting the spectral density of accelerations at the test mass to:

$$S_a^{1/2}(f) \leq 3 \cdot 10^{-14} \left[1 + \left(\frac{f}{3\text{mHz}} \right)^2 \right] \frac{m}{s^2} \frac{1}{\sqrt{\text{Hz}}}$$

in the measurement bandwidth of:

$$1 \text{ mHz} < f < 30 \text{ mHz}$$

This is below one order of magnitude of the requirement for LISA in frequency and amplitude of the noise level.

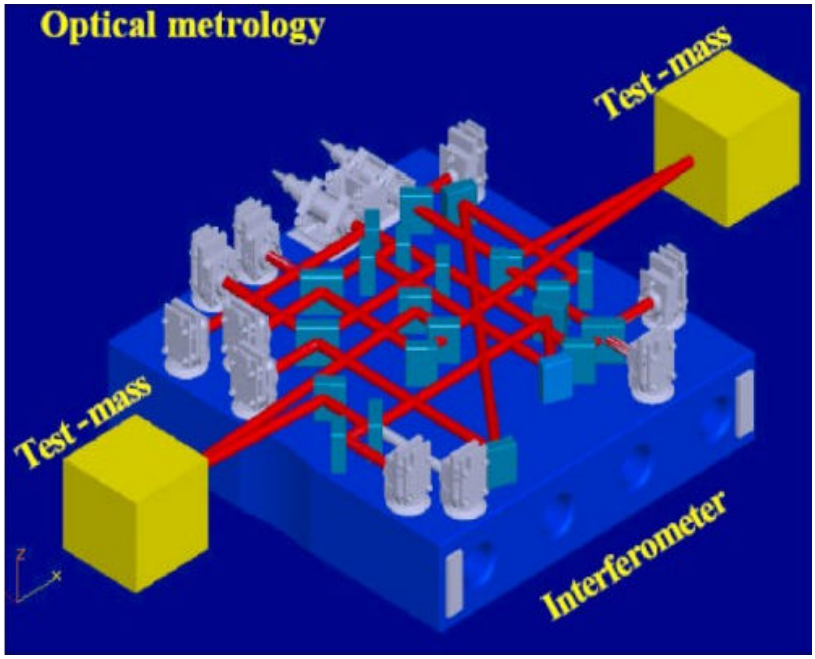

Fig. 1.3-2 *Test masses and laser interferometer*

The sources contributing to the acceleration environment of the proof mass arise from both direct effects on it and the effects on the spacecraft that are

coupled to the test mass through the electrostatic suspension system. These are:

- External forces on the spacecraft, among them:
  - ⇒ Thruster force and thruster noise
  - ⇒ Difference in gravitational acceleration between test mass and spacecraft centre of mass
  - ⇒ Solar radiation pressure
  - ⇒ Interaction with atmosphere, planetary magnetic fields

- Internal forces acting on the proof mass and the spacecraft, including
  - ⇒ Thermal noise
  - ⇒ Pressure fluctuations
  - ⇒ Electrostatic actuation
  - ⇒ Spacecraft self gravity

- Forces that arise from sensor noise feeding into thruster commands

1.3.2 Optical Metrology System Requirement

A laser interferometer for precise measurement of the variation in the distance between the test masses is needed: LISA is expected to detect path length changes of a few picometers within the measurement bandwidth.
The interferometer sensing will have to be able to monitor the test mass position along the sensitive axis (nominal line of connection between the two test masses) with a displacement noise level of:

$$S_n^{1/2} \leq 10 \frac{\text{pm}}{\sqrt{\text{Hz}}}$$

in the frequency range:

$$3 \text{ mHz} < f < 30 \text{ mHz}$$

relaxing as $1/f^2$ towards 1 mHz. This requirement is one order of magnitude bigger, both in noise level and frequency, than the one defined for LISA.

1.4 Contributions of the Thesis

In general, the objective of a Real-Time Test-Bed is to validate the functional performance of the sensors, actuators and control systems allowing open-loop and closed-loop simulation in real time, using real hardware or hardware simulators.

The philosophy of the DFACS team is to have as much hardware in the loop as possible to reduce the risk of unexpected failures and to have an End-to-End (E2E) Simulation that is as close to reality as possible. This is in line with the "lessons learned" by the Gravity Probe B Mission, an already flying Drag-Free mission, operated by Stanford University.

The work done in the scope of the thesis represents a first step toward the build-up of a LISA Pathfinder Real-Time Test-Bed (LTP-RTB) that also includes optical metrology hardware in loop and will aim at the functional testing of the Drag-Free Algorithm Control System (DFACS) in closed-loop.

Therefore, a preliminary Real-Time Test-Bed was built-up. It consists of a Real-Time Computer and a laser interferometer representing the in-loop hardware part of the Test-Bed. The built-up interferometer measures the TMs x_2-x_1 differential displacement in consequence of two tip/tilt mirrors motion. TMs angles are represented by the aforementioned mirrors which are controlled by electronics devices connected to the Real-Time Computer. The RTC, in which the E2E-Simulator was implemented, computes the TMs Equations of Motion (EoM) sending analog signals to the mirrors electronics.

In order to develop and to put the test-bed into operation, the following steps were carried out:

- Implementation of the E2E Performance Simulator (version 3.4) on the dSPACE ® Real-Time Computer.

- Build-up of the so called HP (Hewlett Packard) interferometer, replacing the x_2-x_1 differential test mass displacement readout of the E2E-Simulator interferometer model.
- Connection of the tip/tilt mirrors electronics to Real-Time Computer.
- Connection of the HP interferometer and laser electronics to the LabVIEW® Computer, in order to make the x_2-x_1 measurement available.
- Testing of the RTB proper functioning and performances
- Calibration of the RTB in order to reach consistency between the E2E-Simulator and RTB laser readouts.

1.5 Outline of the Thesis

The first part describes the LISA Pathfinder mission and presents a general overview of the main topics of the thesis.

In Chapter 2, the E2E Performance Simulator implementation on the Real-Time Computer is described, explaining which software-hardware package has been used and how it works. Moreover, an interactive telecommand interface is presented.

The third part gives an overview of the laboratory instrumentation. Chapter 3 explains the HP interferometer design and underlines its principle of operation from both an optical and electronic point of view. The major differences and points in common with respect to the LTP interferometer are presented. This chapter explains the practical interferometer design procedure and describes how some instability problems, revealed during the build-up, have been solved.

In Chapter 4, all the electronic devices involved in the RTB build-up are presented and their specifications and principles of operation are given. Moreover the way in which the various devices are interconnected and a schematic overview of the complete build-up is given.

Chapter 5 shows the final configuration of the HP interferometer and summarizes the achieved RTB performance in non-vacuum environment.

The calibration of the RTB is obtained, finally, in chapter 6.

The entire calibration procedure is then explained and the tests results are analyzed.

The last chapter proposes a summary and suggests guidelines for further work.

Part II

The E2E-Simulator and the Real-Time Environment

Chapter 2

End-to-End Performance Simulator Implementation on Real-Time Computer

The E2E-Simulator implementation procedure required using the Real-Time Workshop® (RTW) software and *real-time* package (software and hardware) called dSPACE®. The dSPACE® package, with respect to other real-time systems, allows to create a C-code, representative of the entire E2E-Simulator, directly on the Real-Time platform (called dSPACE® RTC) in order to make the simulator available to run in real-time. The C-code script is created by means of a procedure that requires the use of the Real-Time Workshop® . The advantage of such a system is the easy connection between the dSPACE® RTC boards with the hardware in-loop parts.

In this chapter, an overview of the E2E-Simulator and the software-hardware package used during the work is given. Then, the entire procedure of the simulator implementation on the Real-Time Computer is described.

Moreover, in order to make the RTB experiments interactive, a particular telecommand interface has been created. In fact, by means of it, the user can change the experiment settings and simulation parameters interactively.

2.1 End-to-End Performance Simulator

End-to-End modeling and simulations aim at verifying the on-orbit performance of a strongly coupled satellite and payload (LTP) system. Consequently, detailed and accurate models of the satellite subsystems have been developed. Modeling work goes far beyond what is typically done for conventional satellite system simulators.

The levels of interaction between different disciplines and subsystems for LISA Pathfinder are much more complex than in traditional space missions, demanding a highly integrated modeling approach. The non-linear system simulator was implemented in the MATLAB/Simulink® environment. All the subsystems are integrated into this environment (fig. 2.1-1) and all models are written in C/C++ in order to speed up the simulation run-time. The following features are included in the E2E Performance Simulator:

- 18 DOF non-linear dynamics of the spacecraft and two test-masses
- Environmental models for Earth, Sun and Moon gravity and gravity gradient
- Solar radiation pressure model accounting for solar irradiance fluctuations
- Detailed μ-propulsion model
- Drag-free, attitude and suspension control system software
- Various internal and external noise sources, as well as coupling effects between spacecraft and test-masses
- Inertial Sensors and Optical metrology models

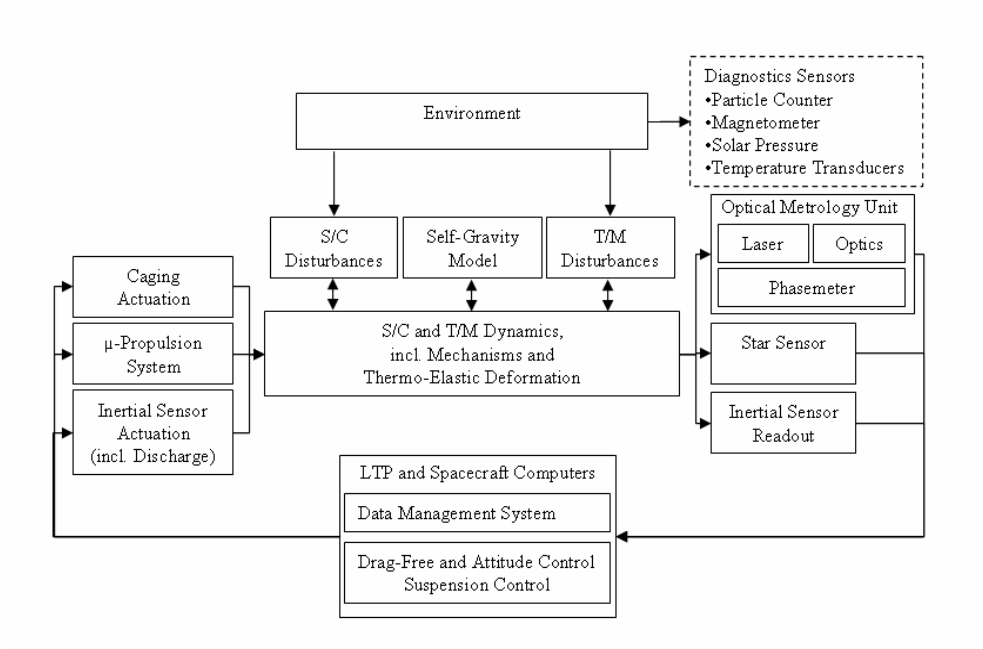

Fig. 2.1-1 *E2E-Simulator top-level architecture*

In order to achieve reasonable simulation times the sampling frequency is equal to 10 Hz.

In this thesis, the simulator (version 3.4) has been implemented on the Real-Time Computer. The required steps for the transfer on the used dSPACE® RTC is described in section 2.3.

2.2 Real-Time Workshop® Software and dSPACE® System

Real-Time Workshop® (RTW) generates optimized, portable code from Simulink® models.

Using integrated *makefile* (1) based targeting support; RTW builds programs that can run on a wide variety of real-time targets.

Through an extensible *makeprocess* and download procedure, RTW creates an executable for the E2E Performance Simulator and places it on the target system, i.e. the dSPACE® Real-Time Computer.

Once the simulator runs in that computer, the processor board (DS 1005 PPC) performs calculations in real-time.

The dSPACE® environment provides a user interface, *ControlDesk*, to monitor, manage and control the experiments tuning parameters online, as explained in [6].

The simulator implementation and running processes require a two PC solution: a host PC to run MATLAB/Simulink® and a target PC, i.e. the RTC, to run the generated code, executing the model in a real-time environment (fig. 2.2-1). Communication between the two boxes is supported via a high-speed fiber optic cable.

The DS1005 PPC board is the core of dSPACE®'s modular hardware (Read [4] and [5]). It provides the computing power for the real-time system featuring a PowerPC (PPC) processor that runs at 480 MHz. This board could be connected to standard serial devices via the UART RS232 connector, and to the others I/O boards (e.g. A/D - D/A converters), via a PHS-bus connector.

(1) Makefile: collection of commands that allow groups of programs, object files, libraries to interact

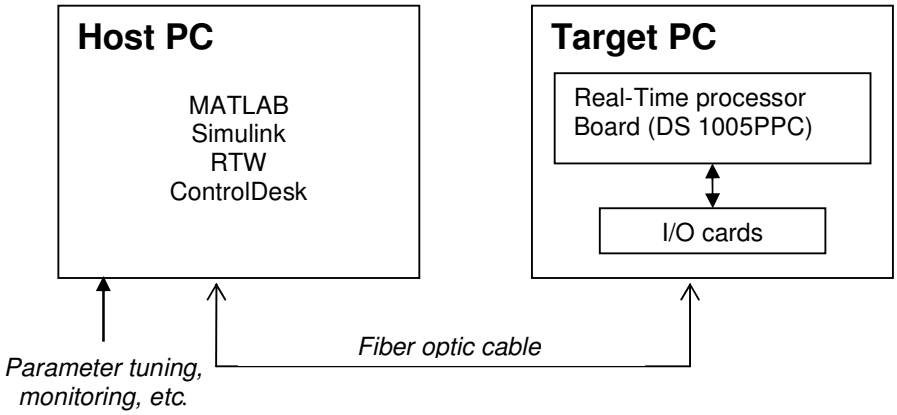

***Fig. 2.2-1** PCs configuration*

The I/O boards installed in the Real-Time Computer, which was utilized in this work, are:

- DS2002 Multi-channel A/D board
- DS2101 D/A board
- DS4201 Prototyping board
- DS4003 Digital I/O board
- DS814 link board (used for the connection with the host PC)

The dSPACE® user can program the DS1005 PPC board from Simulink via Real-Time Interface (fig. 2.2-2). It contains Simulink blocks representing the entire range of I/O boards, as explained in [7].

The user could add these blocks to the simulation model and make settings (e.g. the voltage range for each D/A converter channel) for the specific board to use. This allows a simple and efficient connection of hardware (sensors and actuators) to the existent model of the E2E-Simulator, as required by hardware in-loop simulation.

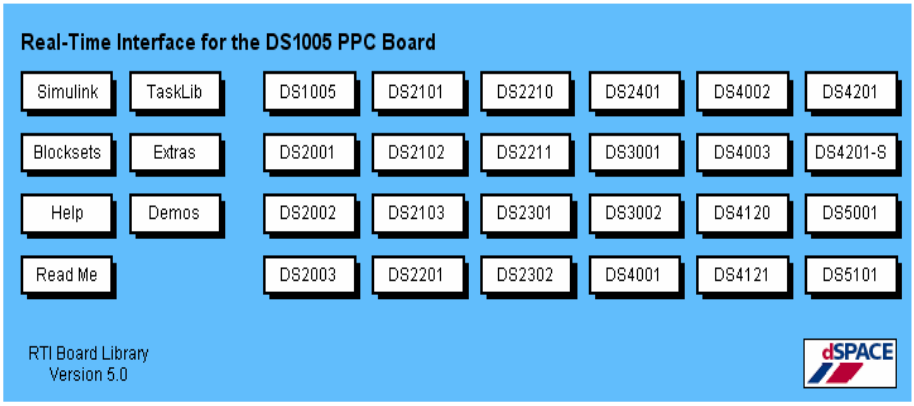

Fig. 2.2-2 *Real-Time Interface (RTI) board library*

2.3 The Implementation Procedure

In order to be able to run the E2E-Simulator on the dSPACE® RTC, it is necessary to generate a simulator C-code format which can be compiled and downloaded in the dSPACE® hardware. This is the so-called implementation procedure and can be accomplished by means of RTW [9].

2.3.1 The General Implementation Procedure

The Implementation Procedure, or "build" process, consists of the following steps (fig. 2.3-1):

- **Analysis of the model:** RTW reads the Simulink model (*model.mdl*) and compiles an intermediate representation of it (*model.rtw*). During this phase, RTW evaluates simulation and block parameters, propagates signal widths and sample times, determines the execution order of blocks within the model, computes vector sizes. The process is stopped if structures, such as S-Functions parameters, or MATLAB functions are present in the model.
- **Generation of the code:** RTW, through the Target Language Compiler (TLC), transforms the intermediate model description stored in *model.rtw* into target-specific code. The TLC program consists of :

⇒ *System Target File* (it is the main file: *rti1005*[(2)]*.tlc*)

⇒ *Block Target File* (it specifies how to translate each block of the model into target-specific code)

⇒ *Target Language Compiler Function Library* (it contains functions that support the code generation process)

- **Generation of a makefile:** the generated makefile (*model.mk*) instructs the "make" utility to compile and link source code from the model. RTW creates such a file from a *System Template Makefile* (*rti1005.tmf*) designed for the target environment.

- **Creation of an executable program:** the build process invokes the "make" utility which runs the compiler to create the executable and downloads it to the dSPACE hardware.

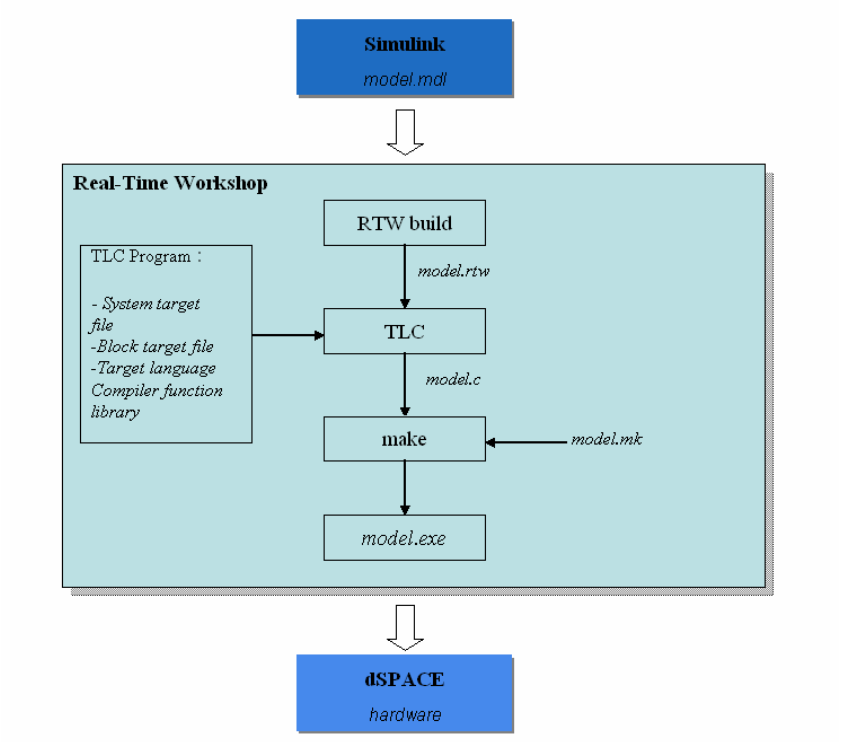

Fig. 2.3-1 *General Implementation procedure diagram*

(2) Rti1005: real-time platform in use

The dSPACE Real-Time Interface (RTI) supports RTW during the "build process", generating *variable description file* (*model.trc*) and *user makefile* (*model_usr.mk*). The former contains the necessary information about the model signals and parameters allowing to modify them by mean of ControlDesk, the latter, if compiled by the user, needs to define extra paths, directories, libraries and also S-functions source code files.

2.3.2 Specifics of E2E-Simulator Implementation Procedure

In order to implement the E2E-Simulator, the RTW limitations have been taken into account. The software does not support MATLAB functions and structures such as S-function parameters. If they are present in the model, the "build" process fails. Therefore, the following modifications have been applied:

- MATLAB functions in the *Telecommands* and *Simulator Commands* blocks have been deleted.

- Structures have been replaced by double-arrays as parameters for the following S-functions:
  - ⇒ x_to_C_sf / C_to_Vs_sf (*Capacitive Readout model* and *Capacitive Actuation*)
  - ⇒ Vact_to_Fcap_inst_sf (*Capacitive Actuation*)
  - ⇒ GravityField_sf (*SC_Environment*)
  - ⇒ SolarForceTorqueInterpolation_sf (*SC_Disturbances*)

Moreover, the user *makefile* that dSPACE RTI generates during the implementation procedure, had to be compiled because of the several S-functions the E2E-Simulator contains (See Appendix A).
Despite these changes, the system, during the "build" process showed some problems. It was discovered that without *GravityField* and *SolarForceTorqueInterpolation* S-functions the implementation procedure

worked properly. For this reason, these S-functions have been replaced by more simple and elementary models (See Appendix A).

2.4 Telecommand Interface

The E2E Performance Simulator's initialization file (*sim_init.m*) contains a list of telecommand files. Before starting a simulation, the user must define which of those files is to be used. They contain information about the commands, the parameter value(s) and the time at which the command has to be applied. The possible commands are:

- set DFACS mode (the baseline modes are an operational concept and define which coordinates are controlled and how, which kind of test masses position measurement is available).
- activate the slew maneuvers
- activate the identification procedure
- define a manual command for each of 15 satellite control coordinates
- define the slew command setting
- define the manual set-points option
- define active set of polynomial coefficients
- define significance of each force/torque command for μ-propulsion system
- define availability of each thruster in the μ-propulsion system
- define the μ-propulsion system (FEEP-Colloidal)

2.4.1 Telecommand Implementation on the dSPACE System

An interactive telecommand interface (TC I/F) was created on dSPACE ControlDesk (Appendix B), once the E2E-Simulator was implemented on the Real-Time Computer. This interface allows the user to activate the

telecommands manually online or from the *telecommands* file loaded with the simulator initialization file.

In the *manual* configuration, it is possible to change the parameter values of the commands, transferring them, directly, to the real-time platform during the simulation.

In the *from file* configuration, the commands are uploaded and visualized on the TC I/F when the simulator is implemented on the Real-Time Computer. During a simulation, the user can switch from *manual* to *from file* configuration and vice versa, setting the proper parameters simply by pushing buttons on the TC I/F.

The impossibility of using MATLAB functions in the Simulink model, because of the Real-Time Workshop limitations, led to the problem of how to load some variables on the MATLAB workspace (for the *telecommands* block).

In fact, the DFACS custom mode 1 and 2, when activated, require different sensor mapping, controller, decoupling, capacitive actuation and slew values with respect to the other DFACS modes. Therefore, when, at a certain simulation time, the corresponding matrices and vectors need to be downloaded on the workspace because of the activation of those modes, by means of *telecommands* files, the MATLAB function in the simulator *telecommands* block executes the file which contains them, thus permitting the downloading. Of course, this task is not available without the MATLAB function, therefore a workaround has been found (See Appendix B).

Suppose that the *telecommands* file in use is the one that activates DFACS custom mode 1 and custom mode 2 (TC_*ACCtoCAL.txt* for example). The workaround is the following:

1) Download the matrices and vectors, that are needed for the custom mode 1 and 2, on the workspace by means of the initialization files (See Appendix B: *sim_init.m* and *workaround.m*)
2) Insert multi-port switches for each of the classes of matrices and vectors which are needed (decoupling, mapping, controller configuration, actuation, slew). Each multi-port switch will have as many inputs as the

number of submodes introduced, plus the first input that is the one responsible for the switch.

3) Create a *simulator command* file (*SC_Workaround.m*) in which two new commands are introduced (*SetCST1* and *SetCST2*). They can assume different values according to the number of the *multi-port switch* inputs. *SetCST1* and *SetCST2* are the first *multi-port switch* input and their values decide the output.

This solution permits, at the TC I/F, simply by pushing the values for *SetCST1* and *SetCST2* to change the rows and columns values of the matrices and vectors, for the custom modes, together and to transfer them immediately to real-time platform, avoiding their changes value by value.

Part III

Laboratory Instrumentation

Chapter 3

Laser Interferometry

The hardware part of the used-sensor in the Real-Time Test-Bed is represented by a HP interferometer (the principle of operation and the electronic devices were developed by the Hewlett Packard Co.).
As the LISA Pathfinder interferometer, it is able to measure the differential displacement between the two test masses, represented by two piezo-actuated mirrors.
The HP interferometer replaces x_2-x_1 E2E-Simulator interferometer model. This is the first step towards a hardware in-loop simulator that will also include the important optical metrology which is a crucial technology of the mission.

3.1 LISA Technology Package Optical Metrology System

The LTP Optical Metrology System (OMS) includes the Optical Bench (OB), the Laser Source Unit, the Phasemeter Front-End (PFE) and the Data Management Unit (DMU).
The LTP non-polarizing heterodyne Mach-Zender interferometer (12 beam-splitters, 10 mirrors) is laid on a Zerodur solid plate, placed on the Optical Bench, between the two test masses that behave as mirrors reflecting the measurement beams.
Optical elements compose four separate interferometers (fig. 3.1-1):

1) x_2-x_1 interferometer: provides the main measurement, i.e. the distance between the two proof masses and their differential alignment

2) x_1 interferometer: reads the position and alignment of TM1 w.r.t. the OB
3) *reference* interferometer: provides the reference phase signal from which x_2-x_1 and x_1 are derived
4) *frequency* interferometer: measures laser frequency fluctuations for stabilization purposes

The principle of operation of the Optical Metrology System is illustrated in figure 3.1-2. A stabilized laser signal (λ = 1064 μm) is generated by the Laser Source Unit, that is, Laser Head, two acousto-optical modulator (AOM) plus an Amplitude Control Unit (ACU).

The laser beam that comes out of the Laser Head is split into two parts that are separately frequency-shifted by one AOM for each beam; the two AOM's driving frequency differ by a constant amount, the so called heterodyne frequency which is on the order of magnitude of 1 kHz. The Amplitude control Unit reads a measured power fluctuation signal and feeds a correction to the AOM driver.

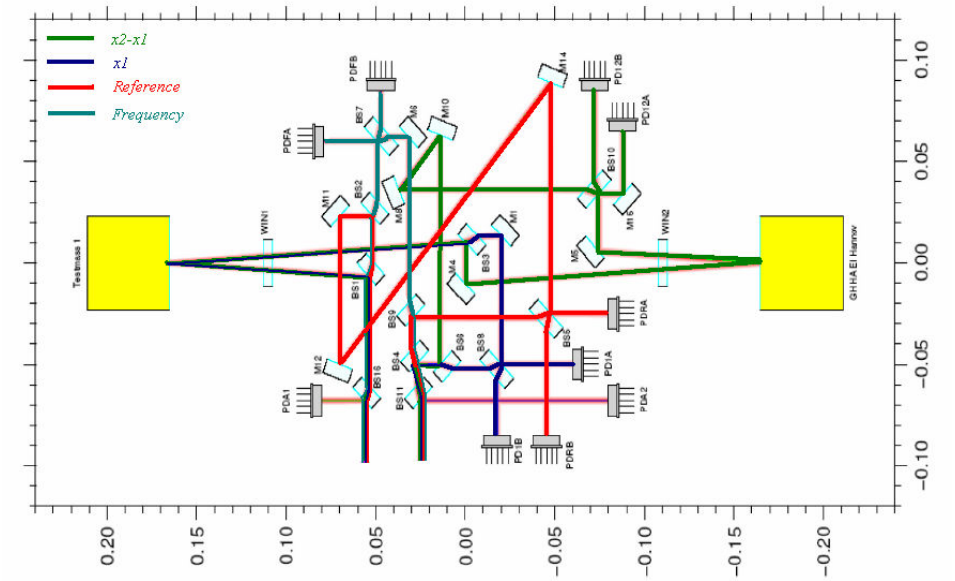

Fig 3.1-1 *LPF four interferometers*

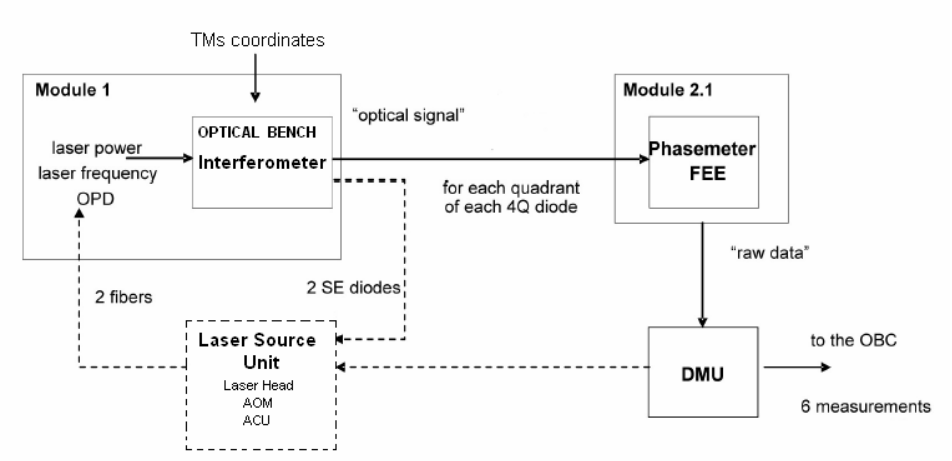

Fig 3.1-2 *OMS principle of operation*

After traveling different paths inside the Optical Bench, the two beams are made to interfere at a beam splitter; the resulting laser signal is detected by a quadrant photodiode that converts it into an "optical signal" (photocurrent signal), that contains a dominant component at the heterodyne frequency.

Any differential pathlength variations cause a phase variation of the heterodyne frequency, and this phase modulation of the heterodyne signal is measured electronically (by the Phasemeter) with respect to the phase reference derived from the *reference* interferometer that is not subjected to pathlength variations. The Phasemeter Front-End processes the optical signal and the resulting "raw data" are transmitted to DMU. It provides the final measurements of TMs' positions and attitudes and correction signals, derived from the *frequency* interferometer and given to the Laser Source Unit for stabilization purposes.

The LTP Optical Metrology System is able to:

- measure difference of displacement between the test masses along the sensitive axis (nominal line of connection between the TMs)
- measure motion of TM1 relative to the spacecraft
- measure angular motion of TM1 and TM2 around the y-axis and z-axis relative to the spacecraft

Therefore, the degrees of freedom which the OMS interferometers measure are: x_1-x_2, x_1, η_1, φ_1, η_2, φ_2 (fig. 3.1-3).

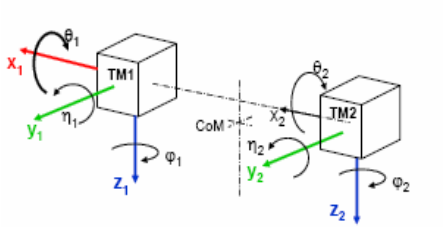

Fig. 3.1-3 *Test Masses degrees of freedom*

3.2 Differences between the LTP and HP Interferometer

The HP interferometer aims at replacing and reproducing, in reality, the functionality of the x_2-x_1 E2E-Simulator interferometer model. It measures the differential displacement (x_2-x_1) between two mirrors which are able to realize the test mass angular motion around the z-axis and y-axis (fig. 3.1-3). The HP interferometer consists of a Laser Head, 9 mirrors, 2 polarizing beam-splitters and the 2 tip-tilt mirrors that represent the test masses (fig. 3.2-1).

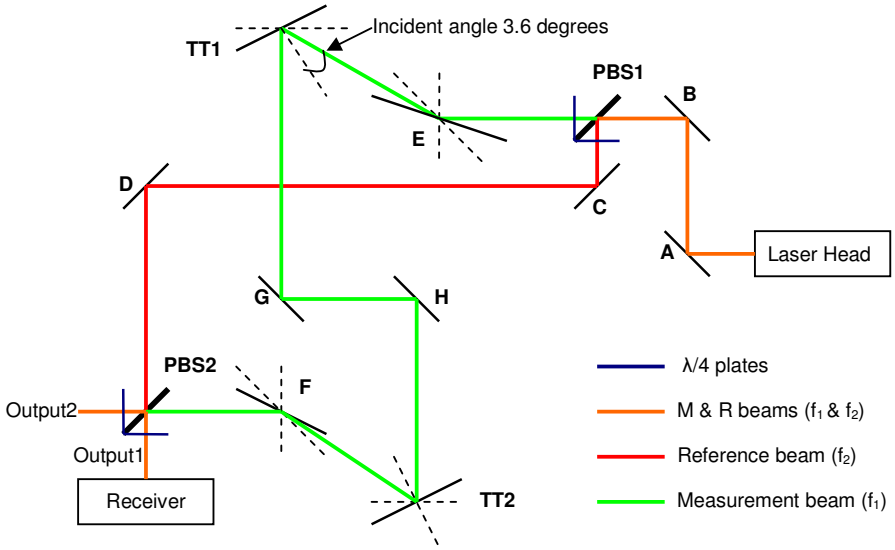

Fig. 3.2-1 *HP interferometer*

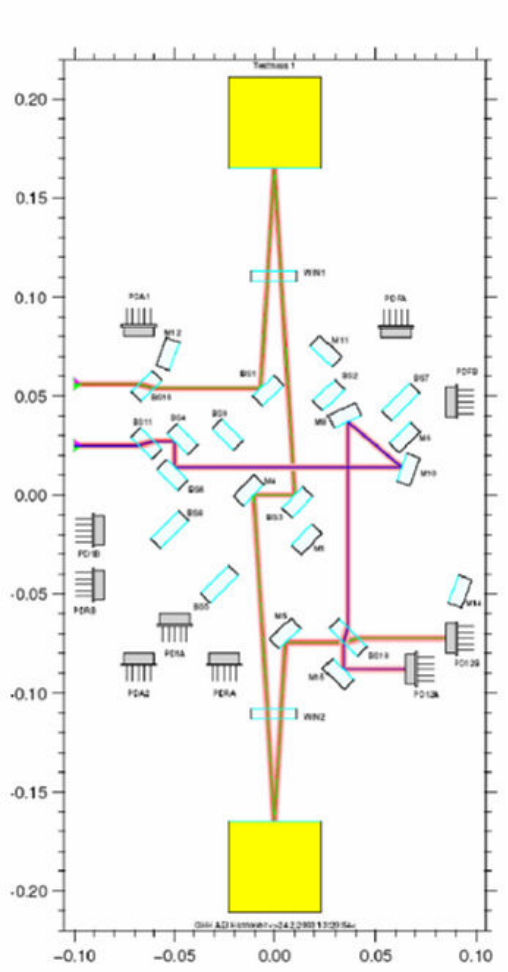

Fig 3.2-2 *LPF x_2-x_1 interferometer*

The x_2-x_1 LTP interferometer aims at verifying the performance of the gravitational sensors by monitoring the distance between the proof masses. The x_2-x_1 HP interferometer only aims at functional testing of the DFACS and no science performance will be reached.

As can be noted, the different targets between the LTP and HP interferometers define the differences between them. This is the reason for which the LTP x_2-x_1 and HP interferometer designs and characteristics are different (fig. 3.2-1, fig. 3.2-2). In fact, for the HP interferometer, it was not necessary to use the same exact number of optic elements, the same laser beam wavelength and measurement electronics of the LTP one, because its goal was simply to realize the same measurement of the E2E-Simulator interferometer model, not to reach the same level of LTP interferometer performance.

The major differences and the points in common between the two interferometers are summarized in the table 3.1 (the reader will find a more detailed description of the HP IFO characteristics in the paragraph 3.3):

	LTP x_2-x_1 Interferometer	**HP x_2-x_1 Interferometer**
Kind of interferometer	Heterodyne	Heterodyne
Measurement	x_2-x_1 differential displacement between TMs	x_2-x_1 differential displacement between TMs
Number of optic elements	9 mirrors 3 beam splitters	9 mirrors 2 beam splitters
Kind of optic elements	Non-polarizing	Polarizing
Test Masses distance	376 mm	385 mm
Incident Angle (Fig. 3.2-1)	3.6 degrees	3.6 degrees
Laser Head	TESAT Nd:YAG laser	HP5517B He-Ne laser
Laser Beam Wavelength	1024 nm	632 nm
Heterodyne Frequency	1 kHz	2 MHz
Kind of photodiode	Quadrant	Single Element
Frequency Modulation	AOM	Automatic in the Laser Head
Measurement Electronics	Phasemeter FEE DMU	HP receiver HP Laser Axis Board
Environment	Vacuum	Air

Table 3.1 *LTP and HP interferometers: differences and points in common*

3.3 Detailed Description of the HP Interferometer

The used HP interferometer thus named because the optical elements and the electronic devices of which it is composed were developed by the Hewlett Packard Co. The electronic and optical principles of operation will be described in the following paragraphs.

3.3.1 Electronic Principle of Operation

The HP interferometer operation is based on the HP 5517B Laser Head (fig. 3.3.1-1).

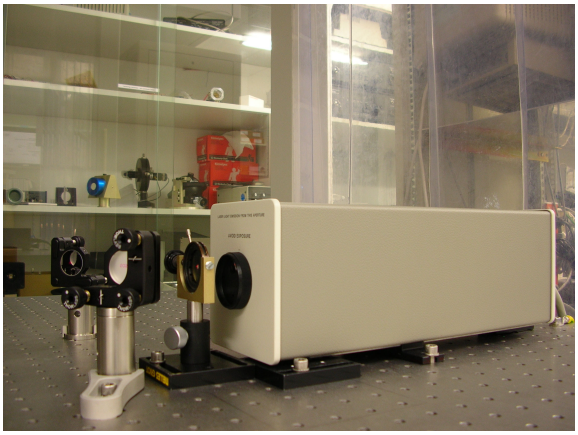

Fig. 3.3.1-1 *Laser Head HP5517B*

This Laser Head is a frequency stabilized Helium-Neon (He-Ne) laser source and the produced light wavelength is 632 nm. It generates a coherent (all light waves in phase), collimated (all waves traveling parallel to each other) light beam consisting of two orthogonally polarized frequency components (f_1 and f_2, in fig.3.2-1). The difference between these two frequencies defines the Heterodyne Frequency (f_{het}) which is on the order of magnitude of 2 MHz [19].

The main portion of the emitted laser beam comes out of the laser head and goes to the interferometer and to an external receiver where a measurement signal is generated. The other portion is directed to the sampler assembly,

inside the source. Most of these samples feed into the reference receiver and the remainder is used to control the laser tuning (fig. 3.3.1-2).

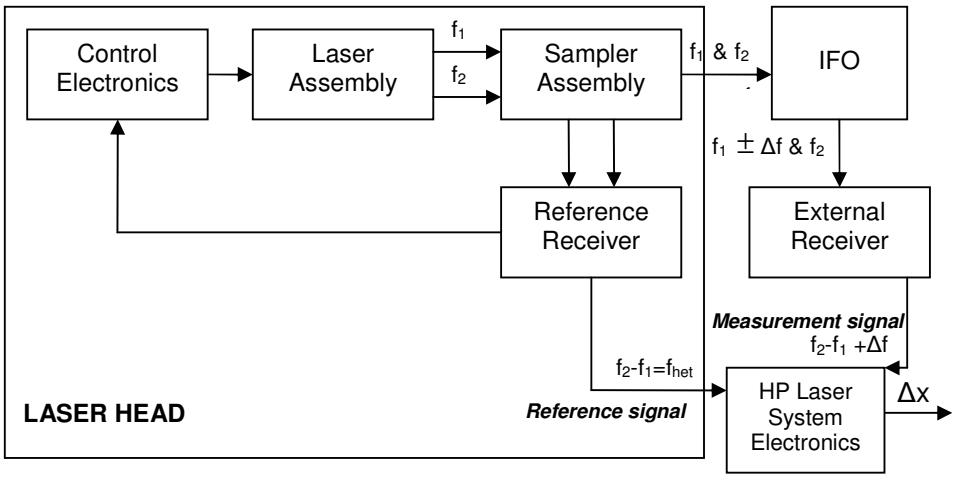

Fig. 3.3.1-2 *HP IFO electronic principle of operation*

The reference receiver generates the reference frequency signal (f_{het}) mixing the two laser frequencies (f_1, f_2).

The HP laser system electronics receives the measurement and the reference signals and compares them, generating the displacement measurement signal (Δx). The Laser Assembly produces the laser beam of the two slightly different frequency components (f_1 & f_2) by exploiting the Zeeman Effect (See Appendix C).

3.3.2 Optic Principle of Operation

The laser beam emitted by the HP Laser Head has two frequency components with linear and orthogonal polarizations (fig. 3.3.2-1).

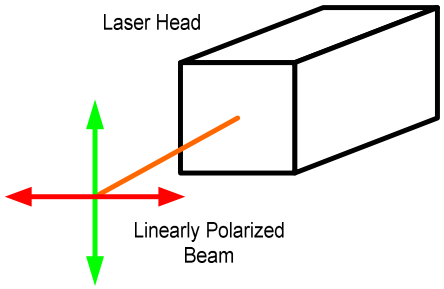

Fig. 3.3.2-1 *Polarizations at the Laser Head*

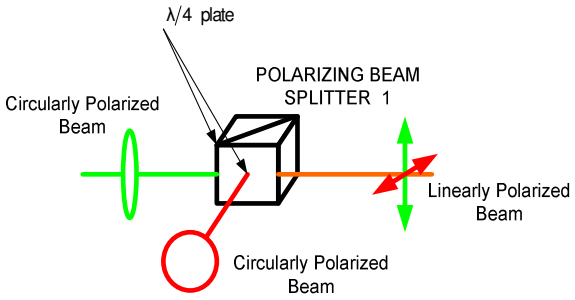

Fig. 3.3.2-2a *Polarizations at the Polarizing Beam Splitter 1*

The polarizing beam-splitter (PBS1 in figure 3.2-1) splits the beam and polarizations. The λ/4 plates mounted on the beam splitter (fig. 3.3.2-2a) switch the polarization from linear to circular. After that, the *reference* (red line in fig. 3.2-1) and *measurement* (green line in fig. 3.2-1) *beams* travel among the mirrors. The measurement beam undergoes a difference in frequency and in the optical path length because of the tip/tilt (TT1/2 in figure 3.2-1)) mirror movement.

At the last polarizing beam-splitter (PBS2 in figure 3.2-1), the two beams interfere; the λ/4 plate, this time, converts the polarizations from circular to linear, orthogonal to each other (fig. 3.2.2-2b).

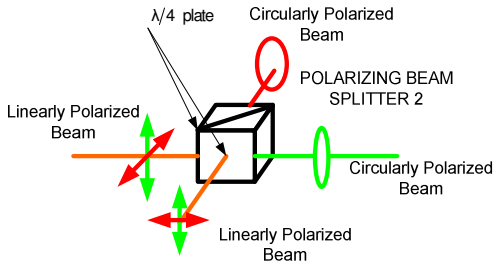

Fig. 3.3.2-2b *Polarizations at the Polarizing Beam Splitter 2*

The resulting optical signal is detected by an HP receiver (fig. 3.2-1). It contains a lens, a polarizer and a photodetector to capture the light and to transform it into electrical signal readable by the Laser Axis Board (see chapter 4) that provides the proper measurement of the displacement due to the mirror movement (Δx in figure 3.2.2-5). To make that measurement

possible, the beam polarizations must coincide (parallel polarizations). The polarizer, oriented to 45° with respect to the incoming beam polarizations, is collocated inside the receiver in order to achieve this aim.

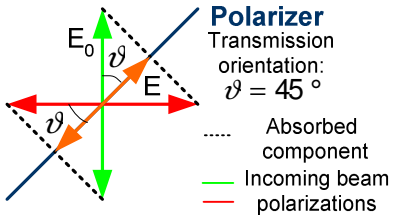

Fig. 3.3.2-3 *Polarizer principle of operation*

In fact, the polarizer is an optic device that converts an unpolarized or mixed-polarized beam of electromagnetic waves into a beam with a single polarization state. The incoming electric field component (E_0) perpendicular to the polarizer transmission orientation is absorbed thus reducing the field amplitude to:

$$E = E_0 \cdot \cos\vartheta \tag{3.1}$$

The transmitted intensity is given by Malus's Law:

$$I = I_0 \cdot \cos^2\vartheta \qquad \textit{Malus's Law} \tag{3.2}$$

The resulting polarizations (orange arrow in figure 3.3.2-3) coincide with the polarizer transmission orientation and are parallel to each other. As soon as the beams overlap perfectly (fig. 3.3.2-4) at the receiver; the laser electronics, whose principles of operation will be explained in chapter 4, calculate the displacement, Δx.

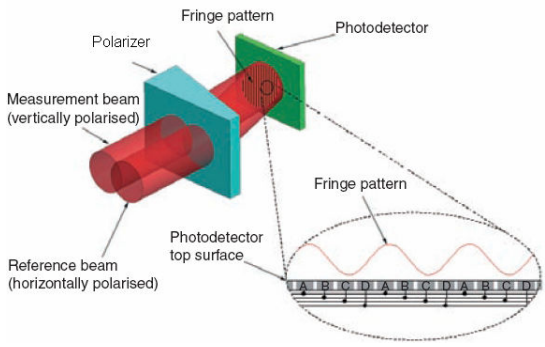

Fig. 3.3.2-4 *Receiver: beams overlap*

The measurement of the differential displacement, between the two moving mirrors, is related to the Optical Path Difference (OPD) between the *reference* path and the *measurement path*. Suppose that a tip/tilt mirror is at rest and the other one moves by the distance of Δx. The Optical Path Difference variation, defined as the length difference between the red beam and the green beam in figure 3.2.2-5,will be:

$$\Delta OPD = \overline{SQ} + \overline{QT} \tag{3.3}$$

The connection between the *OPD* variation and the displacement (Δx) will be:

$$\Delta OPD = 2 \cdot \Delta x \cdot \cos\vartheta \tag{3.4}$$

Where $\vartheta = 3.6°$ is the incident angle. Therefore:

$$\Delta OPD \cong 2 \cdot \Delta x \tag{3.5}$$

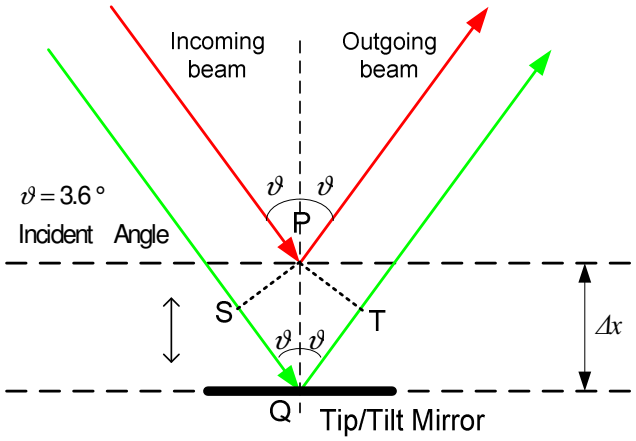

Fig. 3.3.2-5 *Laser Beam at the tip/tilt mirror*

Usually, the resolution of the position measurement that an HP laser system can realize depends on the measurement optics and the electronics that are used. In this HP interferometer, single beam interferometer optic devices were

used [19]. The Polarizing Beam Splitter and the two λ/4 plates visible in figure 3.2-1 together with the Tip/Tilt mirrors contribute to the Single Beam Interferometer working. The name single beam interferometer is due to the fact that the surfaces of the mirrors are hit only twice by the laser light, first by the incoming beam and second by the outgoing beam (fig. 3.3.2-5).

The basic optical resolution is one half wavelength which depends on the *interference fringes*. The interference is obtained by a combination of light coherent waves coming from a unique source, i.e. the Laser Head. In fact, coherent waves, characterized by stationary relations between phases (for any phase changes in one beam originating in source variations are exactly duplicated in the other beam), can superpose and produce visible interference effects because their amplitudes can be combined. When such coherent waves pass through a point, the vibrating medium at this point is subjected to the combined superposed effect of two vibrations and under suitable conditions this leads to stationary waves called *interference fringes*. If the resulting beam intensity at that point is increased with respect to the single beam intensity, the interference is called *constructive,* otherwise *destructive*. Only constructive interference effects, characterized by *bright fringes* (maximum in beam intensity) are able to be detected, on the contrary of the *dark fringes* (minimum in beam intensity), (See [14], [12], [16], [18]).

When the beams that are emitted by the Laser Head are *in phase*, clear fringes will be obtained. Differences in the optical path length due to the Tip/Tilt mirrors movement lead the beam to alternate *in phase* and *out of phase* conditions; in the last case, the interference effects are not detectable (fig. 3.3.2-6).

The phase difference ($\Delta\varphi$) between the two interfering waves is related to the Optical Path Difference variation:

$$\Delta\varphi = \frac{2\pi}{\lambda}\Delta OPD \tag{3.6}$$

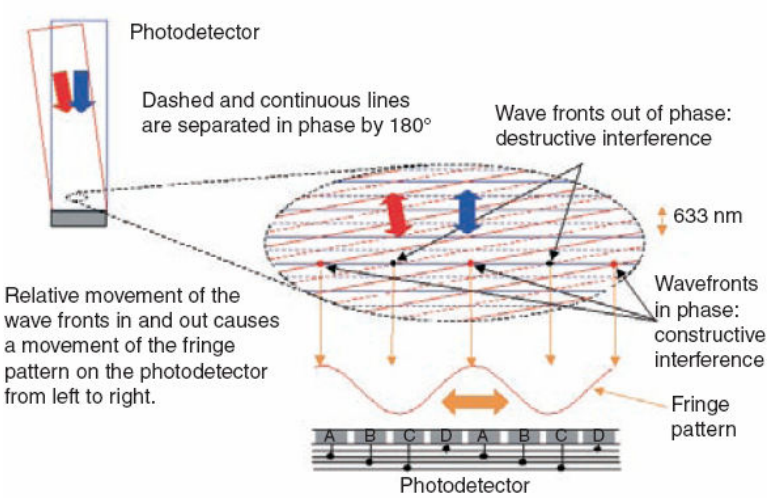

Fig. 3.3.2-6 *Constructive and Destructive interference at the photodetector*

Taking into account equation (3.5):

$$\Delta\varphi = \frac{2\pi}{\lambda/2}\Delta x \qquad (3.7)$$

The phase difference changes by 2π every time the distance Δx increases or decreases by one half of wavelength. If the beams are *in phase,* the phase difference corresponds to an integral number of 2π's or a Δx that is a multiple of one half of wavelength. When the two waves are *out of phase* by π, *destructive interference* will result (See table 3.2). Therefore, an optical resolution of $\lambda/2$ corresponds to the distance between two consecutive detectable bright fringes. As known, in the particular case of the single beam interferometer, the beam has to travel twice the distance Δx to cover it. The factor 2, due to this double path, in equation (3.4), influences the resolution of the optic device. If the HP Plane Mirror interferometer had been used, the factor would have been 4 because of the beam double path; in that case, in fact, the beams would have hit the mirrors four times and the optical resolution would have been equal to $\lambda/4$.

The interference fringes generated by the Tip/Tilt mirrors movement are converted to electrical pulses in the receiver and sent to the measurement electronics (Laser Axis Board) which process them, as required to provide the desired measurement data. The fringes are counted with a counter contained in

the Laser Axis Board. The actual displacement (Δx) is obtained by multiplying the number of counted fringes with the wavelength (λ) divided by a selected interpolation that depends on the electronics used.

	$\Delta\varphi$	Δx
Bright fringes	$2m\pi$	$m \cdot \lambda/2$
Dark fringes	$2(m+1)\pi$	$(m+1/2)\lambda/2$

Table 3.2 *The phase difference and Δx for bright and dark fringes (m an integer)*

The interference fringes generated by the Tip/Tilt mirrors movement are converted to electrical pulses in the receiver and sent to the measurement electronics (Laser Axis Board) which process them, as required to provide the desired measurement data. The fringes are counted with a counter contained in the Laser Axis Board. The actual displacement (Δx) is obtained by multiplying the number of counted fringes with the wavelength (λ) divided by a selected interpolation that depends on the electronics used.

If the optic resolution is equal to $\lambda/2$, using electronic resolution extension, the system resolution increases significantly. The Laser Axis Board HP 10897B, as laser measurement system, introduces an additional 256X resolution extension. Therefore, the overall system resolution is equal to $\lambda/512$.

3.4 Practical Design Knowledge of the Interferometer Built-Up

An interferometer build-up requires considerable precision in fixing the proper mirrors location, in aligning the beams and in handling the sensitive optical instruments involved. An inadequate build-up leads to system instability or to wrong measurement results. These kinds of problems were found in the first version of the interferometer developed in the laboratory. In that case, the two

Voice-Coil mirrors, used as tip/tilt devices, were not fixed in their mounts, leading to instability. In this chapter, the solutions for this problem are presented. Moreover, the entire built-up procedure is described together with the design choices.

3.4. 1 Interferometer Build-Up

Beam Height

The height of the emitted laser beam from the Laser Head is about 80 mm (fig. 3.4.1-1). In laser interferometry, the beam height should be as low as possible and, usually, it is about 75 mm. Therefore, the mirror A (fig. 3.4.1-1) was fixed at 80 mm and tilted, by means of screws behind it, until the beam hit the center of the mirror B at 75 mm.

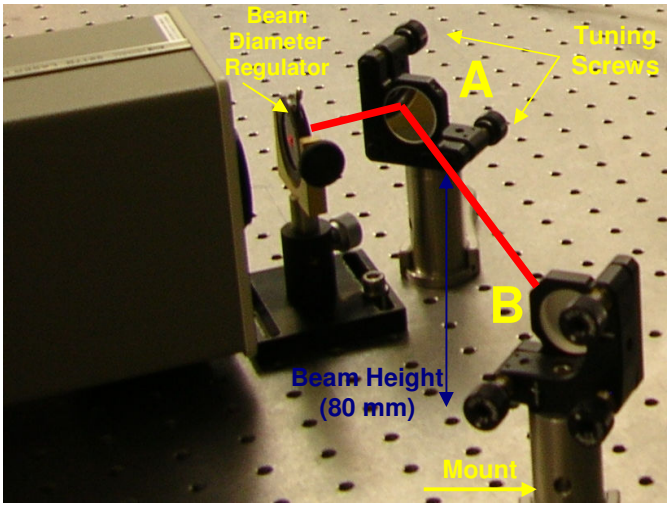

Fig. 3.4.1-1 *Interferometer partial view*

All the other mirrors were fixed at the right height (in such a way that the beam hit the mirror in the center), by means of suitable mounts screwed at the optical bench through fork-clamps (fig. 3.4.1-2). Aluminum plates of the proper height were designed and, then, manufactured by the Astrium machine

workshop, to position the polarizing beam splitters. During the first phase of the interferometer built-up, the Voice-Coil mirrors (representing TMs) were mounted as shown in figure 4.2.2-1.

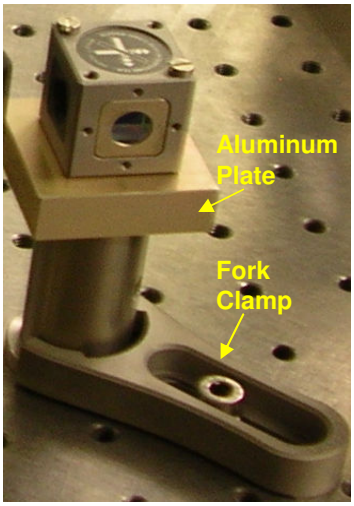

Fig. 3.4.1-2 *Examples of mounting on the optical bench (PBS)*

Mirrors Position and Beams Alignment

In order to operate properly, the receiver needs the perfect overlap of the reference and measurement laser beams (fig. 3.3.2-4), otherwise, the Laser Axis Board loses the signal and no measurement is available.

Therefore, it must be ensured that the beams hit each mirror of the interferometer and maintain a constant distance from the optical bench (75 mm) whether close to the mirrors or very far from them. In order to realize this, a trick was used: a steal post marked with the right beam height was, at first screwed to the OB very close to the mirrors and, then, very far from them. During this procedure, the beam height was adjusted by tuning the screw behind the mirrors (fig. 3.4.1-3). The accurate alignment of the two laser beams at the receiver surface was obtained by the proper and slight movement of the mirror tuning screws.

Observing the mirrors, we can see that, as well as being at the same height, they should be mounted with the right angular position, according to the direction the beam has to assume.

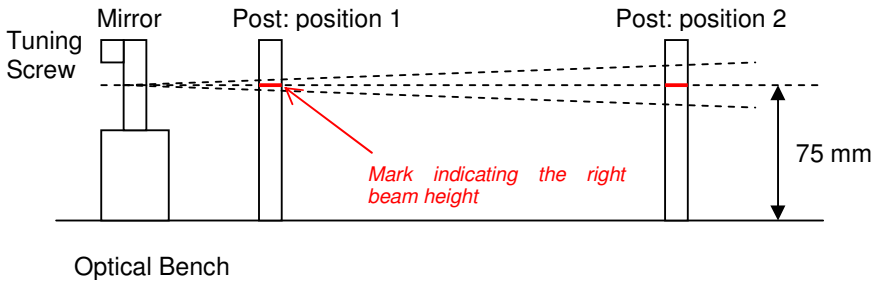

Fig. 3.4.1-3 *Adjusting beams height*

As shown in figure 3.2-1, most mirrors are inclined about 45 degrees with respect to the incoming and outgoing laser light. Before fixing a mirror, definitively, at the OB, it was positioned at about 45 degrees with respect to the incoming beam and laid on the OB in a movable configuration.

To ensure the right outgoing direction (90 degrees w.r.t. the incoming one) and to fix the mirror, the previous post was used. It was screwed at the OB in the expected direction and the mirror was turned a little bit till the beam lighted it (fig. 3.4.1-4a).

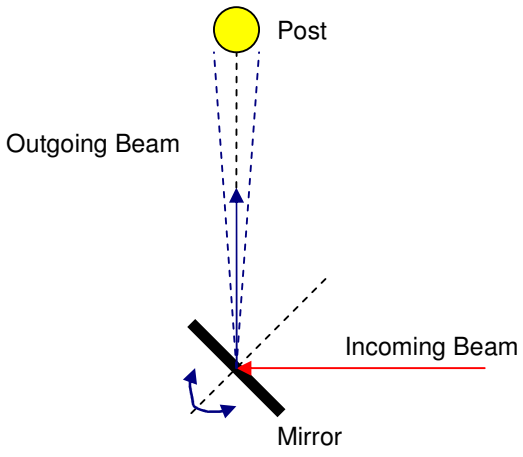

Fig. 3.4.1-4a *Adjusting mirror position*

A bigger effort was required to insert (the two tip/tilt mirrors (E and F mirrors)) in the interferometer because of the incident angle (α = 3.6 degrees)

which needed to be realized. As seen previously in this chapter, that angle is the same for the HP and LTP interferometers, in order to achieve similar optical design and results.

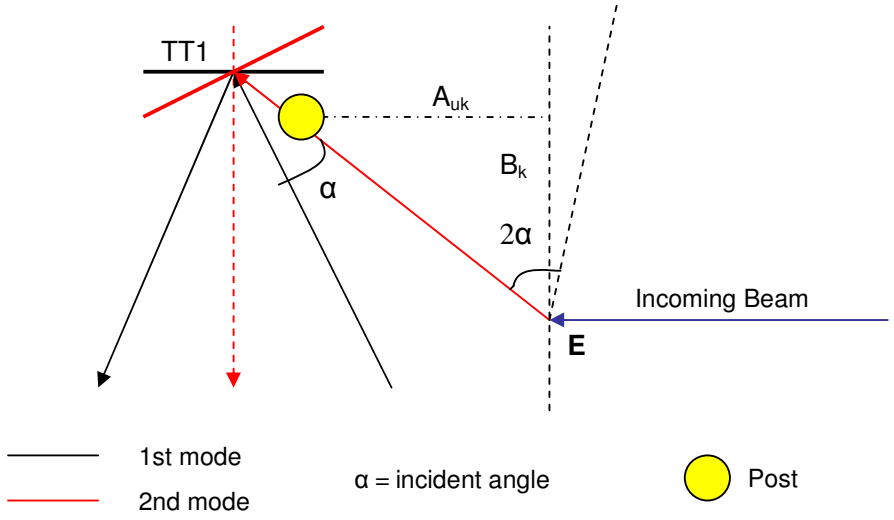

Fig. 3.4.1-4b *Adjusting mirror position*

The procedure was the one previously described. The incoming beam hits the E mirror; therefore, it should be rotated till the outgoing beam realizes an angle that is twice the incident angle. The post was placed in the right direction taking into account the following relation that defines the post position on the OB (A_{uk}):

$$A_{uk} = B_k \cdot \tan(2 \cdot \alpha) \qquad (5.1)$$

where α is the incident angle (3.6 degrees), B_k is a distance chosen on the optical bench and so, known. Once the E mirror was definitively mounted, the Tip/Tilt mirror was easily fixed, taking into account the right direction its outgoing beam had to follow (in dotted red line in fig. 3.4.1-4b).

3.4.2 Stability Problems

During the first working phases the system showed stability problems. The measurement signal LED on the Laser Axis Board (fig. 4.2.7-2) was

extinguished after the start of the testing time. In other words, the signal that came out of the interferometer got lost because of the beam misalignment that disabled the receiver. This happened because the tip/tilt mirror vibrations, were not reduced by the mounts in which they were placed.

As the figure 4.2.2-1 shows, the aluminum mount did not adhere perfectly to the mirror surface causing slight displacements for the mirror itself and for the laser beam. This instability problem also took place, when the optical bench was pushed.

In order to reach the stability, it was evident that a new mount was required. It was not possible to buy a mount that could solve the problem and, at the same time, fix the Voice-Coil mirror in the proper position (right height, right angle). For this reason, first, it was necessary to design the mount and then to manufacture it.

Therefore, within the scope of the thesis, a means to guarantee two degrees of freedom (height, angle) for the mirror and the solution of the instability problem was found. The basic idea was to divide the mount into two parts that permit to accommodate the mirror, keeping it stable and thus reducing the vibrations by means of screws (fig. 3.4.2-1).

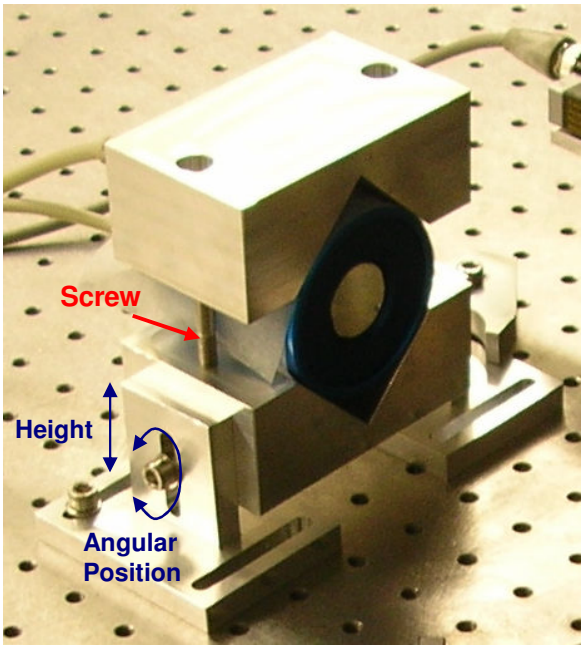

Fig. 3.4.2-1 *New mirror mount*

The two degrees of freedom motion is guaranteed with the system visible in figure (3.4.2-1).

Therefore, the designed and manufactured mount permits to regulate the mirror height and angular position by means of movable parts kept stable by means of screws and to solve the severe problem of the Voice-Coil mirror instability.

Chapter 4

Overview of the Laboratory Build-Up

This chapter describes the functional principle of the Real-Time Test-Bed that was built-up in this thesis. First, the overall system principle of operation is explained. Second, all RTB hardware and software components are explained in detail.

4.1 Principle of Operation

Figure 4.1.1 shows a block diagram which schematically illustrates the functionality the RTB.

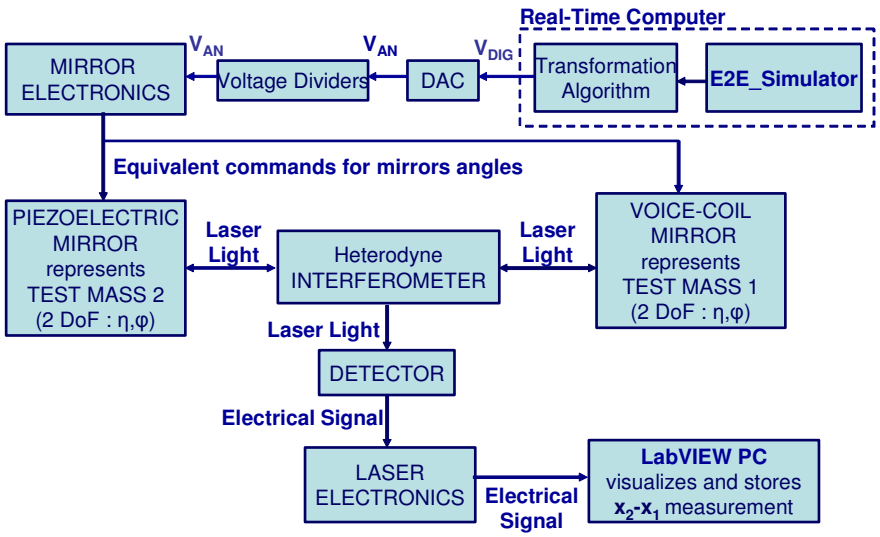

Fig. 4.1.1 *Laboratory instrumentation and interconnection between individual components*

The hardware components used include:

- **Real-Time Computer** with the implementation of the E2E-Simulator (version 3.4) that was adapted so that it runs on the dSPACE® system. The E2E-Simulator also contains a transformation module that commands the desired tip/tilt mirror signals according to the Equation of Motion (EoM).
- **Digital to Analog Converter**
- **Voltage Dividers**
- **Mirror Electronics** for the voice-coil and piezoelectric mirrors
- **Tip/Tilt Mirrors:** voice-coil and piezoelectric mirrors
- **Heterodyne Interferometer**
- **Detector** (or Receiver)
- **Laser Electronics** for the processing of the raw data in order to compute the desired displacement signal.
- **LabVIEW computer** for data visualization and storage

Once the End-to-End Performance Simulator runs on the Real-Time platform, the test masses coordinate (η, φ) values are transformed into digital voltage signals by a transformation algorithm inserted into the simulator dynamics block.

The Digital-to-Analog Converter, installed in the dSPACE® computer, converts the respective test mass angles (η, φ) into corresponding analog voltage values which are finally commanded to the mirror electronics that drive the mirrors.

The voltage dividers bring the input values of voltage to lower levels.

As a consequence of the applied voltage, the voice-coil and piezoelectric mirrors move, producing a change in the optical path length. The differential displacement between the mirrors is measured by the interferometer. The consequential "raw data" are sent to and stored in a separate computer on which the displacement can be visualized, using the LabVIEW® software.

4.2 System Level Overview

The following paragraphs describe each component of the RTB, as depicted in figure 4.1.1. For each component the principle of operation is considered in detail. Specifications, the resolution of the devices and component interfaces are also illustrated in the following.

4.2.1 Transformation Algorithm

The transformation algorithm, shown in figure 4.2.1-2, was introduced in the E2E Performance Simulator in order to transform the TMs angular displacements (η, φ) , as computed by the Equations of Motion (EoM), into corresponding voltages that are required by the tip/tilt mirror driver electronics. The computed voltages, disguised as digital input, are sent to the Digital-to-Analog Converter (DAC) that transforms them into corresponding analog voltages usable for the mirrors electronics. The DAC and electronics devices that control the tip/tilt mirrors introduce gain factors, G_η and G_φ (fig. 4.2.1-1). In order to get the match between the angles as computed from the EoM (η, φ) and the real angles of the mirrors (η^*, φ^*), an off-line calibration is required; it consists in the calculation of the ratio between the latter and the former. The off-line calibration carrying out mode and results are reported in Appendix C.

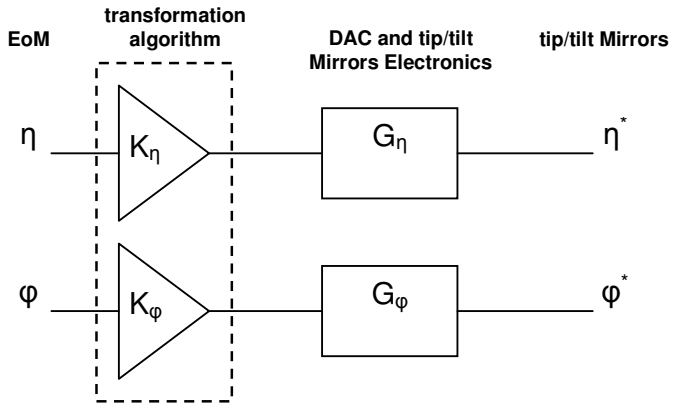

Fig. 4.2.1-1 *Transformation algorithm philosophy*

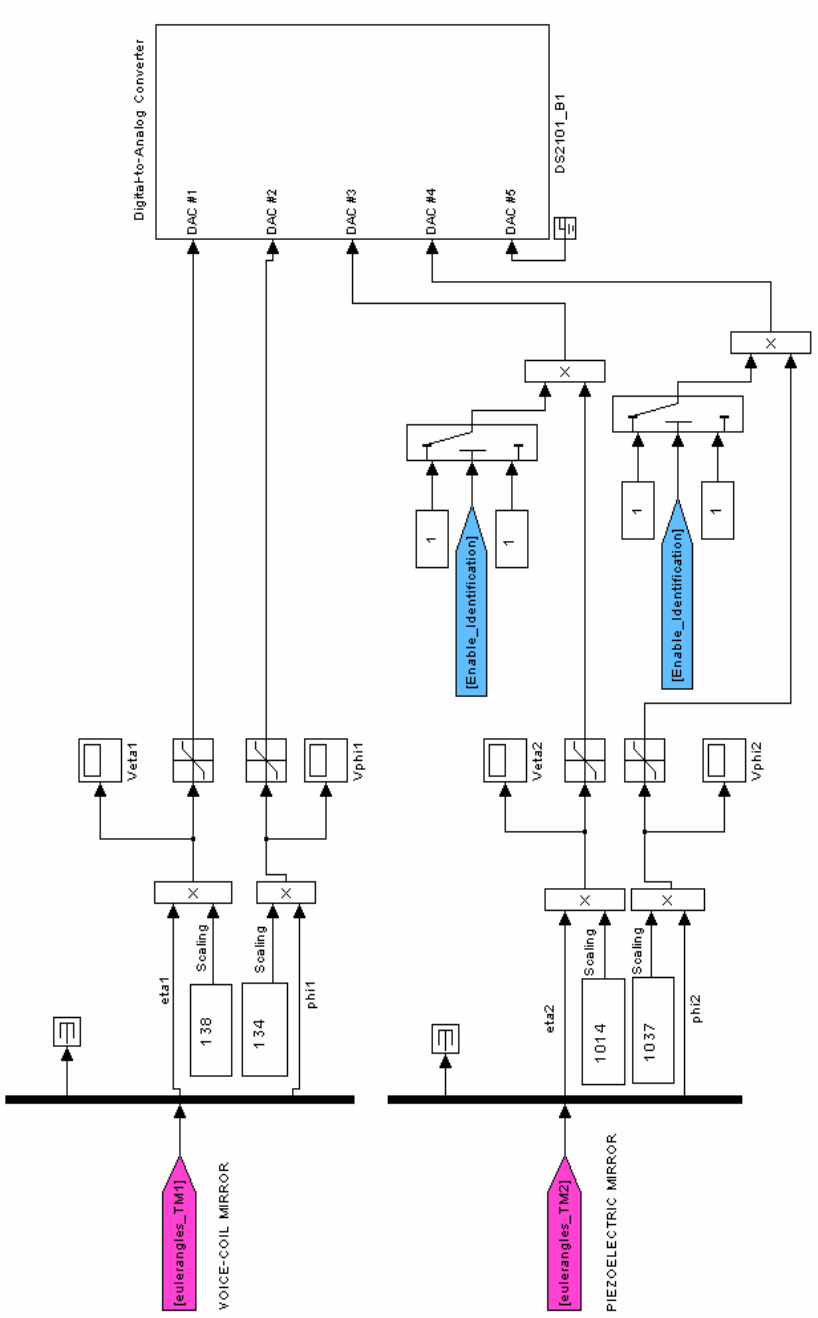

Fig. 4.2.1-2 *Transformation Algorithm: Simulink block*
(No voltage dividers in-line)

The relationship between the EoM outputs and the respective tip/tilt mirrors angles is given by:

$$\begin{cases} \eta \cdot K_{\eta} \cdot G_{\eta} = \eta^{*} \\ \varphi \cdot K_{\varphi} \cdot G_{\varphi} = \varphi^{*} \end{cases} \tag{4.1}$$

Considering that, at the beginning, $K_{\eta}=1$ and $K_{\varphi}=1$, the gain factors that are calculated by means of the off-line calibration are given by:

$$\begin{cases} G_{\eta} = \eta^{*} / \eta \\ G_{\varphi} = \varphi^{*} / \varphi \end{cases} \tag{4.2}$$

Finally, the scaling factors (K_{η}, K_{φ}) introduced to the transformation algorithm to compensate the respective hardware gain of the mirrors and the electronics devices are:

$$\begin{cases} K_{\eta} = 1 / G_{\eta} \\ K_{\varphi} = 1 / G_{\varphi} \end{cases} \tag{4.3}$$

4.2.2 Digital to Analog Converter

As discussed in chapter 2, the DS2101 D/A board is installed in the dSPACE® RTC. It represents a Digital to Analog Converter (DAC) unit featuring 5 parallel D/A converters. They have the following characteristics:

- 12-bit resolution
- ± 5 V, ± 10 V or 0….10 V output voltage range (selectable for each of the converters individually)

The Real-Time Interface board library provides the block that implements the functionality and I/O capabilities of the board (fig. 4.2.1-2) and that was put

into the transformation algorithm block. In the specific case, the following scaling between the analog output and the input of the block was chosen:

Output Voltage Range	**Simulink Input**
± 5 V	± 1

Tab 4.1 *Scaling factor*

It corresponds to a resolution of ± 1.22 mV.

A connector panel provides the connection between the mirrors electronics and the D/A channels.

4.2.3 Voltage Dividers

The minimum amplitude of the Euler angles, η and φ, as calculated from the EoM, is equal to 2 μrad. The Digital to Analog Converter has a resolution equal to ± 1.22 mV that, in terms of tip/tilt angular values at the Voice-Coil and Piezoelectric mirrors (see Paragraph 4.2.4) means:

$$\alpha = 0.01 \cdot V_{DAC} = \pm 12 \ \mu\text{rad} \qquad (\text{Voice} - \text{Coil Mirror}) \qquad (4.4a)$$

$$\alpha = 2 \cdot 10^{-4} \cdot V_{DAC} = \pm 0.244 \,\mu\text{rad} \quad (\text{Piezoelectric Mirror}) \qquad (4.4b)$$

Where α stands for η or φ, and V_{DAC} is the DAC resolution.

The equations 4.4 will become clear in the following paragraph in which the tip/tilt mirror specifications will be considered.

Looking at the results, the value of 12 μrad is considerably higher than the value which is needed to realize, i.e. 2 μrad. To solve this problem, voltage dividers were built-up for both η and φ channels.

The voltage dividers are able to increase the DAC resolution of a factor of 100. The output voltage (V_{out}) of the dividers is proportional to the input voltage (V_{in}) by means of two resistors (R_1 and R_2) that produce a voltage drop between the terminals in accordance with Ohm's law:

$$V_{out} = \frac{R_2}{R_1 + R_2} V_{in} \tag{4.5}$$

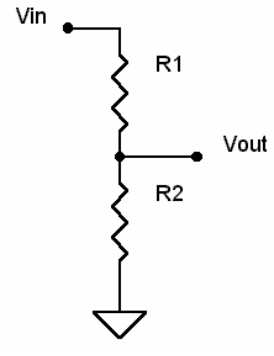

Fig. 4.2.3-1 *Voltage Divider's circuitry*

In the specific case:

$R_2 = 1\ k\Omega$

$R_1 = 100\ k\Omega$

$V_{out} = 1/101\ V_{in}$

The DAC resolution is, now, equal to 0.0122 mV; the realizable amplitude value is about 0.122 μrad.

4.2.4 Tip/Tilt Mirrors

As the name suggests, these mirrors tip and tilt around two axes that correspond to the test masses y-axis and z-axis (fig. 3.1-3), realizing the η and φ angular values. Both of the used mirrors have the same principle of operation: the analog voltage that comes from the DAC is converted in equivalent commands for mirror angles by means of specific electronic devices which, together with the DAC, introduce gain factors. Therefore, the tip/tilt mirrors needed a calibration to ensure that the Euler angles (η, φ) would coincide with the real values obtained at their surfaces.

Before continuing with the mirrors description, it is necessary to pay attention

to the difference between the mechanical (α_{mech}) and the deflection or optical angle (α_{defl}) that the mirrors realize, in order to more readily understand which angle their specifications refer.

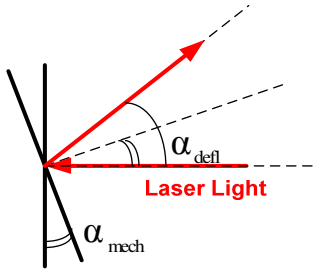

Fig. 4.2.4-1 *Difference between mechanical and optical angles*

The law of reflection says that:

$$\alpha_{defl} = 2 \cdot \alpha_{mech} \tag{4.6}$$

This becomes clear by observing figure 4.2.4-1

Voice-Coil Mirror

According to the specifications [25], the mirror characteristics are:

- Resolution: 5 µrad
- Maximum Input Voltage: ± 10 V
- Maximum mechanical angle: ± 35 mrad (α_{defl}=± 70 mrad)

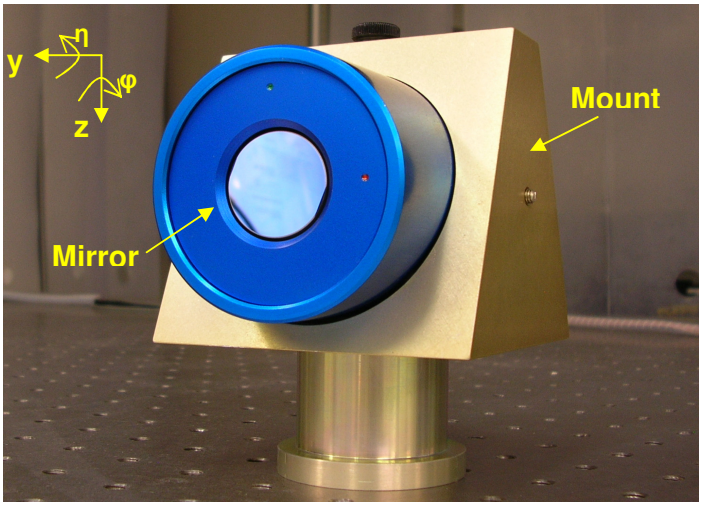

Fig. 4.2.2-1 *Picture of the DKS2/35 mirror*

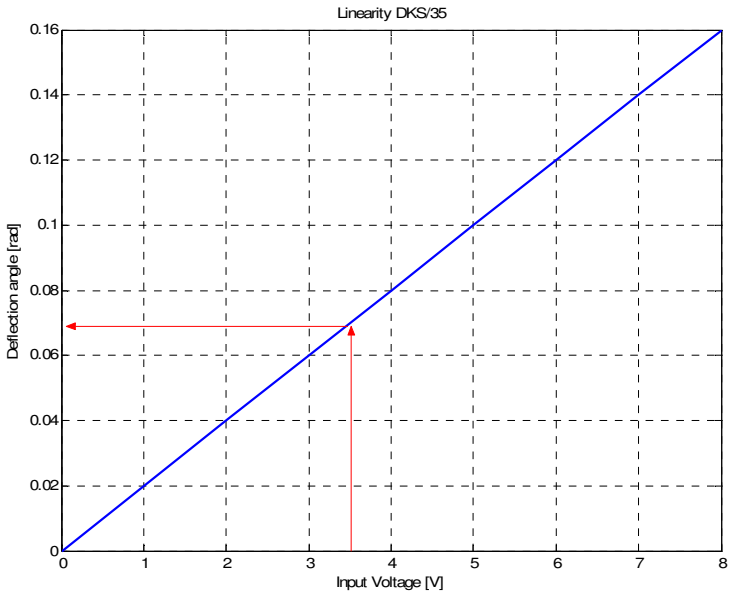

Fig. 4.2.4-2 *Linearity between the voltage and the deflection angle*

The plot in figure 4.2.4-2 shows the relationship between the mirror input voltage (V_{DAC}) and the nominal optical angle (α_{defl}) it reaches after the application of that voltage (see also equation 4.4a):

$$\alpha_{defl} = 0.02 \cdot V_{DAC} \Rightarrow \alpha_{mech} = 0.01 \cdot V_{DAC} \qquad (4.7)$$

The electronics device that transfers the voltage to the mirror accepts as maximum input voltage ± 5 V, consistently with the D/A converter characteristics.

The BNC cables coming from the DAC connector panel transfer the analog voltages (that represent to the η and φ angular values) to the mirror electronics by means of the BNC connectors as represented in the block diagram of figure 4.2.4-3.

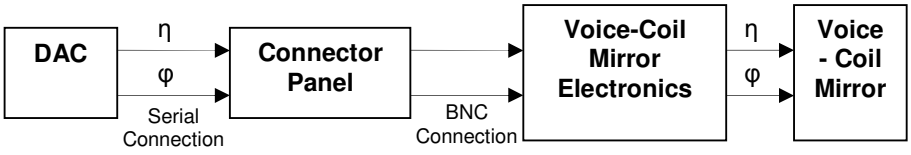

Fig. 4.2.4-3 *Electronic devices connections*

Piezoelectric Mirror

The S-340 piezo actuator is a tip/tilt platform; it permits rotations around the z-axis (φ) and y-axis (η) eliminating the x-axis freedom (fig. 4.2.4-4/5).
The piezo actuator is mounted on a special device that allows us to regulate its height, its angular position and the shift along the y-axis, by means of μ-meter screws (fig. 4.2.4 -4); moreover, if the device is turned of 90°, the piezo moves along the x-axis instead of the y-axis.

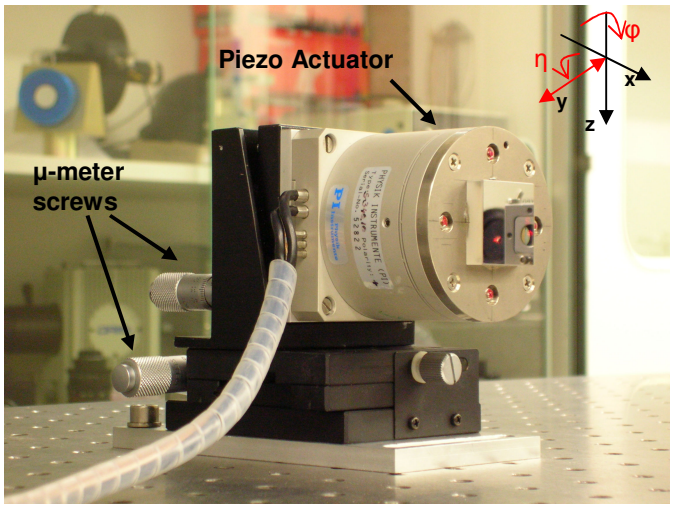

Fig. 4.2.4 -4 *Piezoelectric mirror (Phisik Instrumente: S-340)*

Unlike the Voice-Coil mirror, its electronics makes possible both an open-loop and close-loop operational modes, (see [22], [23]).
The platform incorporates two pairs of Low Voltage Piezoelectric Translator (LVPZT) actuators; in each pair, they are connected in differential push-pull mode. It means that any change in the operating voltage causes one actuator of the pair to see a voltage increase, the other to see a decrease of the exact same magnitude. Each tilt axis requires one controlled operating voltage in the range of 0 to +100 Volts (with an excursion of ± 20 %) and one more constant voltage of +100 V.
The input voltage (V_{DAC}: from the DAC) is 10 times smaller than the piezo voltage (V_{PIEZO}: to the Piezo). In other words, the DAC is connected to an amplifier that, mounted into piezo electronics, introduces a gain factor of 10.

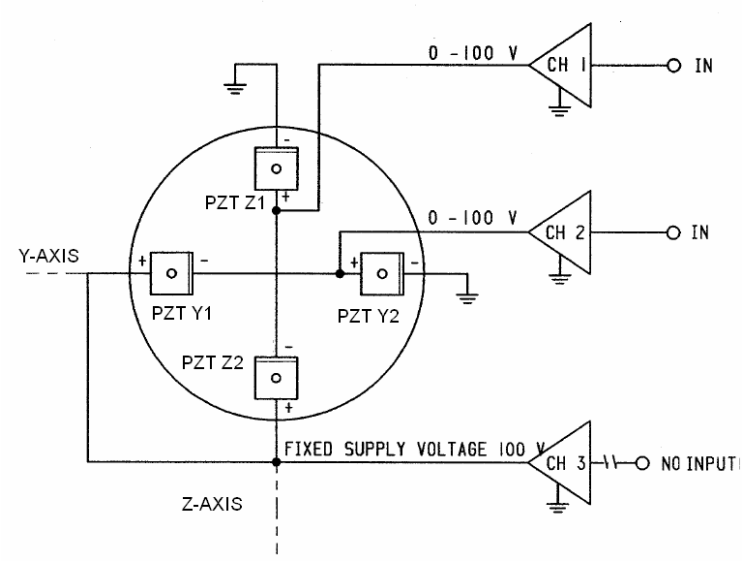

Fig. 4.2.4 -5 *Piezo actuator layouts and wiring*

If the piezo electronics is off ($V_{DAC} = V_{PIEZO} = 0$ V) the piezoelectric mirror assumes a default position corresponding to a mechanical angle equal to -1 mrad, when the device is powered up, both actuators of the pair have a piezo voltage 50 Volts and the mechanical angle is set to zero. Summarizing:

$$\alpha_{mech} = 1\,\text{mrad} + 0.02\frac{\text{mrad}}{\text{Volts}} \cdot (V_{PIEZO} - 100)\text{Volts} \qquad (4.8)$$

Piezo voltages below 50 Volts cause tilting in one direction, above 50 Volts, tilting in the other (fig. 4.2-6). Therefore, 50 Volts can be considered a new origin since that the piezo actuator presents this symmetrical behavior with respect to the zero position ($\alpha_{mech} = 0$). Hence (see equation (4.4b)):

$$\alpha_{mech} = 0.02\frac{\text{mrad}}{\text{Volts}} \cdot (V_{PIEZO})\text{Volts} \qquad (4.9)$$

In closed-loop operational mode (fig. 4.2.-7), the Linear Variable Differential Transformers (LVDT) sensors, attached to the moving parts, send the actual position value to a controller that calculates the difference with respect to the reference signal. The control signal is received by the amplifier that transmits it to the piezo.

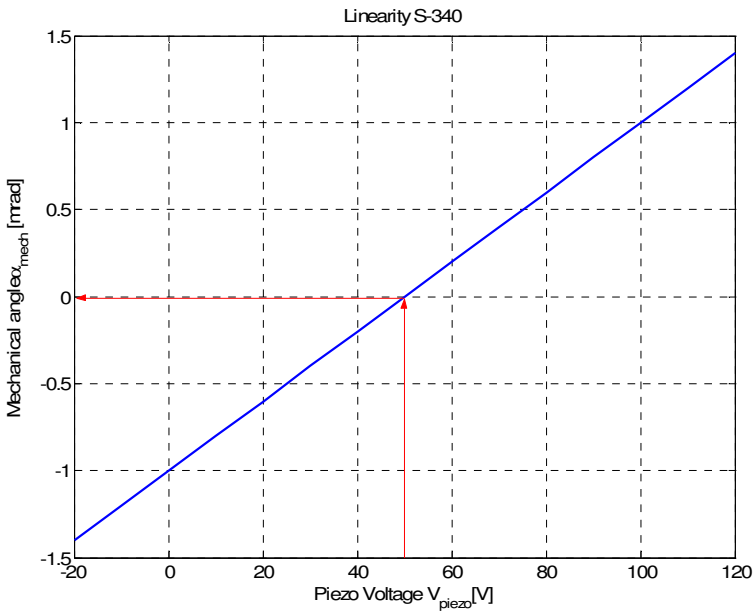

Fig. 4.2.4 -6 *Linearity between the output voltage and the deflection angle*

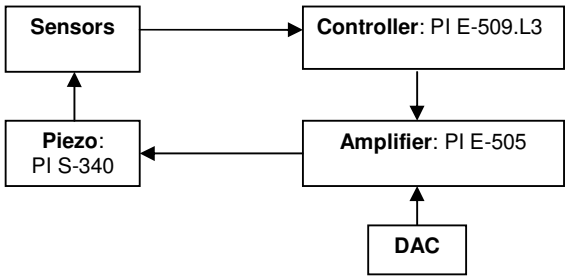

Fig. 4.2.4-7 *Closed-loop operational mode*

From the specifications [22], the position resolution of the piezo actuator is:

- 0.5 µrad in closed-loop
- 0.1 µrad in open-loop

The difference is due to the fact that, in open-loop, there is no sensor which puts additional electronic noise on the control signal.

4.2.5 Functional Overview of DAC, Voltage Divider and Tip/ Tilt Mirror Electronics

Every in-line electronic device introduces a gain factor (fig. 4.2.5-1) obtainable from the specifications.

As seen before, the maximum DAC digital input values correspond to ± 1, that, in the specific case, means ± 1 rad. The voltage dividers limit the angular values that could be obtained as mirror electronics output. Their presence is necessary to increment the DAC resolution and to make the realization of angular displacements, congruent with the EoM solutions, possible at the Voice-Coil mirror.

Given the fact that, during the laboratory tests, the Voice-Coil mirror is kept still (see chapter 5) and, so, no voltage passes through its electronics, removal of the voltage dividers from the line, in order to obtain a more wide angular range could be taken into consideration.

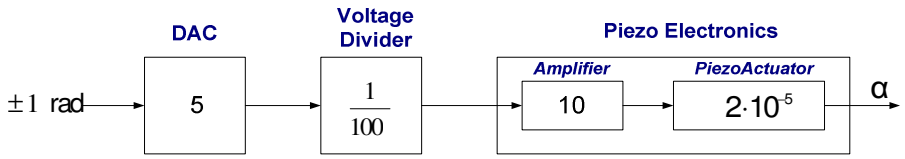

Fig. 4.2.5 -1 *In-line electronic devices and their gain factors*

Looking at the figure 4.2.5-1, the maximum angular value with the voltage divider in-line is the following:

$$\alpha_{max} = \frac{5}{100} \cdot 10 \cdot 2 \cdot 10^{-5} = 10\,\mu\text{rad} \qquad (4.10)$$

The minimum value is given by the equation (4.4b), but that value is smaller than the piezoelectric mirror resolution (0.5 μrad) that corresponds to the minimum available value.

Without the voltage divider, the angular range is, considerably, improved:

$$0.5\ \mu\text{rad} < \alpha < 1000\ \mu\text{rad} \qquad (4.11)$$

4.2.6 The HP Receiver (or Detector)

As explained in chapter 3, in the HP interferometer, once the *reference* and the *measurement* beam interfere at the last polarizing beam splitter (PBS2, fig.3.2-1), the resulting single beam is directed to the receiver (fig. 4.2.6-1).

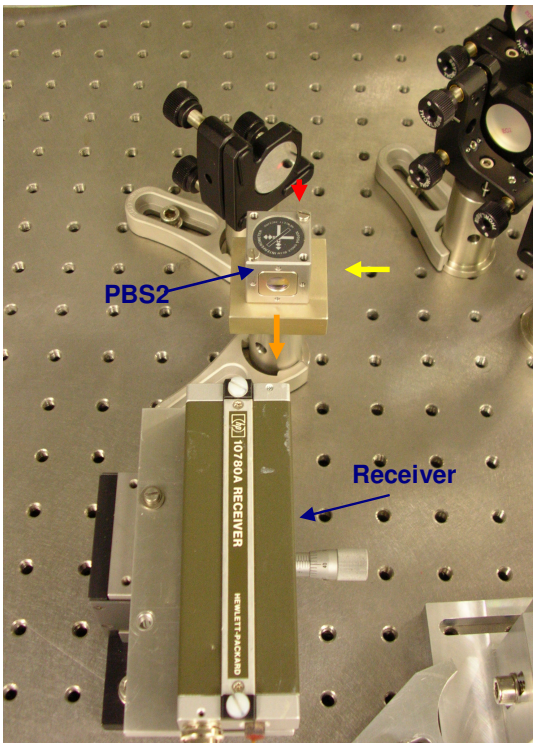

Fig. 4.2.6-1 *HP 10780A receiver*

The receiver converts the Doppler-shifted frequency of the laser beam from the interferometer into on electrical signal for the Laser Axis Board (fig. 4.2.7-1), (see [19]). This frequency shift, resulting from the relative motion between the source (one or both moving mirrors) and the receiver (the observer, at rest) is known as Doppler shift. The PBS1 (fig.3.2-1) splits the beam into the *reference* (frequency: f_1) and measurement beams (frequency: f_2). Since that, in the *reference* path, the mirrors are fixed, no Doppler Effect is present. The movable mirrors in the *measurement* path, instead, produce a shift in frequency proportional to the mirror velocity (v_m).

According to the Relativistic Doppler Effect, the relation between the frequency (υ), seen by the observer at rest, and the frequency (υ_0), seen by the

source moving toward the observer [(1)], is:

$$\upsilon = \upsilon_0 \sqrt{\frac{1 + v_m/c}{1 - v_m/c}} \tag{4.12}$$

Since $v_m << c$:

$$\Delta f = \upsilon - \upsilon_0 = + \frac{1}{\lambda_0} \cdot v_m \tag{4.13}$$

where λ_0 is the wavelength of light at the mirror surface.

The resulting frequency for the *measurement* beam will be: $f_1 \pm \Delta f$ (depending on the direction of the mirrors movement). The light directed to the receiver has two frequency components (f_2 and $f_1 \pm \Delta f$) that interfere at the receiver's polarizing plate (see Chapter 3). This produces a difference frequency (f_2 - $f_1 \pm \Delta f$), which is detected by the receiver's photodetector and converted to an electrical signal (AC current).

The receiver circuitry (fig. 4.2.6-2), then, amplifies the signal and transforms it into a square wave signal (TTL signal). The output signal is a differential square wave at the measurement frequency (f_2 - $f_1 \pm \Delta f$).

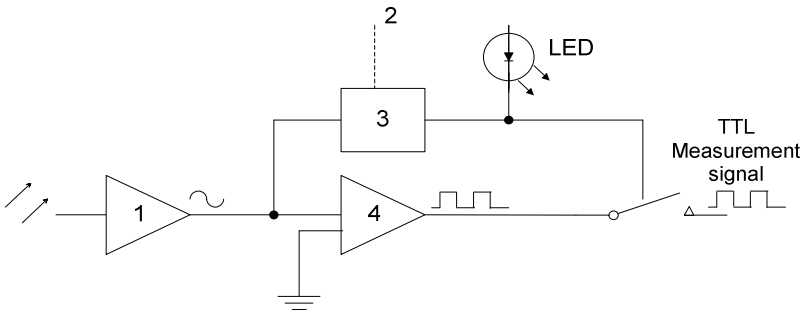

Fig. 4.2.6-2 *Receiver circuitry*

(1): If the observer and the source move away to each other, the mirror velocity should be substituted with (- v_m)

Inside the receiver, a squelch circuit allows the signal output to be turned off automatically if the input signal is not strong enough. A LED indicator on the receiver lights up when the input signal is detected.

Displacement information is obtained in the Laser Axis Board by comparison of the measurement frequency (f_2 - $f_1 \pm \Delta f$) and the reference frequency (f_2 – f_1). The latter is sent to the Laser Axis Board, directly, from the Laser Head (fig. 3.3.1-2)

4.2.7 Laser Electronics

The HP 10897B High Resolution Laser Axis Board is a VME board, (see [20]).

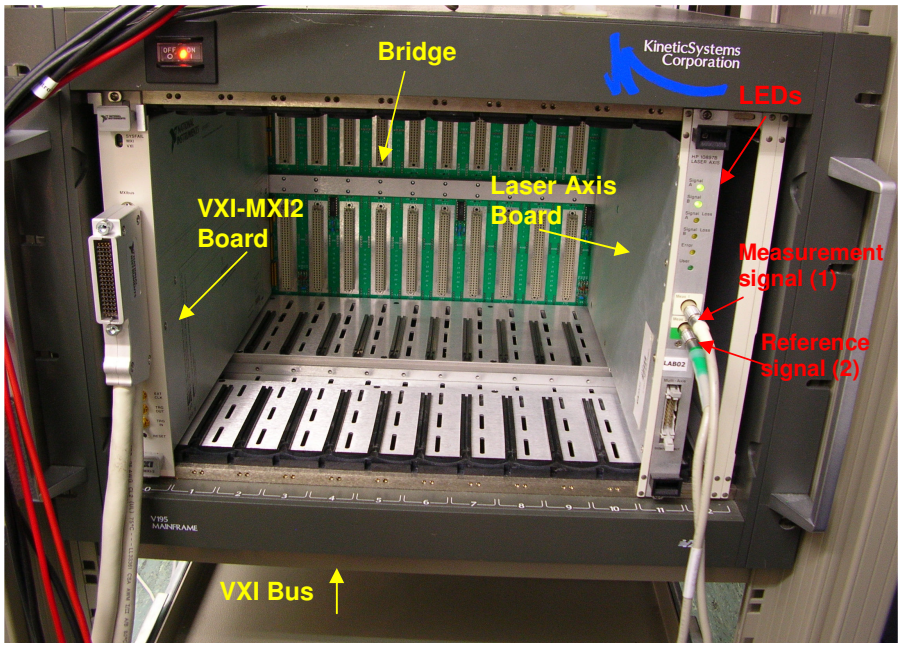

Fig. 4.2.7-1 *HP Laser Axis Board and VXI board installed in the VXI bus*

It converts the reference and measurement signals (fig. 4.2.7-1), in the form of TTL signals coming from the Laser Head and the receiver, to a 32-bit digital word, representing the displacement Δx in fractional wavelengths. The Laser Axis Board contains a fringe counter (Up-Down counter).

Depending on which falling edge of the TTL signal, reference or measurement signal, occurs first, the direction of the count either up or down is defined. The

output is an integer (n) expressed over 32 bits, representing the number of interference fringes, obtained as a consequence of the tip/tilt movement.
The position word is readable by a VXI (or VME) bus system. The position resolution depends upon the used optic and electronic devices (tab. 4.2); it increases with the interferometer precision.

Optics (λ=632.8 nm)	**Resolution**
Linear or Single beam	λ/512 (1.23 nm)
Plane Mirror	λ/1024 (0.625 nm)
High Resolution	λ/2048 (0.3125 nm)

Table 4.2 *HP Laser Axis Board resolution*

As seen in chapter 3, the Single Beam Interferometer and the Laser Axis Board, used in this work, permit a resolution equal to λ/512.
By exploiting the rising and falling edge of the TTL signals an interpolation can be realized, resulting in a resolution enhancement of factor 256. In Fact, without interpolation, one count event relates to a movement of the tip/tilt mirror of λ/2, i.e. the distance between two bright fringes for the Single Beam Interferometer (See paragraph 3.3.2). By using the internal interpolation, a movement of λ/512 corresponds to one count event.
This means that, the measured distance (Δx) is expressed as:

$$\Delta x = n \cdot \frac{\lambda}{512} = n \cdot 1.23 \text{ nm} \qquad (4.14)$$

The main components of the board are the Front-Panel Input/Output, the Laser Axis Processing Unit and the VXI bus interface.
The first receives measurement input signals and isolates these inputs from the internal board's circuitry. It determines if the reference and measurement signals are present, if not, the Light Emitting Diodes (LEDs) on it (fig. 4.2.7-1/2) are switched off.
The Laser Axis Processing Unit generates real-time position information from the laser input signals and stores this data in the appropriate holding registers

for retrieval. It also tests the integrity of measurement input data enabling the LED to light up if an error is present. The VXI bus Interface links the Laser Axis Board to the VXI bus and contains six functional sections which monitor bus activity, respond to appropriate bus cycles, monitor the laser system status and generates VXI bus interrupt requests when specified errors occurs.

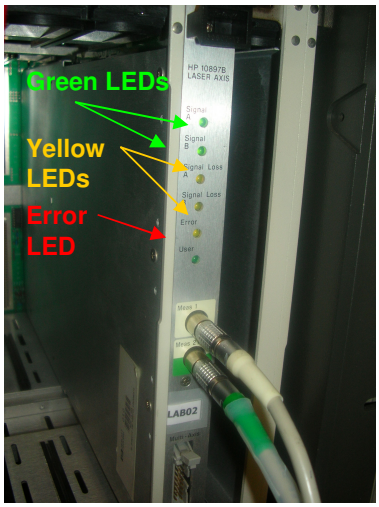

Fig. 4.2.7-2 *Laser Axis Board*

As visible in figure 4.2.7-2, the green LEDs are switched on when the reference and measurement signals are perfectly detected; when the signals are not strong enough, the following two yellow LEDs flash. The fifth LED lights up when an error occurs.

The VXI bus is a powerful test instrumentation technology that is based on the VME bus. Indeed the letters VXI stands for VME eXtension for Instrumentation. The basic building block of this system is the mainframe that contains 13 slots into which various modules (instruments) can be added; this bus also contains all the power supply requirements for the rack and instruments located in it. As shown in the figure 4.2.7-1, the VXI bus, in the specific case, contains the Laser Axis Board (on the right) and the VXI-MXI2 board (on the left). Its tasks consist in receiving measurement data from the laser board, in transmitting it and in initializing the board. Once the National Instruments VXI-MXI2 board receives data, it converts the A24 (address space in which data are stored) VXI bus cycles into MXI bus cycles and vice versa.

4.2.8 LabVIEW® Computer

General Overview

The block diagram of figure 4.2.8-1 illustrates the functional overview of the laboratory build-up. The Euler angles (η and φ), solution of the EoM solved by the dSPACE® RTC, after the passage through the DAC, the voltage dividers and the mirrors electronics arrive in form of equivalent commands at the tip/tilt mirrors.

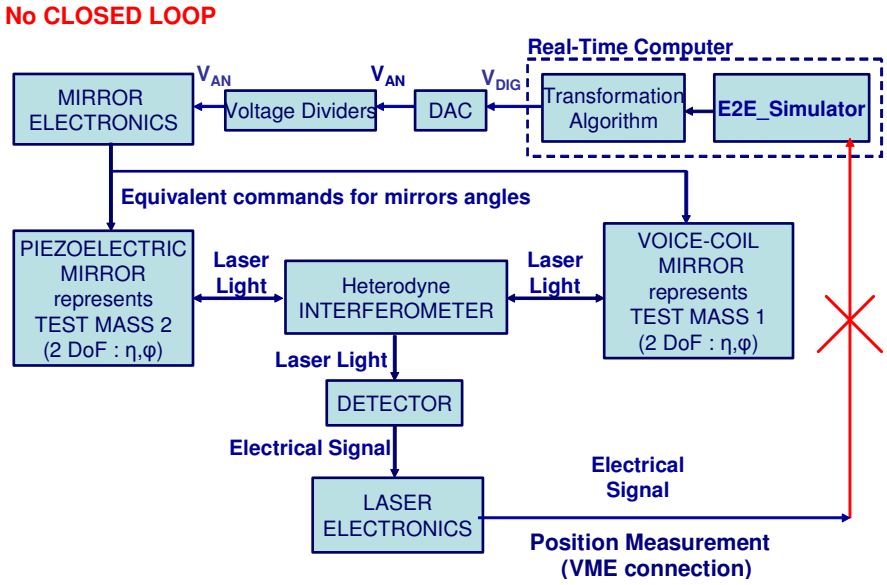

Fig. 4.2.8-1 *Closed loop configuration*

The laser light detected by the receiver is transformed into electrical signals usable by the laser electronics, as explained in this chapter.

Finally, the displacement measurement should be feed back to the dSPACE® RTC in order to create a closed loop system.

However, it was not possible to upload the results by means of the RTC but an external computer, the so-called LabVIEW® computer, was used; it allow us to visualize and store the measurement data.

The DS1005 PPC board (see chapter 2) and the other dSPACE® boards in

commerce do not include VXI connectors or, even if a connection is present, no software package is available with the VISA tasks.
This limit did not permit to make the measured position available as input for the Drag-Free Algorithm Control System (DFACS), inside the E2E-Simulator.
The block diagram of figure 4.2.8-2 shows the connections between the external computer and the laser electronics, and so with the VXI bus.

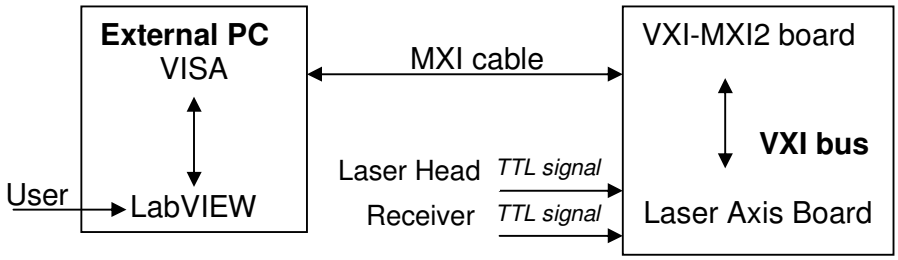

Fig. 4.2.8-2 *Connection between IFO, Laser Axis Board and visualization PC*

The laser head and the receiver send TTL signals to the Laser Axis Board connected to the VXI-MXI2 board by means of the VXI bus.
The MXI bus system (32-bit Multisystem eXtension Interface bus) is installed in an external PC and is linked to the VXI-MXI2 board through a MXI cable.
The user can control the experiment through the LabVIEW® software installed in the external PC.

LabVIEW® Software

The software package that permits to make settings for the boards, to download data to the external PC and to give commands to the VXI bus for the initialization of the boards is represented by VISA (Virtual Instruments Software Architecture) and LabVIEW® ,(See [10], [11]).
VISA is a standard I/O Application Programming Interface (API) for instrumentation programming, it controls the VXI bus; LabVIEW is a general-purpose programming system but it, also, contains libraries of functions and development tools designed, specifically, for data acquisition and instrument control.

By means of LabVIEW Virtual Instruments, the user can activate VISA and, so, control the VXI and its instruments. It permits also to store and visualize the laser measurements graphically.

During this work, two LabVIEW I/O interfaces were used. The first has the role of initializing the Laser Axis Board before starting the measurements. By means of the second interface, the position measurement is read from the board at a sampling rate equal to 500 Hz. The 32-bit digital position word is, then, converted in an integer number that is multiplied by the board resolution ($\lambda/512$). The user can observe the final result via a graph in which the position, expressed in nanometers, is plotted against the time, in seconds.

For major details about the LabVIEW interfaces, see Appendix E.

Chapter 5

Complete Setup and Performance

This chapter shows the final setup of the test-bed and reports the results of the laboratory tests carried out to check the system performance.

5.1 Interferometer Final Configuration

The final and operative version of the test-bed is visible in figure 5.1-1.

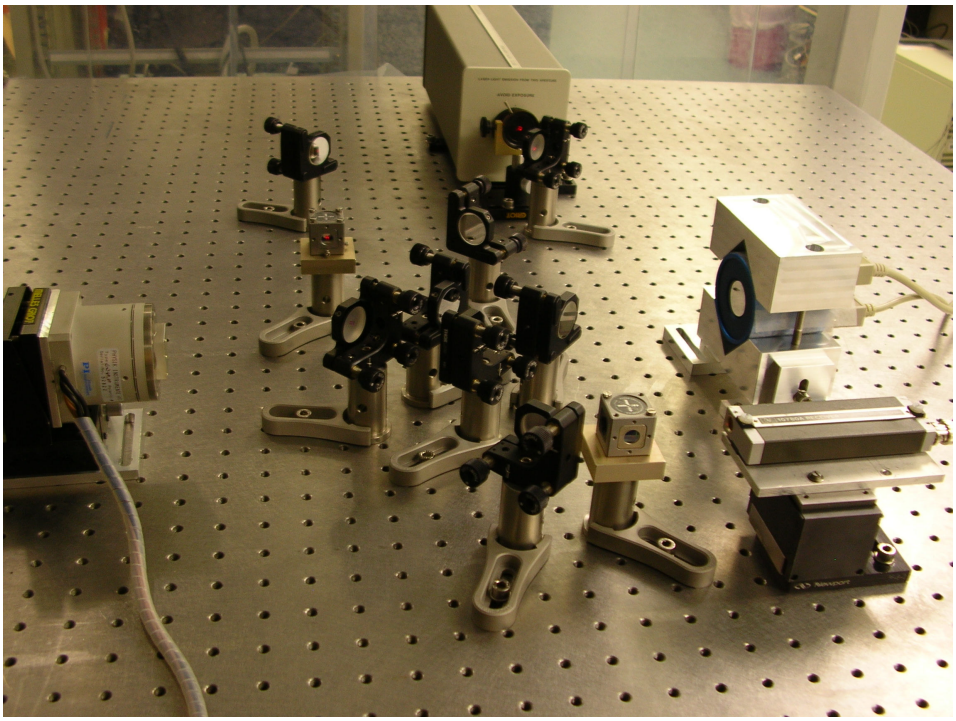

Fig. 5.1-1 *HP Interferometer final configuration (Optic Lab, Astrium FN)*

Among the various DFACS control modes of operation, the one taken into account for the laboratory tests is the so-called SCI1 (M3) mode.

Test Mass 1 (TM1) is Drag-Free controlled and the Test Mass 2 (TM2) is suspension controlled along the x-axis, which is the sensitive axis.
The reason for this choice is that the piezoelectric element is able to realize better angular displacements than those obtainable with the voice-coil one. In order to obtain more precise test results, it was decided to apply the SCI1 (M3) mode considering the piezoelectric mirror as TM2 and the voice-coil mirror as TM1 practically kept at rest because Drag-Free controlled.
The other optical devices are the two Polarizing Beam Splitters and 8 mirrors. As it can be seen in figure 5.1-1, each element of the interferometer is screwed up into an optical table. The threaded holes on its surface are equidistant from each other (25 mm). This kind of optical bench eliminates torsional and bending vibrational modes by means of hydraulic dampers.

5.1.1 Maintenance of the Interferometer

In order to obtain a proper operation, it is necessary to clean the mirrors to remove dust, periodically. Usually, special lens tissues with a solution of 95 % ethanol in water are used.

5.2 System Performance

5.2.1 Stability

The combined action of the optical bench and the proper mounts, that damp the vibrations permitting precise beam alignment, led to obtaining high levels of stability, demonstrable by slightly pushing the table without losing the measurement signal at the receiver. The system sensitivity becomes clear looking at the figure 5.2.1-1; in fact, the test measurement, visible in the plot, is affected by three peaks to which correspond as many slight touches of the optical bench.

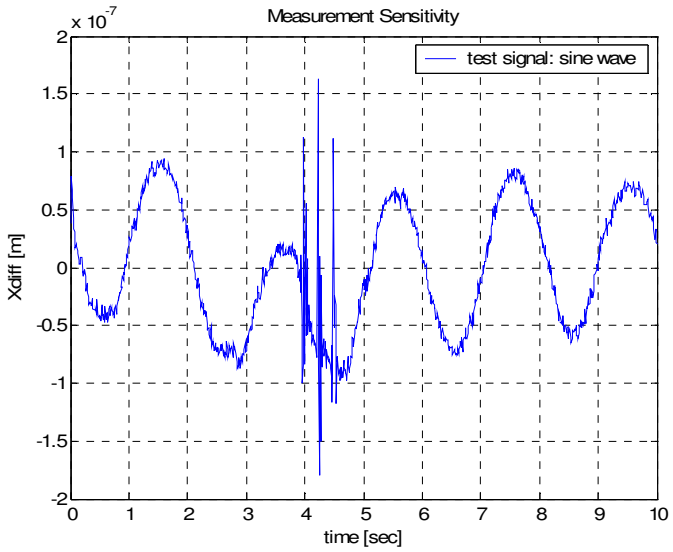

Fig. 5.2.1-1 *Test signal disturbed by 3 slight touches of the OB*

5.2.2 Reached Noise Level Performance

Once the HP interferometer was built-up and made operative, it was necessary to measure how much influence the laboratory environment and the system electronics had upon its sensitivity.

A 3 hours measurement was carried out without applying any external signal to the tip/tilt mirrors. During a first test, the piezoelectric mirror was cold, i.e. switched on to carry out the test. During the second test, the piezo actuator was warm, i.e. powered and in use for some hours.

The noise Power Spectral Densities (PSDs) of the first and second test were calculated and are shown in figure 5.2.2-1.

It can be noticed how the thermal effects due to the piezo actuator over-heating has a very small influence on the noise level.

Usually, in a quiet room in which electrical equipment, air-conditioning and computers are working, noise at 60-500 Hz is generated.

Therefore, in that frequency range, the contributions due to the environment and the thermal effects are present. At lower frequencies, the noise starts to increase relaxing as 1/f towards 10 mHz. The Flicker noise (1/f) is, usually, generated in all the electronic devices and its causes, related to the internal circuitry, can vary greatly. The noise related to the electronic devices becomes more relevant in 10 mHz -1 mHz bandwidth, where it grows as $1/f^2$.

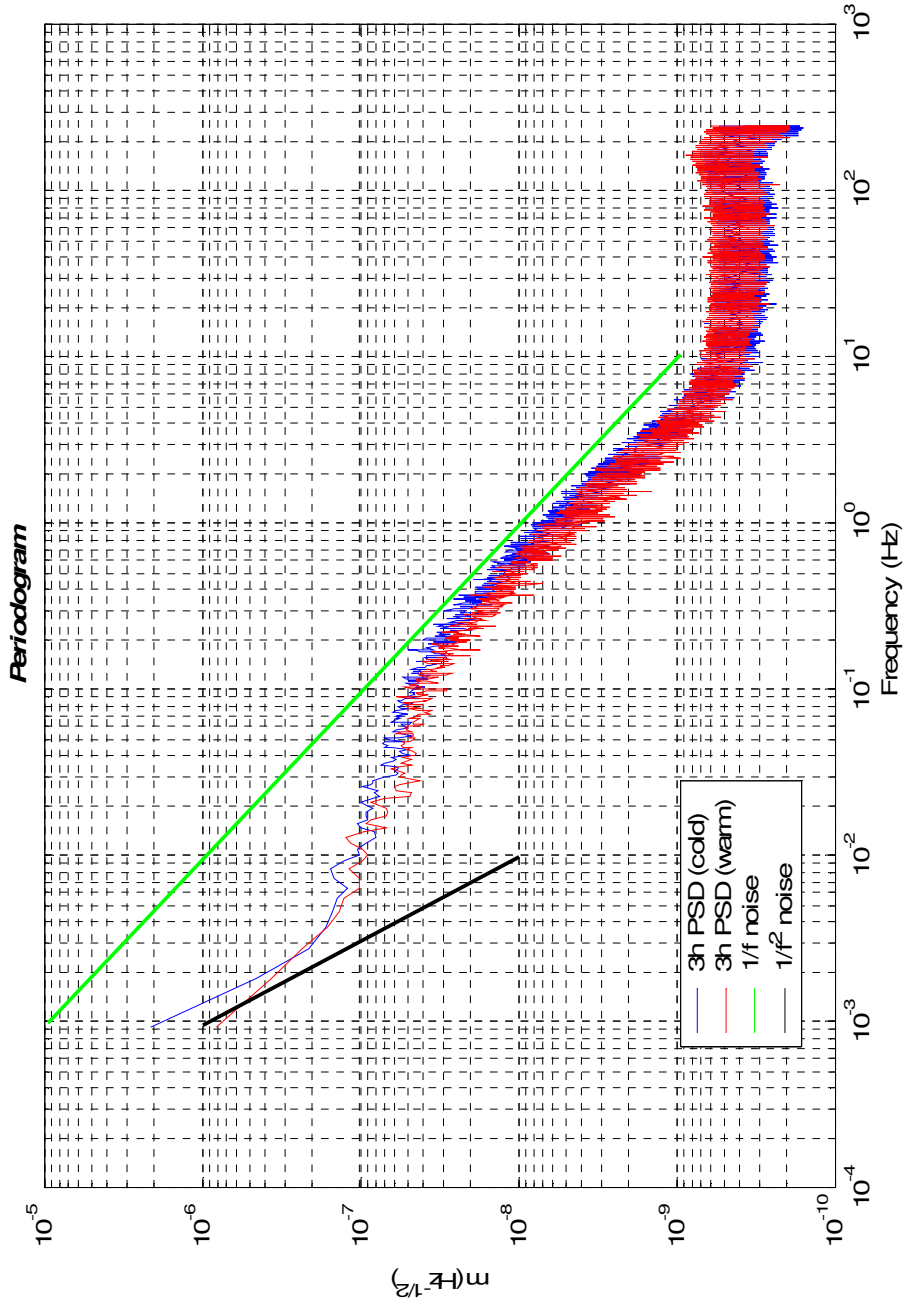

Fig. 5.2.2-1 *Noise Power Spectral Densities relative to 3 hours measurements*

At this point, it is interesting to compare the HP interferometers performances with the DFACS control accuracy in order to verify the DFACS functional testing capability of the used real time test bed.

The more stringent control requirement specified here for the x_1 drag-free coordinate is:

$$S_{x_1} = 5 \cdot 10^{-9} \left[1 + \left(\frac{f}{3\text{mHz}} \right)^2 \right] \qquad (5.1)$$

in the measurement bandwidth (1 mHz -30 mHz) [27].

Figure 5.2.2-2 represents the sensitivity of the HP interferometer and the control requirement on the x_1 coordinate in the frequency range of interest.

As can be noted, the DFACS control accuracy is satisfied in terms of the sensitivity of the build-up.

Even if the HP interferometer is exposed to adverse environmental conditions (air and acoustics), the reached noise level performance permits DFACS testing. In order to dampen the acoustic vibrations and, in so doing improve the performances, a wooden box could be put covering the HP interferometer.

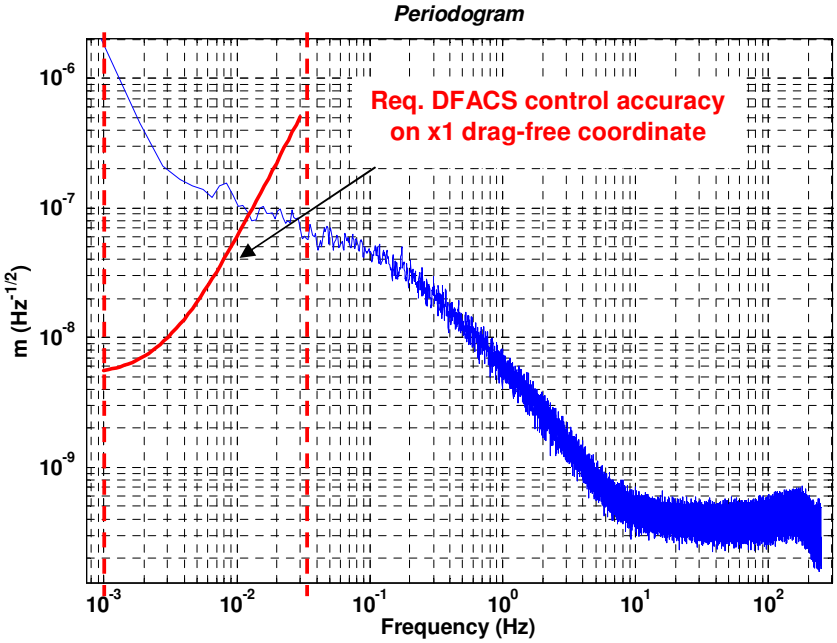

Fig. 5.2.2-2 *DFACS Control requirement and sensitivity of the HP IFO*

5.2.3 X-Axis Test

An x-axis test was carried out in order to know, exactly, how much the displacement measurement was precise and consistent.

Observing the figure 4.2.4-4, it could be seen that the piezo actuator can be moved along the y-axis, because of its assembly. If the mount, at its basis, is turned by 90°, the available movement will be along the x-axis.

Therefore, if, during a measurement, the piezo is moved along the x-axis by a known quantity, the laser system readout, readable in the LabVIEW file, must coincide with that amount.

As seen in paragraph 4.2.8 and in the Appendix E, the numerical value by which the number of the interference fringes is multiplied, coming from the laser electronics, represents the instrumentation resolution that, in the case of the HP interferometer, is equal to 1.23 nm. When the x-axis test was carried out, the resolution value, set in the LabVIEW file, was equal to 0.62 nm [(1)].

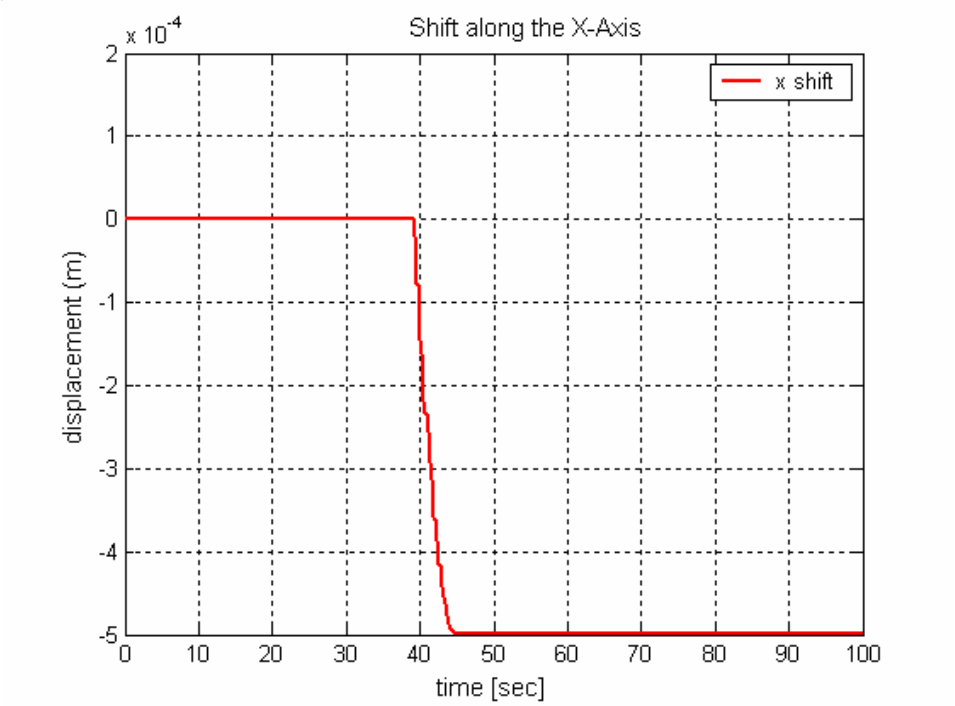

Fig. 5.2.3-1 *X-axis measurement by applying a shift equal to 1 mm*

(1) A resolution equal to 0.62 nm is typical of the plane mirror interferometer (See table 4.1) used in the Optical Delay Line (ODL) built-up (Astrium, Ottobrun). In a first moment, the same LabVIEW file was used for both the ODL and the HP interferometer, without modifying it.

By means of the μ-meter screw, put behind the piezo mount (fig. 5.2.4-2), the Tip/Tilt device, during a 100 seconds test, was shifted along the x-axis by 1 mm. No external test signals were applied at the mirror.

Looking at plot of figure 5.2.4-1, it can be seen that the measured displacement is equal to 0.5 mm.

The reason for this difference, between the imposed and measured value, stands in the erroneous resolution set in the LabVIEW file. Therefore, if *n* is the number of the fringes and:

$$n \cdot 0.62\,\text{nm} = 0.5 \cdot 10^6\ \text{nm} \tag{5.2}$$

setting the proper value of the resolution:

$$n \cdot 1.23\,\text{nm} = 1 \cdot 10^6\ \text{nm} \tag{5.3}$$

will obtained.

The x-axis test demonstrated how much the measurements, effectuated by means of the HP interferometer and its electronics, are accurate and reliable.

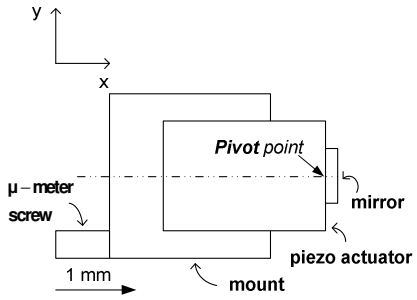

Fig. 5.2.3-2 *Shift along the x-axis*

Part IV

Calibration and Testing of the Real-Time Test-Bed

Chapter 6

Calibration of the RTB

The main goal of the Real-Time Test-Bed build-up, during this work, was to obtain a good match between the E2E-Simulator x_2-x_1 laser readout model and the corresponding laboratory interferometer readout.
Therefore, the designed hardware build-up has to be calibrated. Figure 6.1 shows the ideal case, in which the laser light is perfectly aligned with the centerline, and the real case, in which a misalignment of the beam is present.
The real offset (d_y in figure 6.1) has to be measured and calibrated in order to reach a good correspondence between the real and the simulation results.
In this chapter, the complete RTB calibration procedure and its results are analyzed.

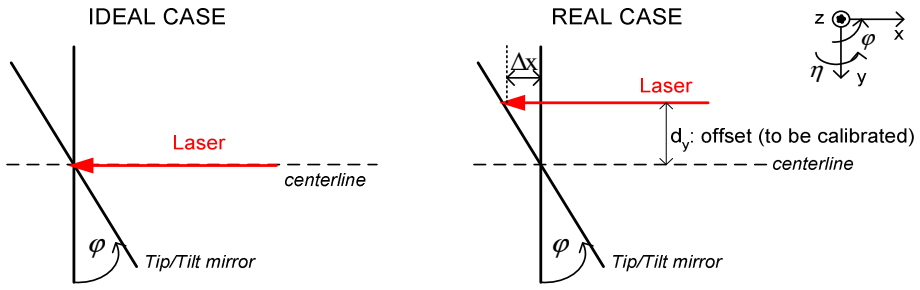

Fig. 6-1 *Beam misalignment*

6.1 Calibration Procedure

The RTB calibration procedure aims at the calculation of the real laser beam position that differs from the nominal one obtained in the ideal case.
The real offset is calculated by means of the identification procedure. Test signals, representing the angles η and φ, are applied to the TM2, i.e. the

piezoelectric mirror (see chapter 5). For this experiment, sinusoidal test signals have been chosen. The relative displacement between TM2 and TM1 at rest, i.e. the voice-coil mirror, is measured by the interferometer.

The distance measurement (Δx) consists of a superposition of the applied sinusoidal signals (see equation (6.2)). The gain and phase variations in the measured Δx signal, calculated by means of the parameter identification, contain the desired information, i.e. the real offset.

The sinusoidal test signals are applied by the dSPACE® RTC and, through a proper Control Desk interface (see Appendix D), it is possible to modify the frequency and the amplitude of the signal as needed.

Looking at the equation (C.10) in Appendix C.3 and neglecting the term due to the quadratic effect, the following relation is given:

$$\Delta x = d_y \cdot \tan\varphi + d_z \cdot \tan\eta \tag{6.1}$$

where d_z and d_y represent the misalignments along, respectively, the z-axis and the y-axis.

Taking into account that η and φ are relatively small, equation (6.1) becomes:

$$\Delta x = d_y \cdot \varphi + d_z \cdot \eta \tag{6.2}$$

In order to simplify the procedure, the test signal is applied just to the rotation around the z-axis (φ). Therefore, the (6.2) becomes:

$$\Delta x = d_y \cdot \varphi \tag{6.3}$$

The equation (6.3) does not take into account that the real angular output of the electronic devices is not really the one that is expected.

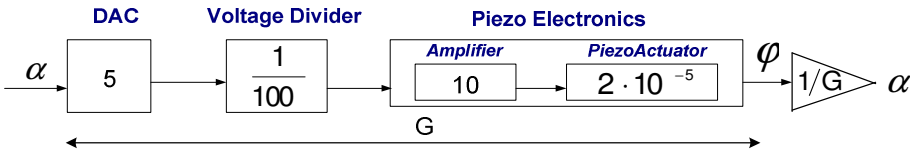

Fig. 6.1-1 *In-line electronics: ideal case*

In the ideal case, the situation would be the one of figure 6.1-1 in which the gains introduced by the electronic devices are represented in the blocks, (see paragraphs 4.2.4/5).
The output angular value will be:

$$\varphi = \underbrace{\left(\frac{5}{100}\cdot 10\cdot 2\cdot 10^{-5}\right)}_{\text{Elecronic devices Gain: G}}\cdot \underbrace{\alpha}_{\text{applied sine amplitude}} \tag{6.4}$$

Considering that, in reality, the hardware gains will be different from the nominal values obtained from the specifications, a factor k has to be taken into account for the calculations (fig.6.1-2).

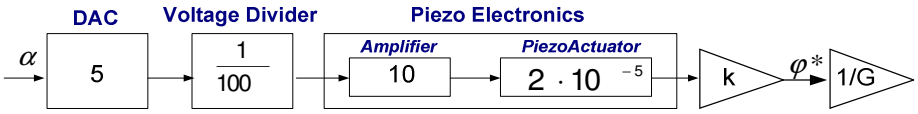

Fig. 6.1-2 *In-line electronics: real case*

Hence:

$$\varphi^* = \underbrace{G\cdot\alpha}_{\varphi}\cdot k \tag{6.5}$$

The factor k is expected to assume a value close to 1 because of the high precision electronics used for the measurement.
By applying the relation (6.5), is obtained:

$$\Delta x = d_y\cdot\varphi^* = \underbrace{\left(d_y\cdot k\right)}_{K}\cdot\underbrace{G\cdot\alpha}_{\varphi} \tag{6.6}$$

where k is equal to 1 in the ideal case. Observing the equation (6.6), it is clear that the multiplicative factor 1/G (fig. 6.1.1/2) has to be taken into account in order to obtain the match between the applied signal (α) and the angle that the mirror effectively realizes (φ).

The identification procedure will estimate the product in parenthesis of the equation (6.6) and not just the misalignment.

However, one can estimate the factor k by using the following procedure, proposed by [32].

Suppose fixing the laser beam at the mirror limit (step 1 in figure 6.1-3). By applying the test signal (φ), it is possible to measure the corresponding value of the relative displacement between the two tip/tilt elements (Δx_1).

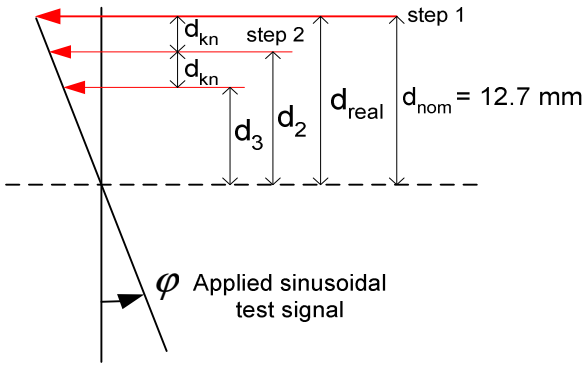

Fig.6.1-3 *Successive measurements*

The equation (6.6), in the specific case, will be:

$$\Delta x_1 = \underbrace{\left(d_{real} \cdot k\right)}_{K_1} \cdot \varphi \qquad (6.7)$$

Observing equation (6.7), it is clear that another measurement is required in order to calculate d_{real} and k separately from each other. Therefore, by moving the piezo μ-meter screw by a known distance (d_{kn}), the laser readout measurement equation, relative to the step 2 in figure 6.1-3, will be equal to:

$$\Delta x_2 = \underbrace{\left(d_{real} - d_{kn}\right) \cdot k}_{K_2} \cdot \varphi \qquad (6.8)$$

From (6.7) and (6.8), it follows:

$$K_2 = \underbrace{d_{real} \cdot k}_{K_1} - d_{kn} \cdot k \tag{6.9}$$

Since K1 and K_2 can be estimated by means of the parameter identification, one is able to obtain k and d_{real} as:

$$\begin{cases} k = \dfrac{K_1 - K_2}{d_{kn}} \\ d_{real} = \dfrac{K_1}{k} \end{cases} \tag{6.10}$$

Obviously, in order to obtain an accurate result, the more measurements carried out the more precise the knowledge of the real laser beam position will be.

Therefore, if *n* is the number of the shifts along the y-axis, will be:

$$\begin{cases} \Delta x_{n+1} = \underbrace{\left(d_{real} - n \cdot d_{kn}\right) \cdot k}_{K_{n+1}} \cdot \varphi \\ k_n = \dfrac{K_1 - K_{n+1}}{n \cdot d_{kn}} \\ k = \dfrac{\sum k_n}{N} \\ d_{real} = \dfrac{K_1}{k} \end{cases} \tag{6.10}$$

where N is the number of the measurements.

Once calculated d_{real}, the actual laser beam position will be known and equal to:

$$d_{act} = d_{real} - n \cdot d_{kn} \tag{6.11}$$

6.2 General Aspects of the Used Estimation Procedure

Each measurement test consists in applying a sinusoidal signal (φ) to the tip/tilt element and in measuring the corresponding relative displacement (Δx) between TMs. During each test, input and output data are recorded so that they can be used for the identification. However, before applying the parameter identification, the data has to be processed.
Therefore, the procedure that led to estimate the beam misalignment is divided into two parts:

- Data Processing
- Parameter Identification

6.2.1 Data Processing

The raw data, Δx and φ, are recorded, respectively, in the LabVIEW® computer and in the Host PC (see chapter 2) containing MATLAB® by means of which the estimation procedure is developed.
These computers are not connected to each other and, so work separately with different clock signals. Therefore, the collected data are characterized in having different sampling frequencies and no synchronization.
Because of these discrepancies and the noise introduced by the surrounding environment, after the data transfer from the LabVIEW® computer to the Host PC, the steps described below are needed.

Length adaptation

The laser readout signal has a sampling frequency equal to 500 Hz (See paragraph 4.2.7); instead, the test signal sampling frequency, set by the user in the Simulink® model implemented in the Real-Time computer, is equal to 100 Hz[(1)] .

(1) In the E2E-Simulator the sampling frequency is set to 10 Hz. During the tests, it was preferred to use a frequency of 100 Hz in order to obtain a DAC output signal, then transferred to the piezo electronics, as much "continuous" as possible

Therefore, when these raw data are imported in MATLAB®, the first signal needs a change in its sampling rate ("resampling").

Detrending

Usually in the measured data slowly variable or linear trends which are not due to the specific physical phenomenon in study (change in the displacement between the TMs as a consequence of their movements) but to other factors, i.e. piezo actuator over-heating, electronics. These trends have to be removed by detrending of data in order to not invalidate the parameter identification. The figure 6.2-1 illustrates an example of Δx detrend.

Coarse Synchronization

As said before, the LabVIEW computer and the Host one, because of the missing connection between each other, start to record data at different times.

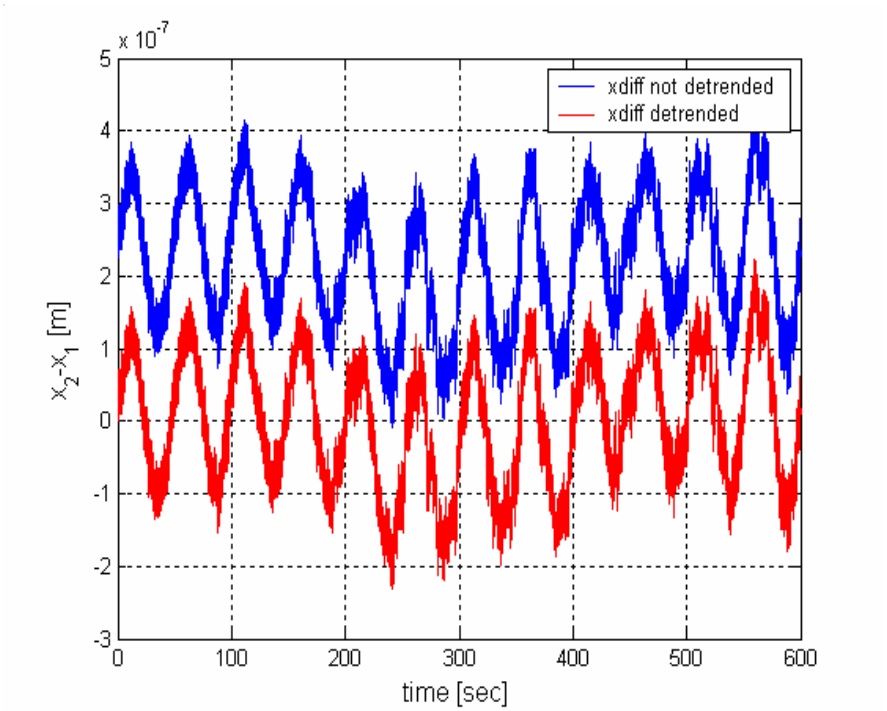

Fig.6.2-1 *Detrending of data*

For this reason, during the tests, it was chosen(2) to start the test signal recording 5 seconds later than the measurement one.
Therefore, during the data processing in order to have correspondence between the two signals, it is necessary to take into account this delay by cutting the first 5 seconds of the laser readout and the last 5 seconds of the test signal.

Filtering

As seen in chapter 5, the external environment (air-conditioning, electronics) introduces high-frequency noise, while other sources could be the cause of low-frequency noise. Therefore, both signals have to be filtered choosing the filter and cut-off frequency.
A low-pass filter passes low frequencies and attenuates those higher than the cut-off frequency. In the specific case, if f is the test signal frequency, the cut-off one was chosen to be:

$$f_{\text{low pass}}^{\text{cut off}} = f + 2 \cdot f \tag{6.12}$$

In order to strictly extract a certain frequency range and to remove the DC offsets and low frequency drifts, a band-pass filter could be used. The chosen pass band is equal to:

$$f_{\text{band pass}}^{\text{cut off}} = \left[f - \frac{f}{2} \quad f + \frac{f}{2} \right] \tag{6.13}$$

Both low-pass and band-pass filter were implemented in the data processing procedure. The one that guarantees better results is the band-pass filter.

(2) The choice is possible because of the Control Desk Interface (Appendix C) that permits to set the time in which starting the recording.

Fine Synchronization

The coarse synchronization does not ensure perfect correspondence between the two signals because of the different clock signals due to the missing connection between the LabVIEW® computer and the Host PC.
In order to match the signals, it is necessary to know the time-shift between them in order to translate one over the other of that quantity.
The fine synchronization is related to the calculation of the cross-correlation function. It is defined as the average product of a signal, X(t), with a time shifted signal, $Y(t + \tau)$:

$$R_{xy} = E\{X(t)Y(t+\tau)\} \tag{6.14}$$

where E denotes the mathematical expectation.
Therefore, the cross-correlation function provides a statistical comparison between the two signals as a function of the time-shift between them.
A MATLAB function was implemented in order to realize the fine synchronization and so, to calculate the cross correlation functions, R_{xy} and $R_{yx.}$ The former is given by the equation (6.14), the latter, on the contrary, is representative of the time shifting of the X signal over the Y signal. When the cross correlation reaches a maximum, X and Y are perfectly correlated. The time value corresponding to that maximum is the one necessary to shift one signal over the other in order to reach the perfect correspondence between them [32]. The found time shift should be as close as possible to zero because the signals had been already coarse synchronized.

6.2.2 Principle of Parameter Identification

The basic principle of the Parameter Identification is to process measured input and output signals of a mechanical system in order to adapt the parameters of a predefined mathematical description so that the accordance between measured and simulated data is as close as possible (Fig. 6.2.2-1).

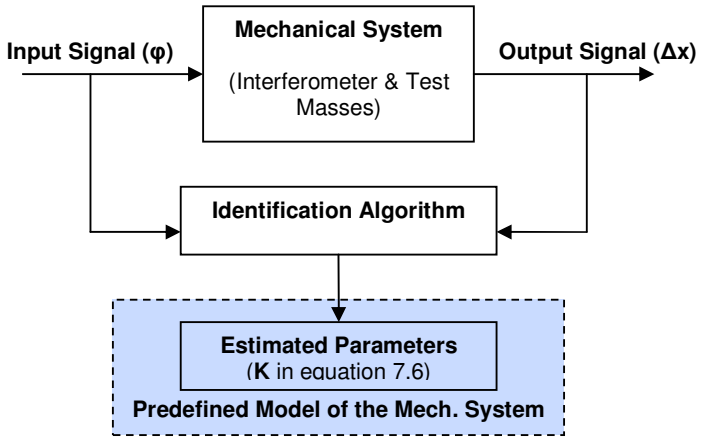

Fig. 6.2.2-1 *Principle of Parameter Identification*

The Identification Algorithm that estimates the parameters is based upon a statistical method, called Least Square method (LSQ).

The mathematical description of the specific physical phenomenon is represented by the equation (6.6). In a more general formulation, the I/O model is given by:

$$\Gamma(N) = \Psi(N) \cdot \Theta \tag{6.15}$$

where:

Γ: vector representing the laser readout

Ψ: test signal vector

Θ: unknown parameter

N: number of components of the vectors Γ and Ψ

The equation (6.15) assumes undisturbed measurement data. Since the measurement data are always superposed by disturbances, the equation changes according to:

$$\Gamma(N) = \Psi(N) \cdot \Theta + \vec{e}(N) \tag{6.16}$$

where $\vec{e}(N)$ is the vector of equation errors.

In least square estimation unknown parameters of a linear model are chosen in such a way that the sum of the squares of the difference between the actually observed and the computed values is a minimum, [31]. For a linear system, i.e. the one in study, this translates into finding the parameter that minimizes the following "loss function":

$$V(\Theta, N) = \frac{1}{2}\sum_{k}^{N}\left(\underbrace{\Gamma(k)}_{\text{process}} - \underbrace{\Psi(k)\cdot\Theta}_{\text{model}} \right)^2 \tag{6.17}$$

Solving for the minimizing parameters the closed form solution as follows is obtained:

$$\hat{\Theta}_{LS} = \left[\Psi^T(N)\cdot\Psi(N)\right]^{-1}\cdot\Psi^T(N)\cdot\Gamma(N) \tag{6.18}$$

where $\hat{\Theta}$ is the estimate of the parameter Θ.

6.3 Calibration Results

Several tests were carried out in order to calculate the laser beam real offset. The results analyzed in this paragraph were obtained by considering three successive measurements.

6.3.1 Set-Up of Identification Experiment

The first measurement test was carried out by fixing the laser beam at the mirror edge; the following two by shifting it each time by 0.004 m, as visible in figure 6.1.3.

As test signal, a sine wave at 0.02 Hz was chosen. Such a low frequency was chosen in order to reduce as much as possible the effects of the missing connection between the LabVIEW and the Host PCs; in fact, for this reason,

the two PCs have different time clocks and if the frequency, *f*, is low enough, whatever value the time assumes, the product $2\pi f \cdot t$, representing the phase shift between the signals, will be small and the mismatch due to different clocks is negligible.

Summarizing, the tests settings are listed below:

- applied sine amplitude: α = 1 rad
- hardware gain: G = 10^{-5}
- test signal frequency: f = 0.02 Hz
- test signal sampling frequency: f_s= 100 Hz
- measurement signal sampling frequency: f_s = 500 Hz
- experiment time: 600 sec
- shifted displacement: d_{kn} = 0.004 m

6.3.2 Raw Data Processing

Figure 6.3.2-1 shows the measurement raw data of the first test that was carried out.

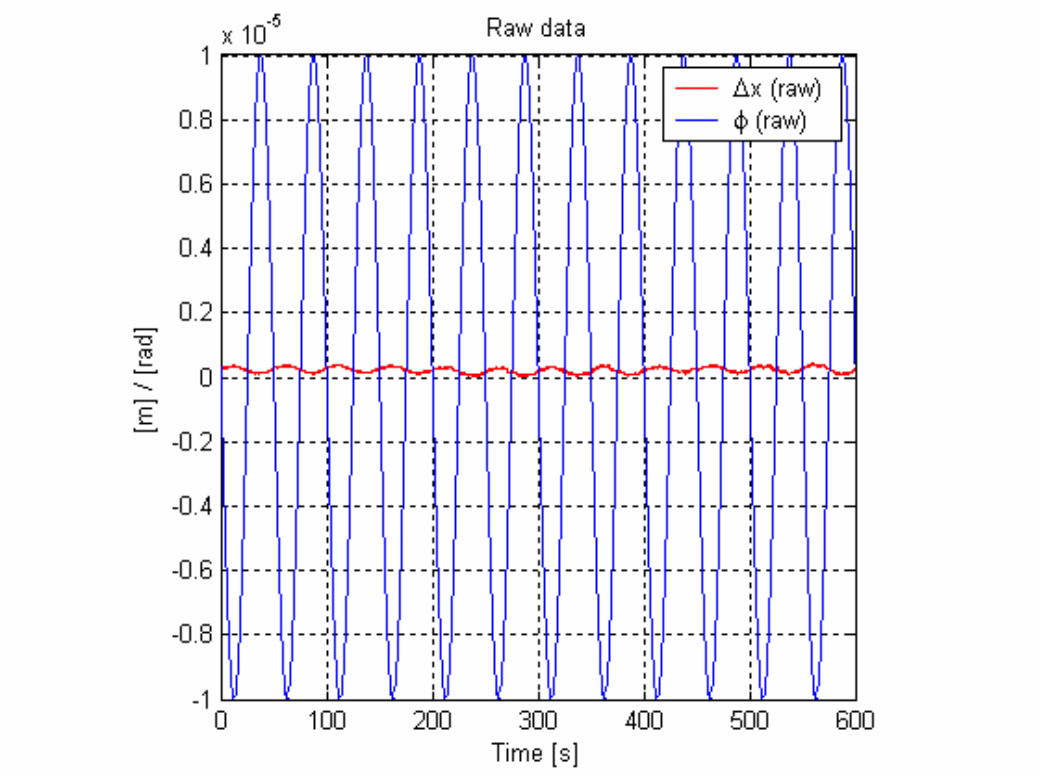

Fig. 6.3.2-1 *Measurement raw data*

In particular, figure 6.3.2-1 shows the test signal, φ, and the laser readout signal, Δx, after the length adaptation. The bias of the two signals has to be removed (figure 6.3.2-2).

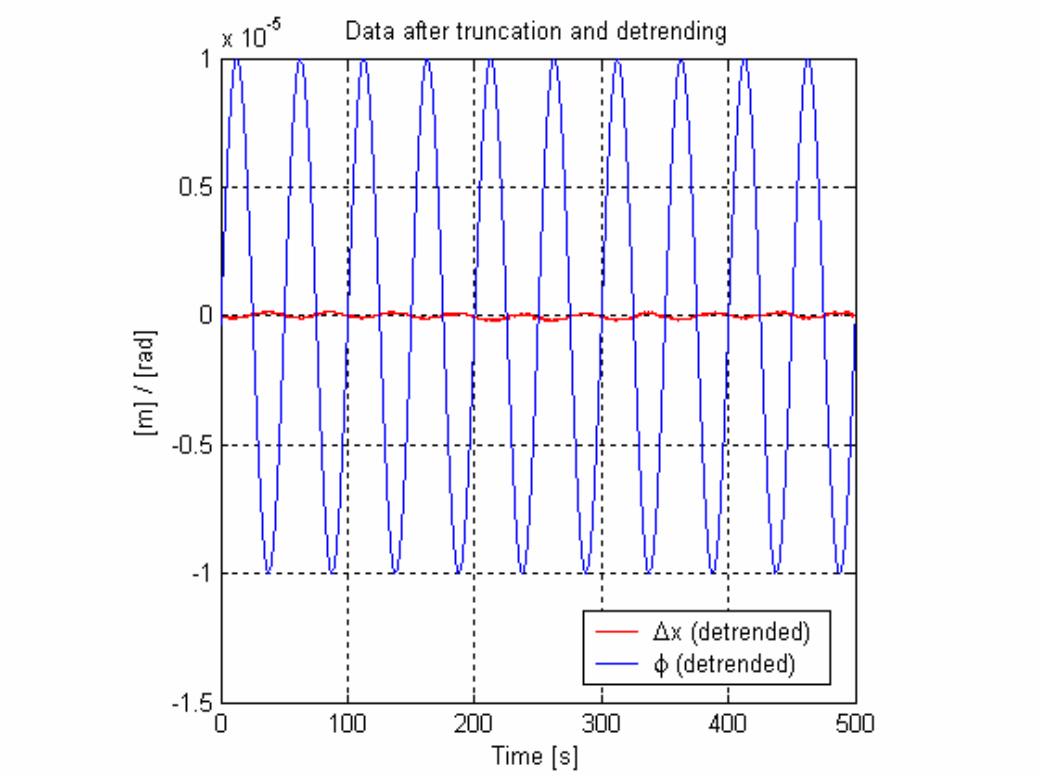

Fig. 6.3.2-2 *Detrended data*

As observable from the above figures, the two signals are out of phase. As seen before, the presence of the mismatch is due to the different time clocks of the LabVIEW and Host PCs. The former is the one that stores displacement data (Δx), the latter is the one that stores the input data (φ).

This becomes clear looking at the cross-correlation function in the plot of figure 6.3.2-3. A time-shift of 5.36 seconds corresponds at the maximum point of the function.

After the coarse and fine synchronizations, the two signals are perfectly correlated.

Before the parameter identification can be accomplished the signals need to be filtered.

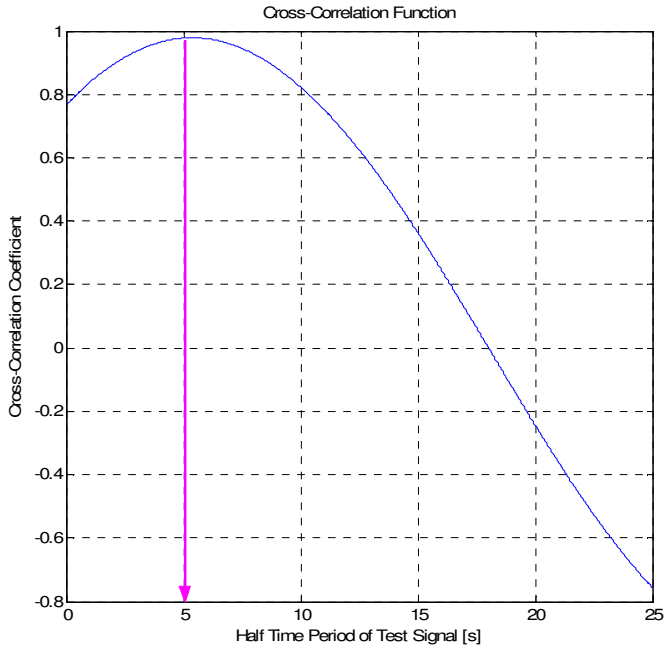

Fig. 6.3.2-3 *Cross-Correlation function*

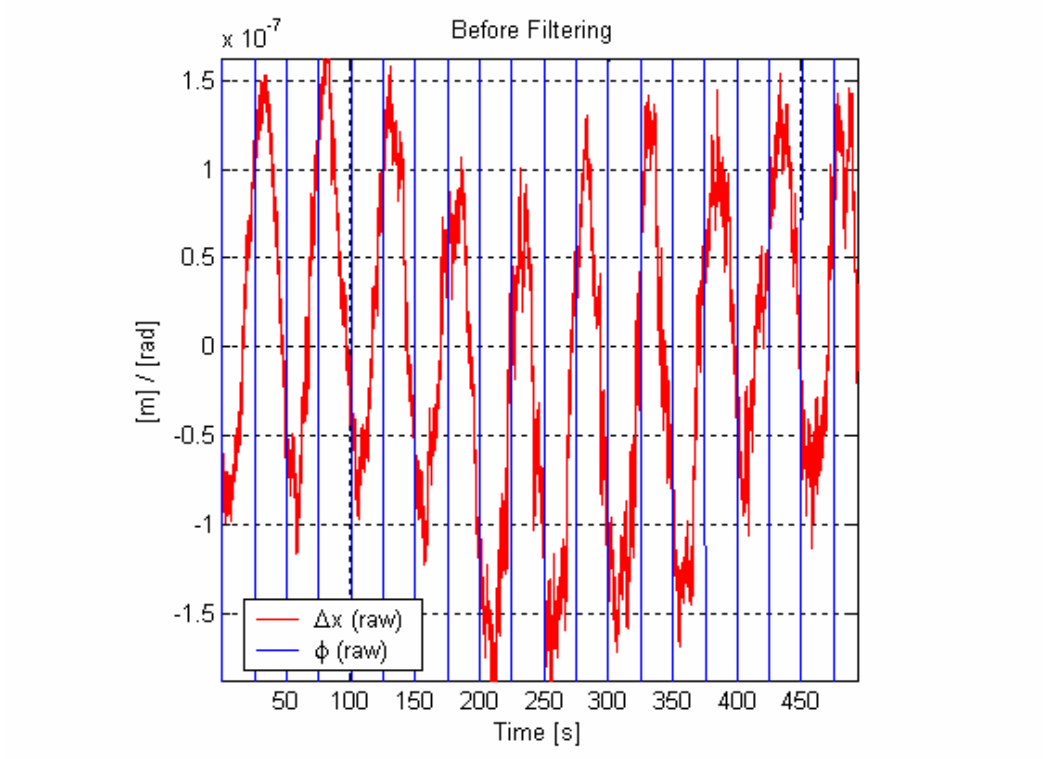

Fig. 6.3.2-4a *Filtering effects*

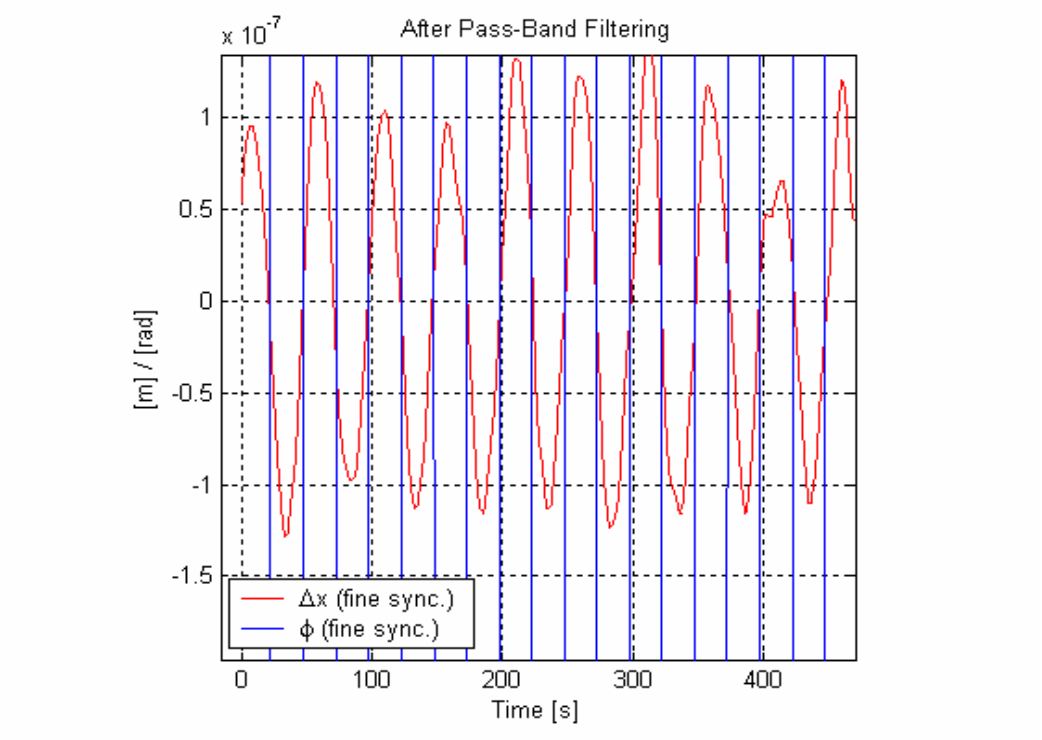

Fig. 6.3.2-4b *Filtering effects*

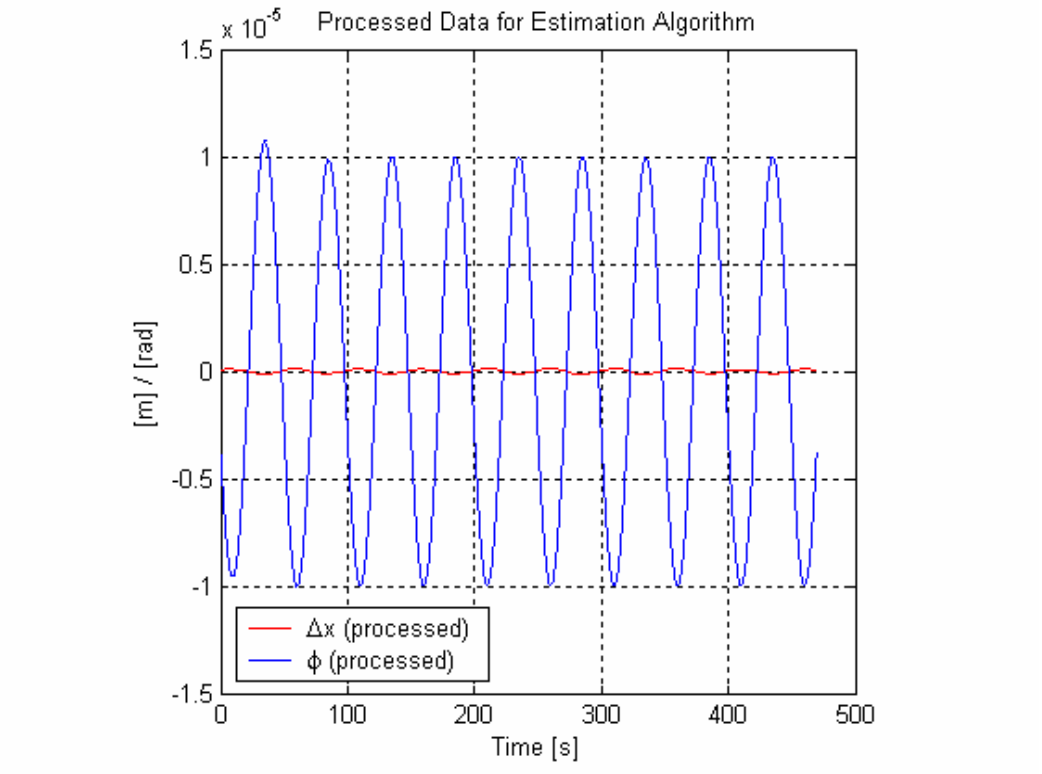

Fig. 6.3.2-5 *Processed data*

Figures 6.3.2-4a/b show how the laser readout looks after and before the application of a pass-band filter with cut-off frequencies given by the relation (6.13). The processed signals ready for the Parameter Identification are visible in figure 6.3.2-5.
The collected raw data relative to the other tests carried out, underwent to the same data processing.

6.3.3 Final Results Obtained from Statistical Estimation Methods

The estimation procedure based on the least square method led to the following solutions:

	Parameter ($K = k \cdot d$)
1st test	- 0.011575 m
2nd test	- 0.007745 m
3rd test	- 0.003745 m

Table 6.1 *Parameter Identification Results*

According to the iterative calculation as described by the equations (6.10), the obtained values of the factor k and of the misalignment d_{real} are:

- k = - 0.9788
- d_{real} = 0.011855 m

Because of the high precision electronic system used the k factor is expected to be more or less 1.
As calibration results shows, the k real value differs from the k ideal value by a 2% error. Therefore, effectively, the electronic devices involved together with a closed-loop functioning and the resolution of the piezo actuator guarantee a high level of accuracy and precision.
The calibration performance reached is good but it is limited by some factors:

- errors in d_{kn} (the μ-meter screw is moved manually, it does not guarantee high measurement precision)
- disturbances due to the no vacuum and noisy environment
- errors in the test signal (α) application due to the eventual delays in transmitting the signal among the electronic devices.

The laser beam real position d_{real} does not differ from the nominal one (fig. 6.1-3) very much. Its determination is really important in order to know the actual laser position once the beam of a known quantity is shifted, according the relation (6.11).

In order to reach the match between the simulation and the laboratory laser readout, the real misalignment could be introduced in the OMU initialization file (*Sens_OMU_init.m*), inside the E2E-Simulator, so that the simulated and the real laser beam assume the same position.

Chapter 7

Summary and Outlook

7.1 Conclusions

During this work, a first stage real-time test-bed for LISA Pathfinder was implemented.

The hardware part of the used-sensor in the RTB is represented by a HP interferometer that replaces the x_2-x_1 E2E-Simulator interferometer model. The HP interferometer is able to measure the relative displacement between two moving mirrors representing the LISA Pathfinder test masses. These mirrors are tip/tilt elements which realize the two degrees of freedom test mass motion, namely: the rotation around the y-axis (η) and the rotation around the z-axis (φ).

These angular values are the solutions for the nonlinear equations of motion, which are provided by the E2E-Simulator. The E2E-Simulator, implemented on the RTC, transformed the angular values into the required actuation signals for the tip/tilt mirrors (Voice-Coil and Piezoelectric mirrors).

Due to the mirror movement, the position information, detected by the laser electronics in terms of changes in the interferometric fringes number, is expressed in nanometer and visualized on the LabVIEW computer, VME connected with the laser electronics devices.

Such RTB built-up represents an open loop system (no feedback of the optical measurement to the DFACS). In fact, unfortunately, the dSPACE® RTC does not permit a VME connection that could close the loop.

Moreover, the RTB was calibrated by means of a calculation procedure that led to estimate the real laser beam position on the tip/tilt mirrors surface, in

order to obtain a good match between the E2E-Simulator and the laboratory interferometer readouts. The accuracy is of about the 98%.
The test-bed final configuration, that was implemented in the scope of the thesis, presents performances which are, obviously, lower than the LTP x_2-x_1 interferometer ones; however, better performances could be achieved simply by finding solutions to isolate the interferometer from the external environment.
Despite the noisy working environment (no vacuum, presence of electronic devices, etc.), the results demonstrated that the RTB is usable for functional DFACS testing in the measurement bandwidth of 1 mHz- 30 mHz.
In conclusion, the implemented RTB represents a first step toward a more advanced test-bed with as much hardware in loop as possible.

7.2 Prospects for Future Work

The actual RTB could evolve toward an LTP-RTB that will aim at testing the DFACS in closed-loop, including the hardware of the Optical Metrology System and the sensors/actuators stimulus/feedback equipment.
The procedure that will lead to develop the LTP-RTB is summarized in the block diagram of figure 7.2-1.
Considering the present RTB as a starting point, the following two developing strategies could be realized in future work:

- **Mode A1**

  This option realizes the connection between the VME bus containing the Laser Axis Board and the dSPACE® computer in order to obtain a closed loop system. The currently used dSPACE® Real-Time Platform, (DS1005 PPC) does not permit a VME connection. Moreover, the dSPACE Inc. supplies boards with VME connection but no specific software support is available. Therefore, another solution should be found.

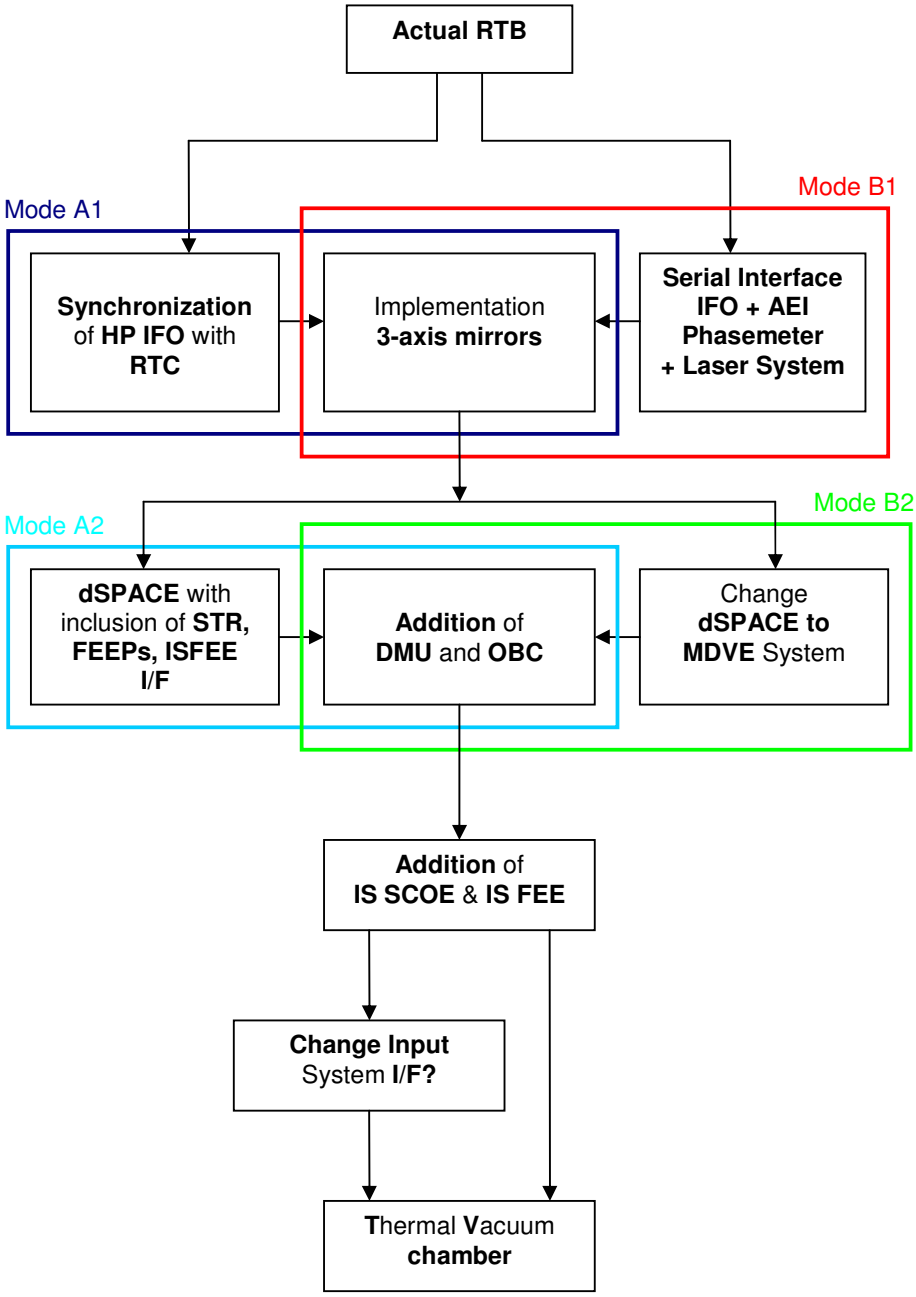

Fig.7.2-1 *Developing procedure for the LTP-RTB*

- **Mode B1**

  If this solution is adopted, the HP interferometer and its laser electronics should be substituted with a table-top interferometer very similar to the LTP one with the same laser system, i.e. the Phasemeter Front-End and Laser Assembly. This interferometer has a serial interface that can be easily connected with the DS1005 PPC.

Whether the mode A1 or the mode B1 will be adopted the test masses should be represented by 3-axis mirror; it means that, for example, the Voice-Coil and piezoelectric mirrors have to be replaced by at least 3 DoF (η, φ, x) elements in order to better simulate the test masses motion.
As a second step one of the following modes could be followed:

- **Mode A2**

  This solution provides for the possibility of using in parallel two dSPACE processors, one containing the Phasemeter Back-End (DMU eventually) algorithms and the DFACS on-board algorithms, the other working as Real Time Simulator (RTS) that will load and execute the environment simulation code (fig. 7.2-2). This RTB configuration will include STR, FEEPs and IS FEE interfaces.

- **Mode B2**

  In this case, no dSPACE platform will be used and the DMU and OBC Simulator interact with a Power PC containing the environmental simulation code according to the Model based Development Verification (MDV) procedure (fig.7.2-3). In this situation, also, the sensors and actuators will be represented by stimulation/monitoring interfaces.

The third step consists in the addition to the RTB of the IS SCOE and IS FEE. The former converts sensing signals simulated into realistic analog sensing currents that are injected into the coax input of the IS electronics. The latter is the Engineering Model of the Inertial Sensor Front-End Electronics.
The *final step* foresees putting the OMS into a thermal vacuum chamber.

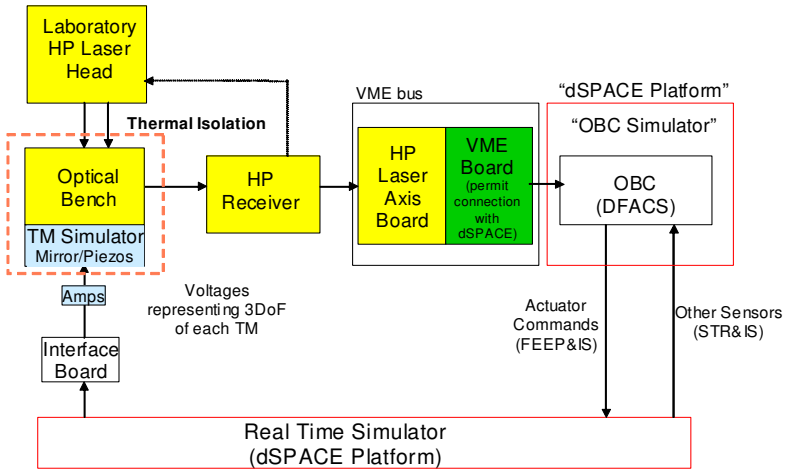

Fig.7.2-2 *RTB: Combination of A1 and A2 modes*

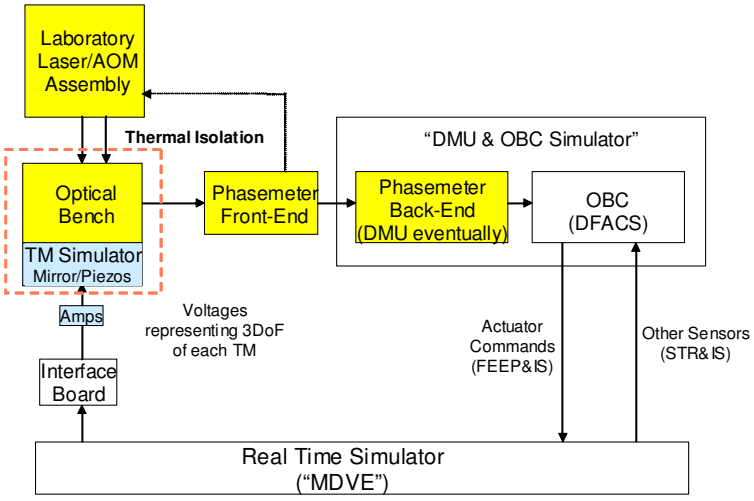

Fig.7.2-3 *RTB: Combination of B1 and B2 modes*

Appendix A

A.1 E2E-Simulator S-functions Modifications

Before describing the implementation procedure, it necessary to report the simplified models introduced in the E2E Performance Simulator instead of *GravityField* and *SolarForceTorqueInterpolation* S-functions because of the problems they introduced during the procedure.

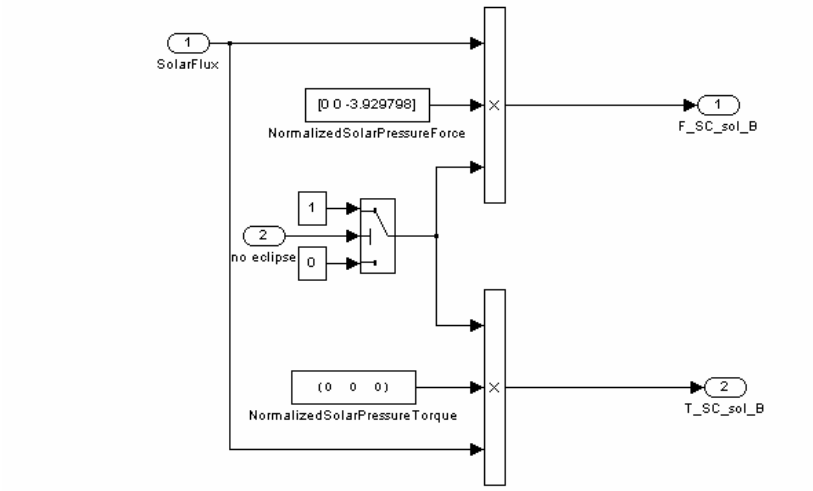

Fig. A.1-1 *Simplified SolarForceTorque model*

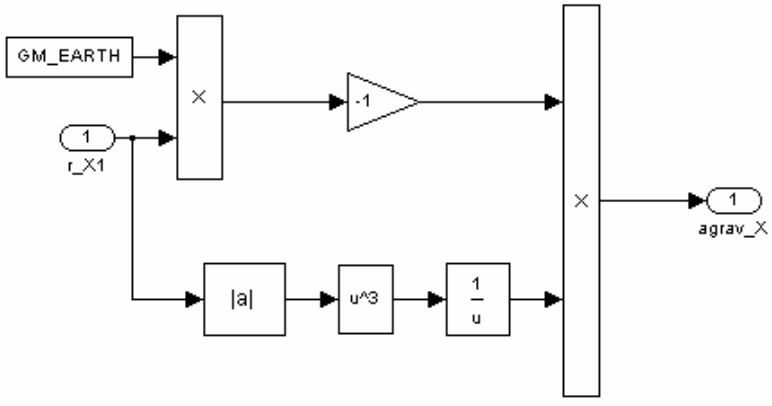

Fig. A.1-2 *Simplified GravityField model*

A.2 Implementation Procedure

In order to obtain a good organized and optimized code for the model all the options had to be set in a proper way in the Simulation Parameter window (Simulation menu):

Solver pane

The stop time was set to INF, in this way the generated program runs on the real-time platform indefinitely. In Control Desk, when the Animation Mode is chosen (it permits to transfer data from/to the platform), the user could set the stop time as parameter, modifying it as needed.

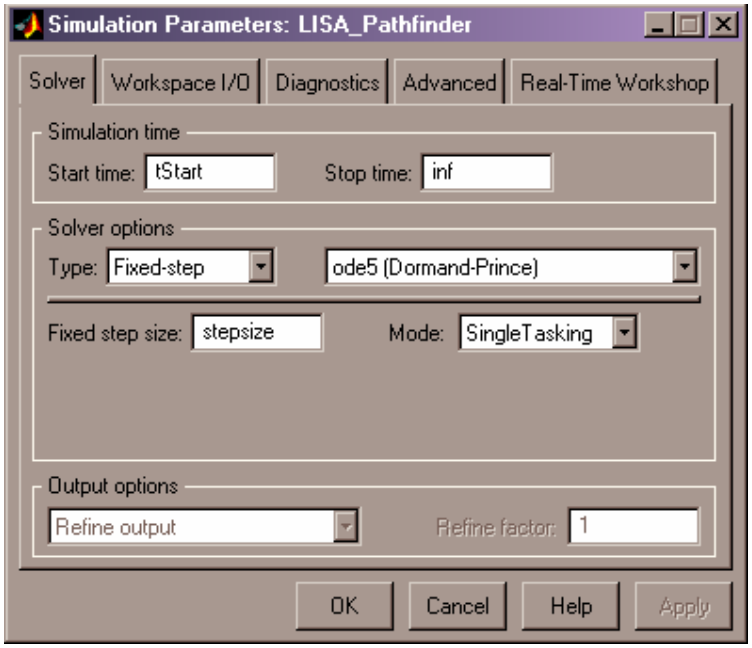

Fig. A.2-1 *Solver pane*

The solver options must be equal w.r.t. the Simulink model.

Advanced Pane

This pane is used to specify options that define the behavior for various blocks. The "inline parameter" option must be unchecked, in this way the block parameters are generated as variables, so they are modifiable during the

real-time simulation. The optimizations were chosen as suggested by dSPACE HelpDesk:

Block reduction	Off
Boolean logic signals	On
Conditional input branch	Off
Parameter pooling	On
Signal storage reuse	Off
Zero crossing detection	On

***Fig. A.2-2** Optimizations*

Real-Time Workshop pane

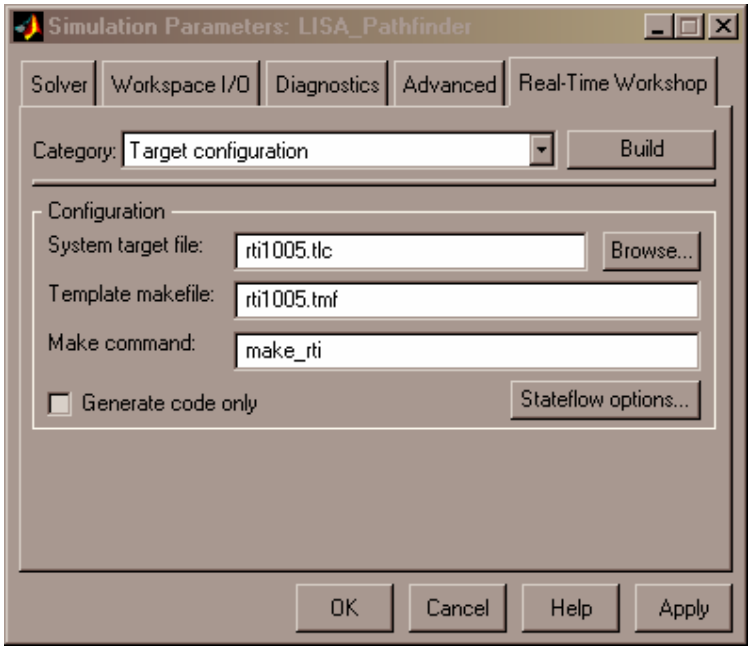

***Fig. A.2-3** Real-Time Workshop pane*

This pane is used to specify the RTI driver programs that control the automatic build process, to set different Real-Time Workshop and RTI simulations, build variable description file, and download options. The following categories contain settings relevant to RTI:

- Target configuration category: when a new model is created, RTI automatically selects the correct system target file, the template makefile and the make command (fig. A.2-3)
- General code generation options category (default configuration)

- General code generation options (cont.) category (default configuration)
- RTI simulation options category: the initial simulation state was set to RUN (the simulation is started right after the download) and "real-time" was selected, as execution mode.
- RTI general build options category (default configuration)
- RTI load options category (default configuration)
- RTI variable description file options category: signal labels, virtual blocks were made available in the variable description file.
- RTI variable description file options category: the "include initial parameter values" was checked to make the initial parameter values available in the variable description file.

The implementation procedure starts by pushing the "build" button (fig. A.2-3). In this way, the Real-Time Workshop® and the dSPACE® RTI start to generate the E2E-Simulator C-code that, at the end of the process, will be downloaded on the *real-time* platform.

A.3 User Makefile

If there are S-Functions in the Simulink model, the first time the user starts the implementation process it fails, creating a *user makefile* in the MATLAB working directory. This happens because RTW is not able to find the S-Functions source and include files. Therefore it is necessary to compile the created *user makefile* specifying the extra paths, directories and missing source files.

```
# ===========================================================================
#  Make include file actuators_model_usr.mk:
#
#   RTI1005 5.0 (19-Apr-2004)
#   Thu Feb 09 10:10:34 2006
#
#   Copyright (c) 1999-2002 dSPACE GmbH, GERMANY
# ===========================================================================

# ===========================================================================
# ===== Define file version macro. Never change this value. ================
# ===========================================================================
USER_MAKEFILE_VERSION = 2
# ===========================================================================
```

```
# ------------------------------------------------------------------------------
# Macros for user-specific settings.
#
# All macros below may list several items (files or directories). You can
# separate multiple items with blanks or list them on several lines using
# the \ (backslash) as line continuation character.
#
# The directory names may include absolute or partial path
# descriptions, e.g., .\project1\file3.c
#
# Blanks in directory or file names are not allowed.
#
# Examples:
#
# USER_SRCS = file1.c file2.c file3.c
#
# USER_SRCS = \
#   file1.c \
#   file2.c \
#   file3.c
#
# ------------------------------------------------------------------------------
# Enable C++ support
USER_BUILD_CPP_APPL = ON
# Directories where S-Function C source files are stored.
SFCN_DIR =\
D:\Marianna\E2E_Simulator\Sfunctions\IS_model \
D:\Marianna\E2E_Simulator\DFACS_Algorithms\Sfunctions\meas_processing \
D:\Marianna\E2E_Simulator\DFACS_Algorithms\Sfunctions\sensor_mapping \
D:\Marianna\E2E_Simulator\DFACS_Algorithms\Sfunctions\guidance \
D:\Marianna\E2E_Simulator\DFACS_Algorithms\Sfunctions\reference_attitude \
D:\Marianna\E2E_Simulator\DFACS_Algorithms\Sfunctions\controller \
D:\Marianna\E2E_Simulator\DFACS_Algorithms\Sfunctions\manual_commands \
D:\Marianna\E2E_Simulator\DFACS_Algorithms\Sfunctions\decoupling\
D:\Marianna\E2E_Simulator\DFACS_Algorithms\Sfunctions\ThrusterActuation\
D:\Marianna\E2E_Simulator\DFACS_Algorithms\Sfunctions\capacitive_actuation \
D:\Marianna\E2E_Simulator\Sfunctions\SolarForceTorqueInterpol \
D:\Marianna\E2E_Simulator\Sfunctions\STARS \
D:\Marianna\E2E_Simulator\Sfunctions\Charge_management \
D:\Marianna\E2E_Simulator\Sfunctions\Gravity_Gradient \
D:\Marianna\E2E_Simulator\Sfunctions\Additional_Dynamics \
D:\Marianna\E2E_Simulator\Sfunctions\Collision_Dynamics \
D:\Marianna\E2E_Simulator\Sfunctions\EoM_18DoF \
D:\Marianna\E2E_Simulator\Sfunctions\OMS_simple

# Additional C source files to be compiled (file name extension .c).
USER_SRCS = \
is_initialize_rtw.c Vact_to_Fcap_rtw.c Vact_to_Fcap_inst_rtw.c
x_to_C_rtw.c \
IS_processing.c IS_processing_data.c meas_processing.c OMU_processing.c
STR_processing.c matvec.c \
       sensor_mapping_data.c sensor_mapping.c mat_func.c \
       guidance.c guidance_data.c \
       reference_attitude.c \
       controller.c controller_data.c \
       manual_commands.c \
       decoupling.c decoupling_data.c \
       mat_func2.c PinvSolve.c thruster_actuation.c thruster_actuation_data.c \
       capacitive_actuation.c capacitive_actuation_data.c \
SolarForceTorqueInterpol_sf.cpp Matvec.cpp matAlloc.c math2.c   errorHandler.c
ForceTorqueInterpolation.cpp InFile.cpp \
       GravityField.cpp SphericHarmonic.cpp matvec.c \
numrec.c mat_func.c gravityField_sf.cpp TM_gg_accel.c MatrixN.cpp
errorHandler.c \
tm_charge.c tm_discharge.c MJ_Matrix.c apparentSunPos_Q.c gmst.c EQ_Matrix.c
nutationParameters.c \
       precessionParameters.c moonPos_M.c QM_Matrix.c \
       Additional_Dynamics.cpp Additional_Dynamics_sf.cpp \
EoM_18DoF.cpp EoM_18DoF_sf.cpp Hit_detection.c mat_func3.c Hit_calculation.c
distance_calculation.c zbrent_double.c \
       OMS_simple.c is_initialize_rtw.c x_to_C_rtw.c C_to_Vs_rtw.c

# Additional assembler source files to be compiled (file name extension .asm).
USER_ASM_SRCS =
```

```
# Directories where additional C and assembler source files are stored.
USER_SRCS_DIR =\
D:\Marianna\E2E_Simulator\Sfunctions\IS_model\Source\
D:\Marianna\E2E_Simulator\DFACS_Algorithms\Sfunctions\meas_processing\Source\
D:\Marianna\E2E_Simulator\DFACS_Algorithms\Sfunctions\sensor_mapping\Source\
D:\Marianna\E2E_Simulator\DFACS_Algorithms\Sfunctions\guidance\Source\
D:\Marianna\E2E_Simulator\DFACS_Algorithms\Sfunctions\reference_attitude\Source
\
D:\Marianna\E2E_Simulator\DFACS_Algorithms\Sfunctions\controller\Source\
D:\Marianna\E2E_Simulator\DFACS_Algorithms\Sfunctions\manual_commands\Source\
D:\Marianna\E2E_Simulator\DFACS_Algorithms\Sfunctions\decoupling\Source\
D:\Marianna\E2E_Simulator\DFACS_Algorithms\Sfunctions\ThrusterActuation\Source\
D:\Marianna\E2E_Simulator\DFACS_Algorithms\Sfunctions\capacitive_actuation\Sour
ce\
D:\Marianna\E2E_Simulator\DFACS_Algorithms\Sfunctions\Common\Source\
D:\Marianna\E2E_Simulator\Sfunctions\SolarForceTorqueInterpol\Source \
D:\Marianna\E2E_Simulator\Sfunctions\STARS\Source \
D:\Marianna\E2E_Simulator\Sfunctions\Charge_management\Source \
D:\Marianna\E2E_Simulator\Sfunctions\Gravity_Gradient\Source \
D:\Marianna\E2E_Simulator\Sfunctions\Additional_Dynamics\Source \
D:\Marianna\E2E_Simulator\Sfunctions\Collision_Dynamics\Source\
D:\Marianna\E2E_Simulator\Sfunctions\EoM_18DoF\Source \
D:\Marianna\E2E_Simulator\Sfunctions\OMS_simple\Source \
D:\Marianna\E2E_Simulator\Sfunctions\Common\Source
# Path names for user include files.
USER_INCLUDES_PATH =\
D:\Marianna\E2E_Simulator\Sfunctions\IS_model\Include\
D:\Marianna\E2E_Simulator\DFACS_Algorithms\Sfunctions\meas_processing\Include\
D:\Marianna\E2E_Simulator\DFACS_Algorithms\Sfunctions\sensor_mapping\Include\
D:\Marianna\E2E_Simulator\DFACS_Algorithms\Sfunctions\guidance\Include\
D:\Marianna\E2E_Simulator\DFACS_Algorithms\Sfunctions\reference_attitude\Includ
e
D:\Marianna\E2E_Simulator\DFACS_Algorithms\Sfunctions\controller\Include\
D:\Marianna\E2E_Simulator\DFACS_Algorithms\Sfunctions\manual_commands\Include\
D:\Marianna\E2E_Simulator\DFACS_Algorithms\Sfunctions\decoupling\Include\
D:\Marianna\E2E_Simulator\DFACS_Algorithms\Sfunctions\ThrusterActuation\Include
\
D:\Marianna\E2E_Simulator\DFACS_Algorithms\Sfunctions\capacitive_actuation\Incl
ude\
D:\Marianna\E2E_Simulator\DFACS_Algorithms\Sfunctions\Common\Include\
D:\Marianna\E2E_Simulator\Sfunctions\SolarForceTorqueInterpol\Include \
D:\Marianna\E2E_Simulator\Sfunctions\STARS\Include\
D:\Marianna\E2E_Simulator\Sfunctions\Charge_management\Include\
D:\Marianna\E2E_Simulator\Sfunctions\Gravity_Gradient\Include\
D:\Marianna\E2E_Simulator\Sfunctions\Additional_Dynamics\Include\
D:\Marianna\E2E_Simulator\Sfunctions\Collision_Dynamics\Include \
D:\Marianna\E2E_Simulator\Sfunctions\EoM_18DoF\Include \
D:\Marianna\E2E_Simulator\Sfunctions\OMS_simple\Include\
D:\Marianna\E2E_Simulator\Sfunctions\Common\Include\

# Additional user object files to be linked.
USER_OBJS =

# Additional user libraries to be linked.
USER_LIBS =

# EOF -------------------------------------------------------------------------
```

RTI and RTW work only with C-code S-Functions. By mean of dSPACE integration kit, it was possible to implement the C++ code S-Functions contained in the E2E Performance simulator. RTI's C++ support is enabled by setting the USER_BUILD_CPP_APPL to the ON value in the *user makefile* (yellow in the script). RTW does not recognize an S-Function as C++, it assumes that an S-Function is C code and therefore tries to locate and compile

a C source instead of a C++ source. To work around this limitation two steps are necessary:

- To provide an empty dummy C source with the same file name as the original C++ source (e.g. Additional_Dynamics.cpp / Additional_Dynamics.c) inserting it in the directory where the S-Function C source file is stored.
- To add the original C++ source to the USER_SRCS of the *user makefile* (yellow in the script).

A.4 Simulink/Real-Time Simulations: Matching of Results

After implementing the E2E Performance simulator on the dSPACE platform, the perfect match between Simulink and Real-Time simulations was verified. The plots below show the simulations results:

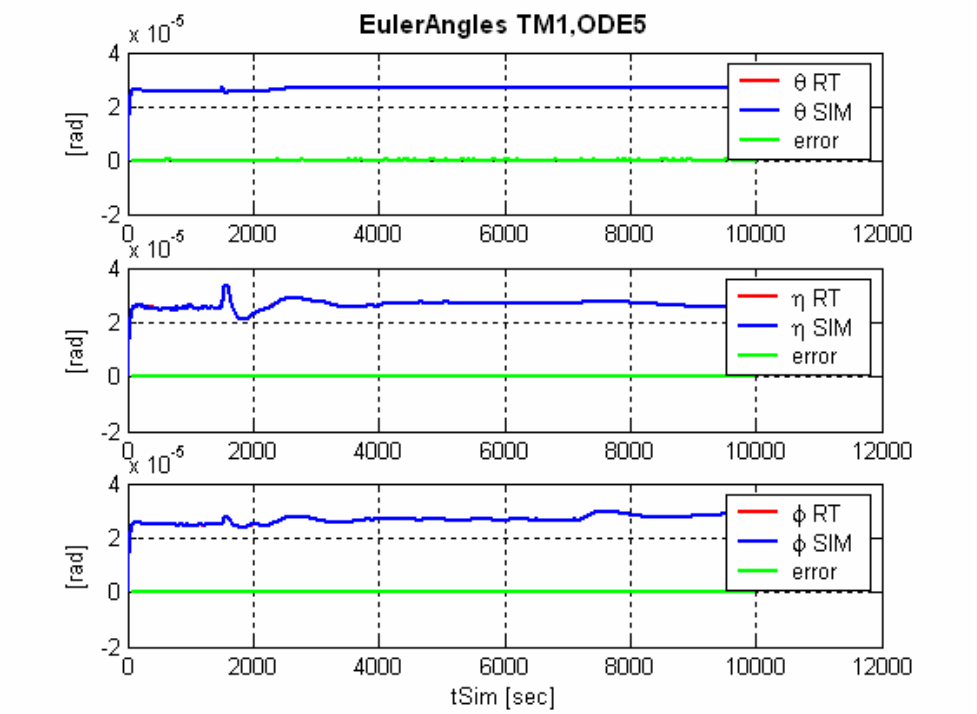

Fig. A.4-1 *Euler Angles of test mass 1*

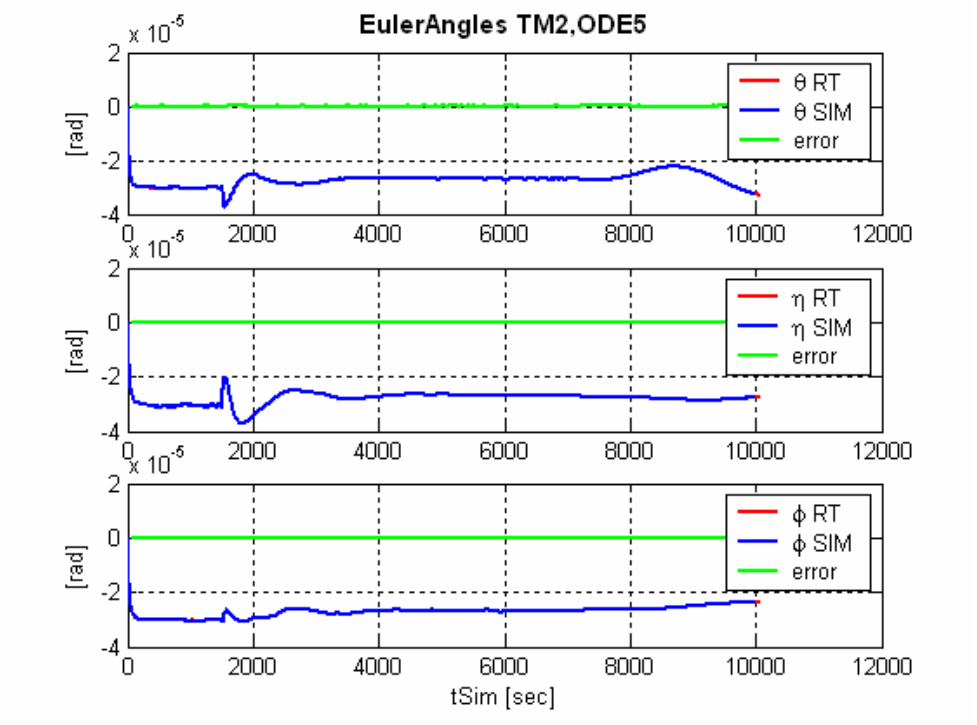

Fig. A.4-2 *Euler Angles of test mass 2*

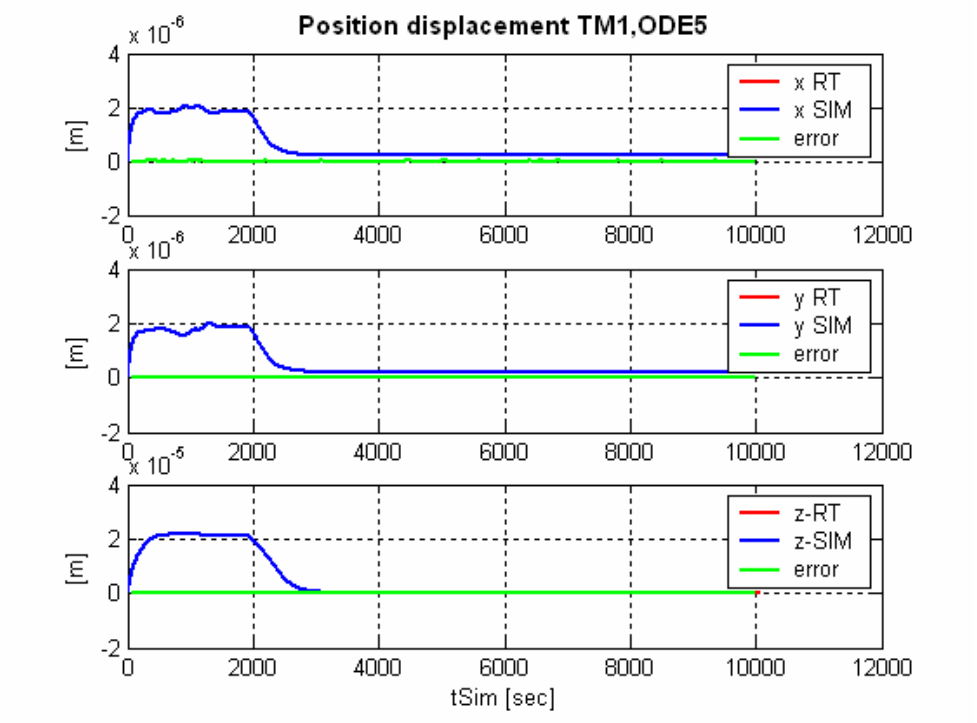

Fig. A.4-3 *Position displacement of test mass 1*

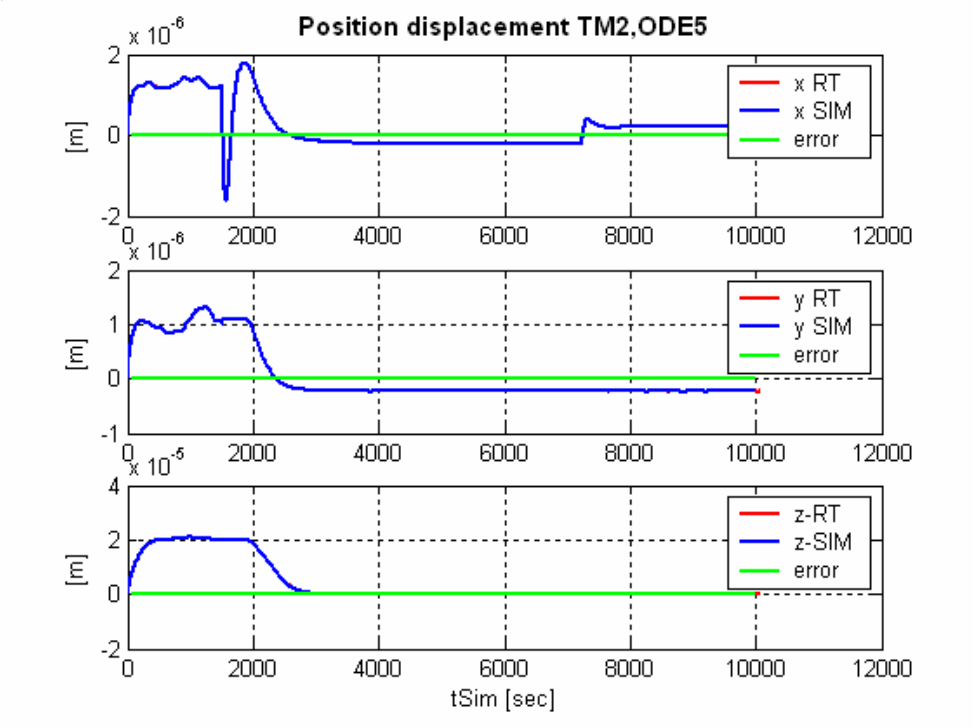

Fig. A.4-4 *Position displacement of test mass 2*

Appendix B

B.1 Telecommands Modification

The task of the MATALB functions that were deleted in the telecommands block, because of the RTW limitations, was to call the m-files containing the values of sensor mapping, controller, decoupling, capacitive actuation and slew to load them on the MATLAB workspace, at the proper simulation time.
Those values are the same for all the DFACS modes except for the DFACS custom mode 1 and 2. Therefore, when those modes are activated, they need the proper values of the aforementioned parameters. In the absence of the MATLAB functions, a trick was found (fig. B.1-1):

1) Download the matrices and vectors, that are needed for the custom mode 1 and 2, on the workspace by means of the initialization files (*sim_init.m* and *workaround.m*)
2) Insert multi-port switches for each of the class of matrices and vectors are needed (decoupling, mapping, controller configuration, actuation, slew). Each multi-port switch will have as much inputs as the number of submodes had been introduced, plus the first input that is the one responsible for the switch.
3) Create a *simulator command* file (*SC_Workaround*) in which two new commands are introduced (*SetCST1* and *SetCST2*). They can assume different values according to the number of the *multi-port switch* inputs. *SetCST1* and *SetCST2* are the first *multi-port switch* input and their values decides the output.

Therefore, the following files were involved:

- *Sim_init.m*: initialization file
- *Workaround.m*: it downloads the matrices and vectors in the Matlab workspace
- *TC_ACCtoCAL.txt*: telecommands file that activates DFACS custom mode 1 and 2

- *SC_workaround*: defines the commands *setCST1* and *setCST2* that represent the input values for the *multi-port switch* placed in the telecommands block.

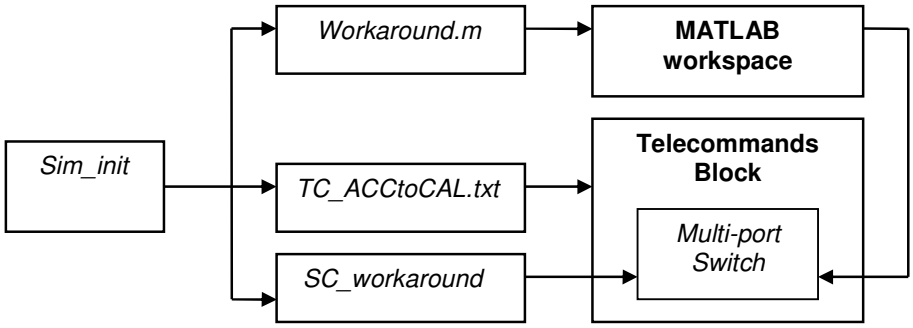

Fig. B.1-1 *Principle of Operation*

B.2 Telecommands Interface

The following figures represent the telecommands user interface in dSPACE ControlDesk. If the user pushes the buttons relative to the DFACS custom mode 1 or 2 (DF_CST1 / DF_CST2), the commands *SetCST1* and *SetCST2* immediately activate the proper aforementioned matrices and vectors (fig. B.2-3/4).

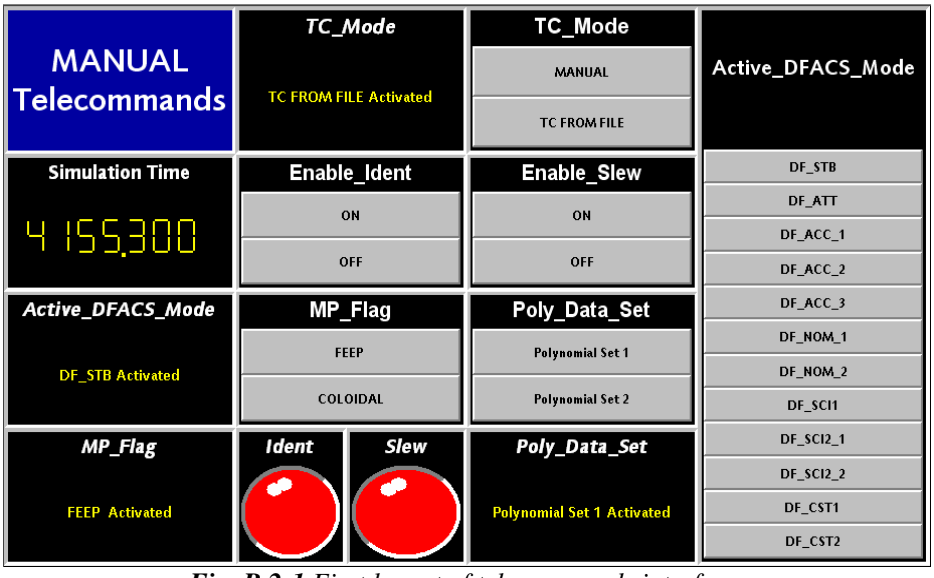

Fig. B.2-1 *First layout of telecommands interface.*

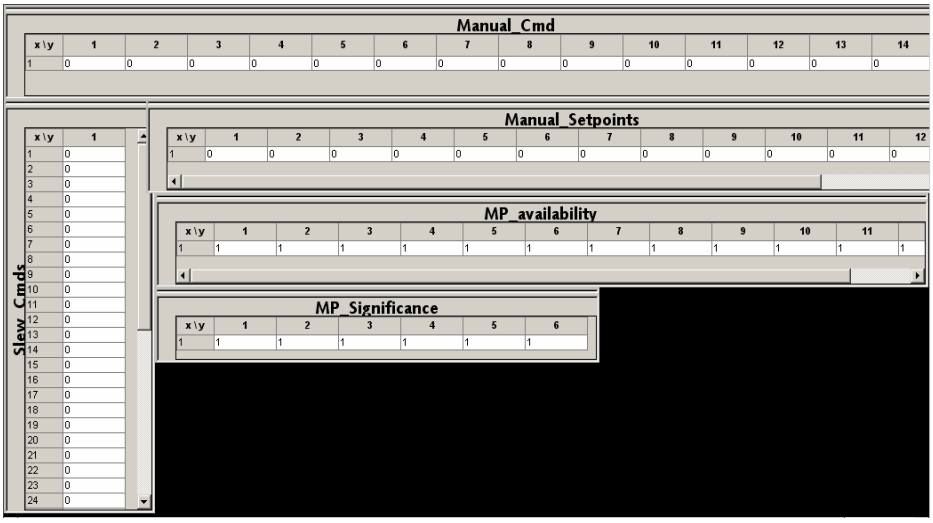

Fig. B.2-2 *Second layout of telecommands interface.*

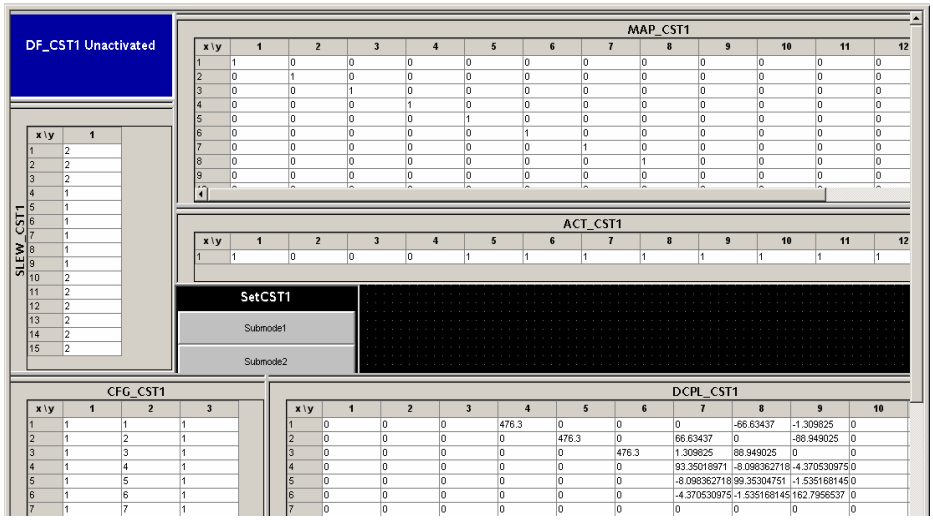

Fig. B.2-3 *Third layout of telecommands interface*

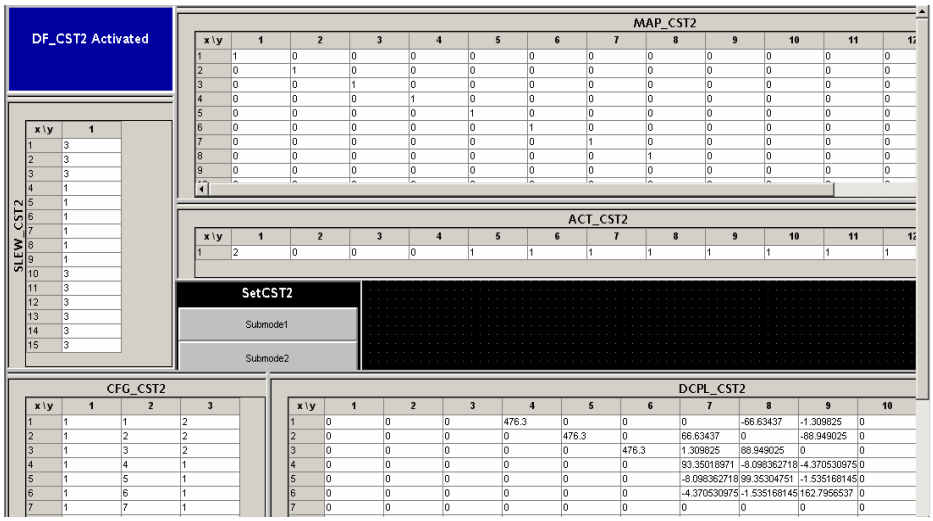

Fig. B.2-4 *Fourth layout of telecommands interface*

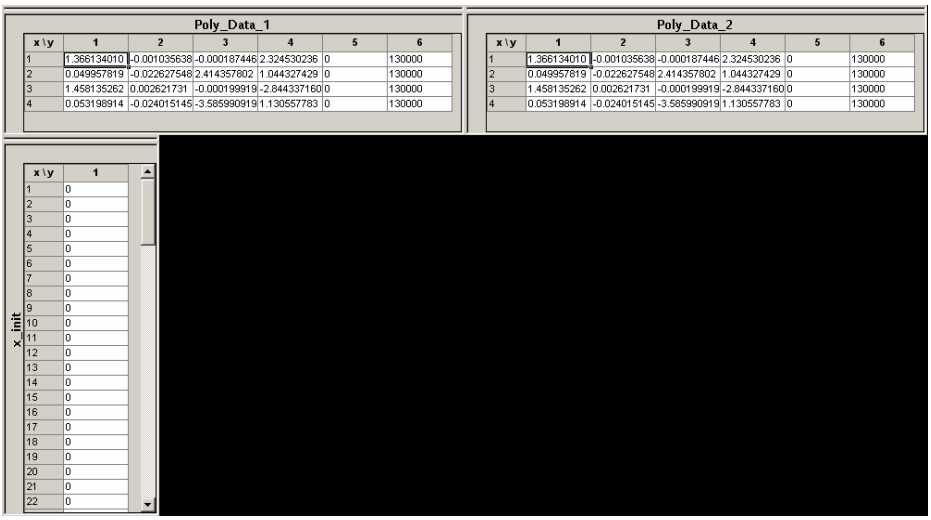

Fig. B.2-5 *Fifth layout of telecommands interface*

Appendix C

C.1 The Zeeman Effect

The Zeeman Effect is the splitting of spectral lines when an atom is placed in an external magnetic field. It was looked for by Faraday, predicted on the basis of classical theory by Lorentz, and first observed by Zeeman for whom the effect is now named, (See [14], [17]).

In quantum mechanics, the electron is thought of as a dual entity, it is a particle and an undulation of energy at the same time. The wavelength depends upon the electron's energy. If the energy increases, the frequency arises (v_0) and the wavelength (λ_0) diminishes:

$$\varepsilon = h \cdot v_0 = h \cdot \frac{c}{\lambda_0} \qquad \text{(C.1)}$$

Where:

c: Light speed

h: Planck's constant

The *state* of an electron is fixed by four quantum numbers:

- n: principal quantum number (any integer from 0 to infinity)
- l: azimuthal quantum number (any integer from 0 to n-1). It determines the electron's orbital angular momentum.
- m_l: magnetic quantum number (any integer, including zero, from $-l$ to $+l$. This totals to $2 \cdot l + 1$ numbers). It determines the specific orientation of the angular momentum in the presence of an external magnetic field.
- m_s: quantum spin number ($\pm$ 1/2)

The energy is dependent upon the quantum numbers. When an external magnetic field is not present, in most atoms, there exist several electronic

configurations that have the same energy, so that transitions between different pairs of configurations correspond to a single line or *energy level*. Therefore, it could happen that the energy levels are the same but the *states* (defined by the quantum numbers) are different (*degeneracy*).

The presence of a magnetic field breaks the *degeneracy*, since it interacts in a different way with electrons with different quantum numbers, slightly modifying their energies. The result is that, where there were several configurations with the same energy, now there are different energies, which give rise to several very close spectral lines. Therefore, a shift in the energy level of the states involved a shift in frequency and wavelength of a spectral line.

When placed in an external magnetic field, the energy of the atom changes because of the energy of its magnetic moment (**μ**) in the field, which is given by:

$$\Delta E = -\boldsymbol{\mu} \cdot \mathbf{B} = -\mu_z \cdot B \qquad \text{(C.2)}$$

where the *z* direction is defined by the direction of **B.** The z-component of the orbital magnetic dipole moment is:

$$\mu_z = -\mu_B m_l \qquad \text{(C.3)}$$

where μ_B is the physical constant of magnetic moment (Bohr Magneton), defined in S.I. units by:

$$\mu_B = \frac{e \cdot h}{2 \cdot m_e} \qquad \text{(C.4)}$$

with:

e: elementary charge

m_e*:* electron rest mass

Therefore, the change in the atom energy is:

$$\Delta E = \mu_B \cdot B \cdot m_l \qquad \text{(C.5)}$$

Since there are $2 \cdot l + 1$ values of m_l, each *energy level* splits into $2 \cdot l + 1$ levels. Figure C.1-1 shows the splitting of levels for the case of a transition between a state with $l = 2$ and one with $l = 1$.

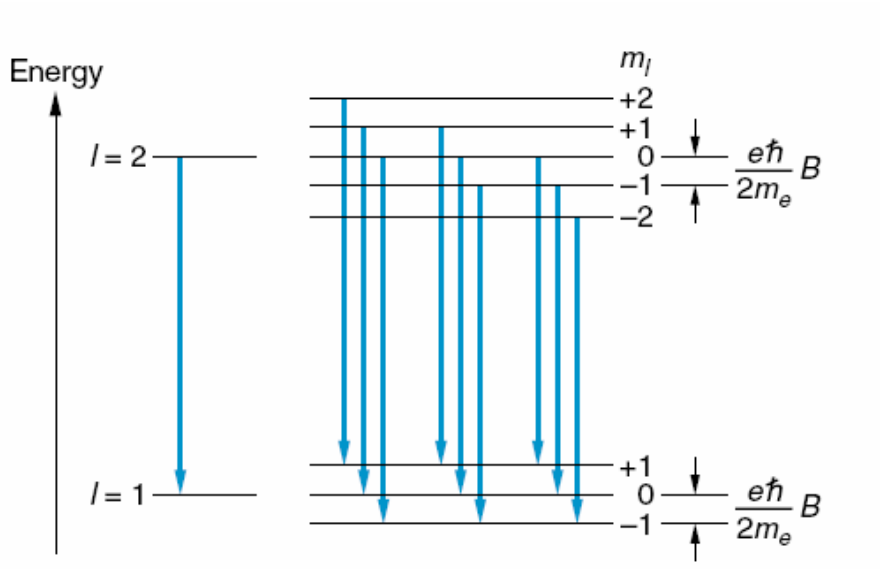

Fig.C.1-1 *The Zeeman Splitting*

Because of the uniform splitting of levels, there are only three different transition energies:

$$\begin{aligned} \varepsilon &= h \cdot \nu_0 + \frac{ehB}{2m_e} && m_l = 1 \\ \varepsilon &= h \cdot \nu_0 && m_l = 0 \\ \varepsilon &= h \cdot \nu_0 - \frac{ehB}{2m_e} && m_l = -1 \end{aligned} \qquad \text{(C.6)}$$

It could be seen that there will be only these energies for any initial and final values of *l*. The change in the frequency of the emitted spectral line is the energy change divided by *h*. The frequency changes are therefore $\pm eB/2m_e$ or 0.

In the specific case, the laser beam is obtained by stimulated emission of photons by excited Neon atoms. The Neon atoms are led to metastable states by means of excited He atoms.

A Neon atom excited to metastable state may transition to ground state and emit a photon of the proper wavelength (λ_0 = 632.8 nm). If an external magnetic field is applied inside the Laser Head, the emitted photons will have slightly different wavelengths, i.e. frequencies.

C.2 Off-line Calibration

The off-line calibration was conducted by setting the amplitude (α_{mech}) of a test signal (sine wave) on the real-time computer and by observing the displacement, s, traced by the laser light on a millimeter paper placed at a certain distance, x, from it. The ratio between the real mechanical angle and the set one (equation (4.2)) was calculated.

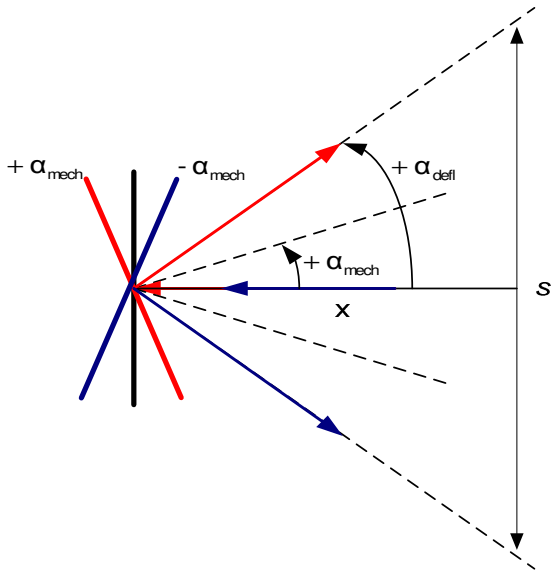

Fig. C.2-1 *Off-line calibration*

Looking at the geometry of figure C.2-1:

$$\alpha_{defl} = \arctan\left(\frac{s}{2 \cdot x}\right) \qquad \text{(C.7)}$$

Considering that the arctangent argument is relatively small (s << x):

$$\alpha_{mech} \cong \frac{s}{4 \cdot x} \qquad \text{(C.8)}$$

The results of table C.1a/b were obtained for the Piezoelectric and the Voice-Coil mirrors:

PIEZOELECTRIC MIRROR x = 2475 mm Without Voltage Divider					
z-axis (φ)			**y-axis (η)**		
Set α_{mech} (rad)	y (mm)	Real α_{mech} (rad)	Set α_{mech} (rad)	y (mm)	Real α_{mech} (rad)
1	9	$0.909 \cdot 10^{-3}$	1	9	$0.909 \cdot 10^{-3}$
0.7	6.75	$0.681 \cdot 10^{-3}$	0.7	6.5	$0.656 \cdot 10^{-3}$
0.5	5	$0.505 \cdot 10^{-3}$	0.5	5.5	$0.505 \cdot 10^{-3}$

***Table C.1a Off**-line calibration of the Piezoelectric mirror*

VOICE-COIL MIRROR x = 1840 mm Without Voltage Divider					
z-axis (φ)			**y-axis (η)**		
Set α_{mech} (rad)	y (mm)	Real α_{mech} (rad)	Set α_{mech} (rad)	y (mm)	Real α_{mech} (rad)
0.6	33	$4.48 \cdot 10^{-3}$	0.6	32	$4.34 \cdot 10^{-3}$
0.4	22	$2.98 \cdot 10^{-3}$	0.4	21	$2.85 \cdot 10^{-3}$
0.2	11	$1.49 \cdot 10^{-3}$	0.2	11	$1.49 \cdot 10^{-3}$

***Table C. 1b** Off-line calibration of the Voice-Coil mirror*

According the equations (4.2) and (4.3) and considering the mean values:

	PIEZOELECTRIC MIRROR		**VOICE-COIL MIRROR**	
	G	**K**	**G**	**K**
η	$0.985 \cdot 10^{-3}$	1014	$7.26 \cdot 10^{-3}$	138
φ	$0.964 \cdot 10^{-3}$	1037	$7.45 \cdot 10^{-3}$	134

***Table C. 2** Off-line calibration: definitive results*

C.3 Quadratic Effect

It is interesting to analyze the power spectral density that is obtained by applying a test signal at one of the Tip/Tilt elements, i.e. the piezoelectric mirror. As a consequence of the sine wave at 2.5 Hz that is applied as piezo actuation signal, the PSD is the one of figure C.3-1:

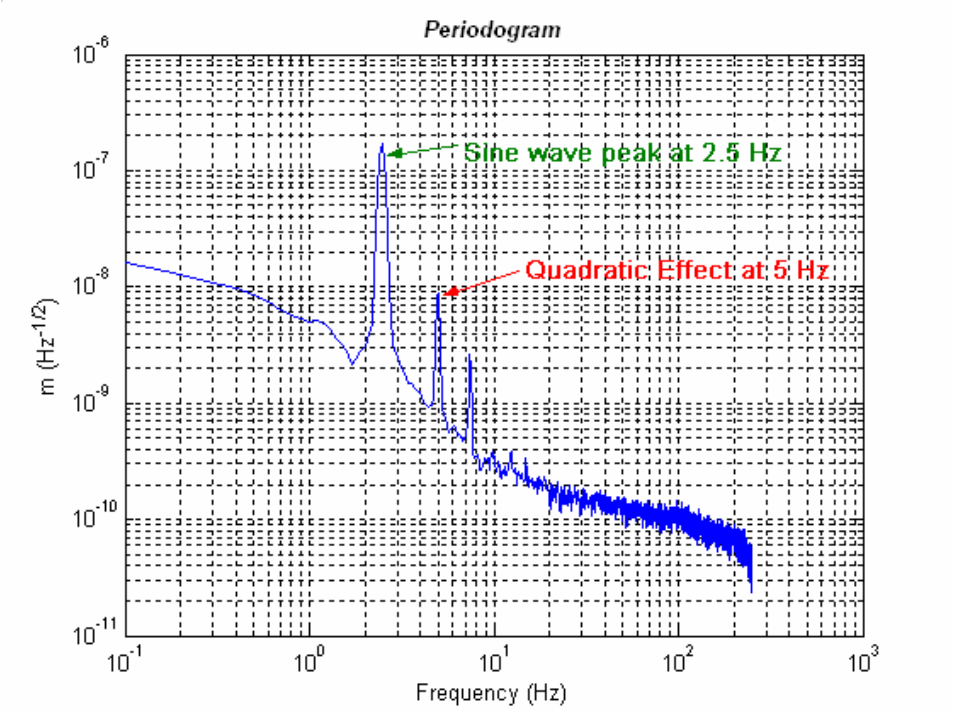

Fig. C.3-1 *Test signal: Power Spectral Density*

As would be expected, the PSD presents a peak, representative of the sine wave, at 2.5 Hz. The second peak is due to a quadratic effect to be imputed to the piezo actuator functioning. In fact, the pivot point, with respect to which the tip/tilt movement is defined, is placed on the piezo actuator surface (fig. 5.2.4-2/ C.3-2) and, therefore, is distant from the mirror surface by a quantity equal to the mirror thickness ("c" in figure C.3-2).

The quadratic effect will be null if the laser beam hits the pivot point surface directly and, if so, the mirror would coincided with that surface.

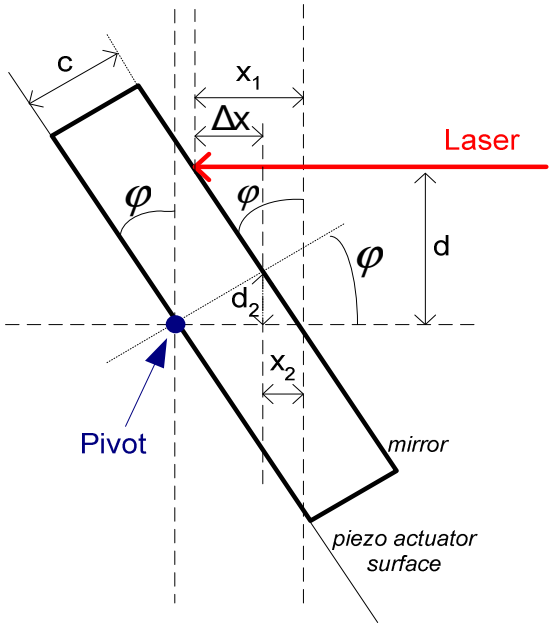

Fig. C.3-2 *Quadratic effect*

The phenomenon is, now, treated analytically.

Looking at the figure C.3-2, the following system can be solved:

$$\begin{cases} \Delta x = x_1 - x_2 \\ x_1 = d \cdot \tan\varphi \\ x_2 = d_2 \cdot \tan\varphi \\ d_2 = c.\cos(90° - \varphi) \end{cases} \tag{C.9}$$

Therefore, the displacement along the x-axis is equal to:

$$\Delta x = d \cdot \tan\varphi + c \cdot (1 - \sec\varphi) \tag{C.10}$$

where $\sec\varphi = 1/\cos\varphi$.

Considering that φ is small and Taylor's expansion of secφ is the following:

$$\sec\varphi = 1 + \frac{\varphi^2}{2} + \frac{\varphi^4}{24} + \ldots \tag{C.11}$$

It is obtained:

$$\Delta x = d \cdot \varphi - c \cdot \frac{\varphi^2}{2} \tag{C.12}$$

Taking into account that, in the specific case, it is:

$$\varphi = \sin(\omega_0 \cdot t) \tag{C.13}$$

where $\omega_0 = 2\pi f$ and f = 2.5 Hz.
The final result is the following:

$$\Delta x = d \cdot \sin(\omega_0 \cdot t) - c \cdot \left[\frac{1}{2}(1 - \cos(2\omega_0 \cdot t)) \right] \tag{C.14}$$

Differentiated into three terms:

$$\Delta x = \underbrace{d \cdot \sin(\omega_0 \cdot t)}_{\text{1st term: main component}} + \underbrace{\frac{c}{2}\cos(2\omega_0 \cdot t)}_{\text{2nd term: quadratic effect}} - \underbrace{\frac{c}{2}}_{\text{3rd term: constant}} \tag{C.15}$$

In the PSD, the first peak is due to the main component of the relation (C.15), the second peak at the second term. The constant part of the (C.15) is not visible in the PSD because of the data detrending effectuated before plotting the power spectral density of the signal.

Appendix D

D.1 Starting a Measurement: Step by Step Procedure

In order to put the laboratory instrumentation into operation and to make a measurement available, the user has to proceed following the steps listed below:

1) Switch the orange multi-port plug (fig. D.1-1) on

It gets power, immediately, to the Power Supply for the Laser Head(1) (laser is on). It activates the current connection for the following instruments:

- Oscilloscope
- Piezoelectric mirror electronics
- Voice-Coil mirror electronics
- VME bus

Fig. D.1-1 *Multi-port plug*

2) Switch the Real-Time Computer (dSPACE computer) on

(1) Before starting a test the laser must be ready, it means that the user has to wait for the laser warm-up (10 minutes, usually)

3) **Switch the Host PC (See Chapter 2, fig. 2.2-1) on**
4) **Open the dSPACE ControlDesk on the Host PC desktop**

⇒ *To load the E2E-Simulator on the RTC*:

- Click on: Platform/Application/Load Application
- Open: D:\ Marianna\E2E_Simulator\lisa_pathfinder.sdf
- Click on: File/open experiment
- Open:
  D:\Marianna\E2E_Simulator\experiment\telecommands.cdx

⇒ *To load the testing sine wave on the RTC:*

- Click on: Platform/Application/Load Application
- Open: D:\ Marianna\LAB\mirror_calib.sdf
- Open the layout files:
  D:\ Marianna\LAB\Lab1.lay
  D:\ Marianna\LAB\Lab2.lay
  D:\ Marianna\LAB\Cap.lay

5) **Switch the oscilloscope on**
   It is always useful to observe what is running on the RTC watching at the oscilloscope
6) **Switch the piezoelectric and voice-coil mirror electronics on**
7) **Switch the VME bus on**
8) **Switch the LabVIEW computer on**
   When "Auswahl" compares on the DOS, the user has to push "1"
9) **Open the Resource Manager on the LabVIEW PC desktop**
   In this way, the VME Bus is initialized.
10) **Open the LabVIEW icon on the PC desktop**
11) **To initialize the Laser Axis Board:**

⇒ Open the Virtual Instrument:
C:\ LABTests\LASERAXISBOARD_initializationfile.vi

⇒ Click on the first arrow on the right (this is the "run" command, it executes the file)

⇒ Check the LEDs on the Laser Axis Board (See paragraph D.2)

10) To start a measurement:

⇒ Open the Virtual Instrument :
C:\ LABTests\xdiff_IFO (writetofile).vi
This LabVIEW file permits to download the measurement data that comes from the VME bus on the PC, to store and to visualize them on a plot

⇒ Set the simulation time samples on the Front Panel of aforementioned file (the uploading frequency is 500 Hz. It means that, for example, to have a simulation time of 3 hours, the corresponding number of samples is 5.4e+6). In the file's Block Diagram is present the number 1.25, it is relative to the interferometer resolution (See Chapter 4).

⇒ Click on the first arrow on the right (it is the "run" command that executes the file, starting the experiment)

The LabVIEW files principle of operation is described in a more detailed way in Appendix E of the present thesis.

D.2 Importance of the LEDs on the Laser Axis Board

When the Laser Axis Board is initialized, it is important to check the status of the Light Emitting Diodes (LEDs) placed on it. Before starting a measurement, the green LEDs in figure D.2-1 must be on, while the others rigorously off. If this situation is present, it means that the measurement and reference signals are received perfectly by the board (Chapter 4, Paragraph 4.2.7).

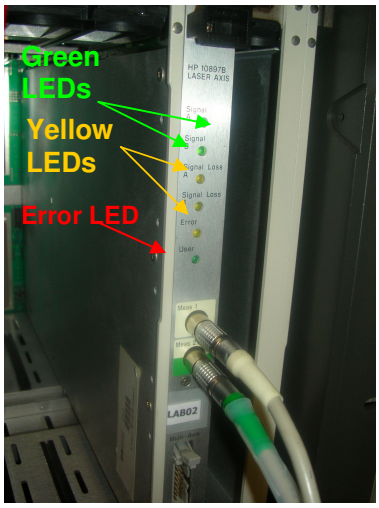

Fig. D.2 -1 *Laser Axis Board*

When the signals are not strong enough, the yellow LEDs flash and, immediately, an error occurs (the fifth LED is on). The cause of this behavior is the laser beam misalignment at the receiver. Therefore, it is necessary to align them in close proximity of the receiver and very far from it, in order to be sure of the perfect overlapping.

D.3 Managing dSPACE ControlDesk

The test signal that has been applied at the Tip/Tilt mirrors, during the tests, is represented by a sine wave. It could be applied by means of the E2E-Simulator running on the Real-Time computer but it was preferred to use a simpler model to speed-up the tests proceeding. In fact, in the dSPACE® computer, a simple Simulink® model whose output is a sine wave was implemented.

As observable from the figure D.3-1, by means of a proper Control Desk interface, it is possible to modify the frequency and the amplitude of the test signal as needed.

Through the *Capture Layout* visible in figure D.3-2, the user can set the simulation time and store the data.

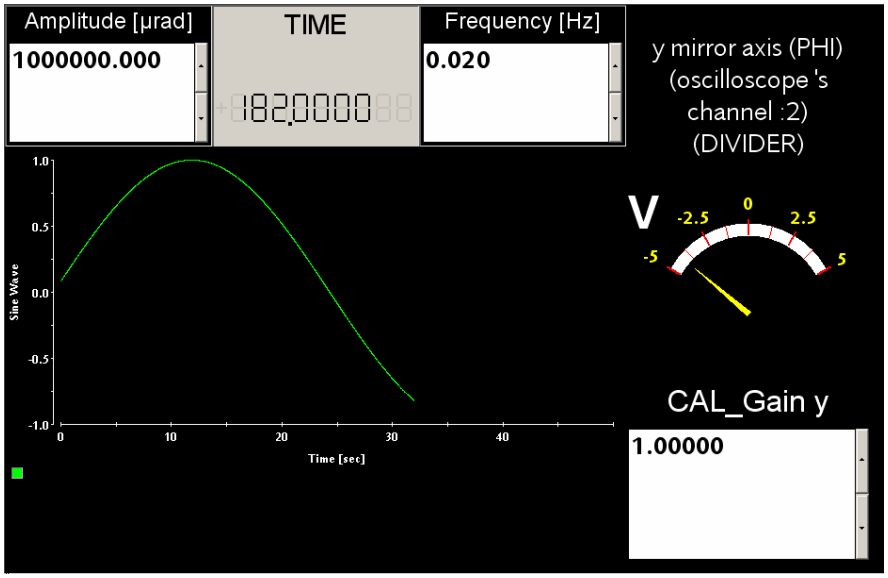

Fig. D.3 -1 *Sine Wave ControlDesk Layout*

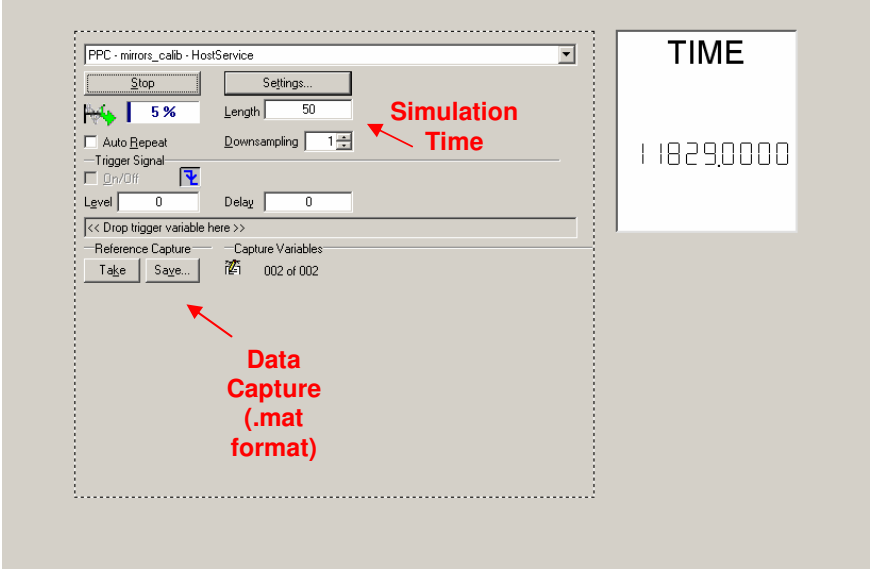

Fig. D.3 -2 *Sine Wave ControlDesk Capture Layout*

Appendix E

VISA is a driver software architecture created by the National Instrument Inc. By means of a LabVIEW application with VISA calls, it is possible to communicate with instrumentation buses, as the VXI bus.
Before starting to explain in detail the LabVIEW files used in this work, it is necessary to introduce the exact terminology.
A VISA Resource is represented by any instrument in the system, in the particular case, the VXI bus. An Instrument Descriptor is the exact name of the instrument. It specifies the interface type (VXI), the address of the device (Logical Address) and the session type (INSTR). A VISA Session is a path of communication to a VISA Resource, so it is necessary to open a VISA Session any time it is necessary to start VISA communication to an instrument.

E.1 Laser Axis Board Initialization File

Each LabVIEW interface is divided into two parts: the Front Panel and the Block Diagram. The Block Diagram of the Laser Axis Board initialization file is visible opening the following file:

- C:\ LABTests\LASERAXISBOARD_initializationfile.vi

In order to initialize the board, the user has to push the arrow icon on the left of the Block Diagram toolbar; in this way a Session is opened. It means that a communication link between the LabVIEW program and the Resource is present. This link is created by VISA.
To open a session the Instrument Descriptor, i.e. the Laser Axis Board coordinates, have to be specified.
In the block diagram of the initialization file, four VISA functions are present. The first represents the Open function; the Resource name input is the VISA Instrument Descriptor for the Resource to which a Session will be opened (In the specific case: VXI::0::INSTR).

The only way to communicate with a VXI instrument is through register access. In fact, the second and the third functions are used to, respectively, write on and read from the configuration register a 16-bit value expressed in hexadecimal numbers (Tab. E.1).
The Address Space input (number 2 in the block diagram of the initialization file) indicates which VXI Address Space to use (in the specific case: "2" corresponds to A24 address).

Offset Array	Value Write	Value Read
0	300	3300
4	201	201
8	1010	1010
9A	FF	FF
9E	0	0
A6	7F	7F
BE	4	4
88	0	0
8C	0	0
B6	80	80
BA	10	0
B2	7F	0
B2	0	0
0	100	FFFF

Tab. E.1 *Initialization file: Front Panel*

The fundamental address in each Address Space is called *base memory address*. VISA keeps track of the base memory address that the device requests in each Address Space. The offset array input is relative to this base address and it is also expressed in hexadecimal numbers. The last function closes the session and if, during the initialization of the board, an error occurs, this function connects to a dialog box that informs the user of the error and displays the text message associated with the VISA error code.

E.2 Laser Axis Board Upload and Visualization File

The Block Diagram of the LabVIEW file (C:\LABTests\xdiff_IFO (writetofile).vi), that permits to upload the position measurement from the Laser Axis Board storing and visualizing it, is observed in figure E.2-1.

The gray window, divided into 3 parts, guarantees the consequentiality of the actions. The function that permits to upload the 32-bit position word from the board is put into the so called “For loop” window.

It executes a section of code a defined number of times (samples). Its count terminal (the “N” input terminal in figure E.2-1) is visualized on the Front Panel; the user has to choose and write down the number of samples to execute the loop. For example, considering that the upload frequency is 500 Hz, in order to obtain a simulation time of 500 seconds, the number of samples will be 250000.

At each sample, i.e. every 0.002 seconds, a position value corresponds. The position word expressed in binary digits is, then, transformed in an integer number and multiplied by the board resolution (0.62 nm in figure E.2-1; 1.23 nm in the specific case).

The uploaded values of time and position are plotted and visualized on the Front-Panel. The measurement data are stored at the end of the test.

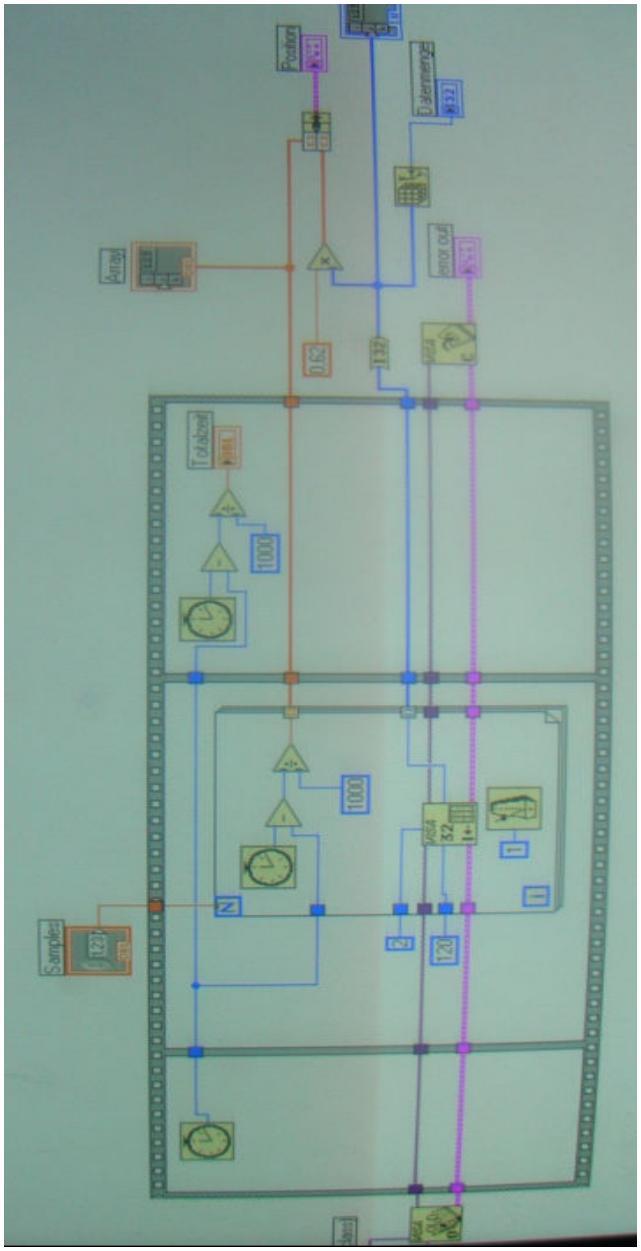

Fig. E.2-1 *Upload and visualization file: Block Diagram*

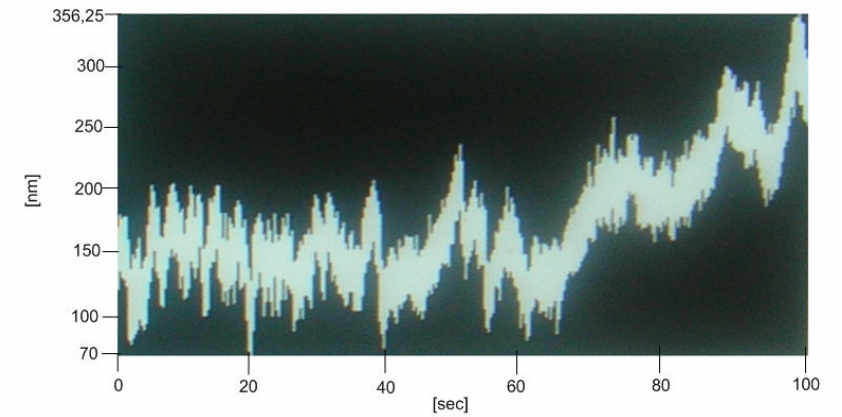

Fig.E.2-2 *Example of measurement data plot*

References

[1] Astrium Ltd, *Proposal for SMART-2 in response ESA ITT AO/2-2524/03/NL/HB,* Proposal Number TP1589, May 2003

[2] Fichter, W., Schleicher, A., Brandt, N., Vitale, S., Bortoluzzi, D., *Control Tasks and Functional Architecture of the LISA Pathfinder Drag-Free System*, February 2005

[3] Montemurro, F., LISA Pathfinder Simulator User Manual, Technical Note, EADS Astrium GmbH, July 2005

[4] dSPACE®, *Modular Systems based on DS1005: Installation and Configuration Reference* (for release 3.5), 2002

[5] dSPACE®, *Modular Systems based on DS1005: Installation and Configuration Guide* (for release 4.0), 2003

[6] dSPACE®, *Control Desk: Experiment Guide* (for release 4.0), 2003

[7] dSPACE®, *Real-Time Interface (RTI and RTI-MP): Implementation Guide* (for release 4.0), 2003

[8] dSPACE®, *C++ Integration Kit Version 1.0.2: Implementation Guide for RTLib and RTI, 2005*

[9] The MathWorks, Inc., *Real-Time Workshop®: User's Guide* (Version 4), 2000

[10] National Instruments, Corp., *LabVIEW®: Data acquisition Basics Manual* (Version 7.0), 2003

[11] National Instruments, Corp., *LabVIEW®: User Manual* (Version 7.0), 2003

[12] Hecht, E., *Optics,* Addison Wesley, 2002

[13] Bass, M., *HANDBOOK OF OPTICS Volume 1: Fundamental, Techniques & Design*, 2nd edition, McGraw Hill, NewYork, 2000

[14] Bass, M., *HANDBOOK OF OPTICS Volume 2: Devices, Measurements & Properties*, 2nd edition, McGraw Hill, NewYork, 2000

[15] Hobbs, P.C.D., *Building Electro-Optical Systems Making It All Work*, John Wiley & Sons, 2000

[16] Tolansky, S., *An Introduction to Interferometry*, Longmans, London, 1955

[17] Brown, E.B., *Modern Optics*, Reinhold, New York, 1965

[18] Born, M., Wolf, E., *Principles of Optics*, Pergamon Press, London, 1965

[19] Agilent, *Laser and Optics: User's Manual*, Web Site: http://www.agilent.com

[20] Agilent, *HP10897B High Resolution VME Bus Laser Axis Board: User Manual,* Web Site: http://www.agilent.com

[21] National Instruments, Corp., *VXI-MXI2 User's Manual,* August 1996

[22] Physik Instrumente GmbH, *S-340 User Manual PZ 75E Tip/Tilt Platform* (Release 2.20), Web Site: http://www.physikinstrumente.com

[23] Physik Instrumente GmbH, *PZ62E User Manual* (Release 2.20)

[24] Thorlabs, Inc, Catalog, Volume 18, Web Site: http://www.thorlabs.com

[25] Laser2000 GmbH, *DKS/35 Produkt Information*, Web Site: http://www.laser2000.de

[26] Heizel, G., *SMART-2 Interferometer*, Albert Einstein Institute, Hannover, August 2002

[27] Fichter, W., *DFACS Requirements Specifications*, Technical Note, EADS Astrium, July 2005

[28] Brandt, N., *Noise Generation and Data Analysis,* Technical Note, EADS Astrium GmbH, April 2003

[29] Fichter, W., *DFACS Test-Bed with OMS*, Technical Note, EADS Astrium GmbH, December 2005

[30] Ziegler, T., *Calibration of Electrostatic Actuation*, Technical Note, EADS Astrium GmbH, January 2006

[31] Ziegler, T., *Basics of Parameter Identification for Multibody Systems*, Technical Note, EADS Astrium GmbH, January 2006

[32] Ziegler, T., *Personal Communications*